CHEMICAL REVIEWS

Review

Cite This: *Chem. Rev.* 2020, 120, 36−78

pubs.acs.org/CR

Single-Molecule Analysis and Engineering of DNA Motors

Sonisilpa Mohapatra,[†] Chang-Ting Lin,[†] Xinyu A. Feng,[‡] Aakash Basu,[†] and Taekjip Ha*[,†,§,∥,⊥]

[†]Department of Biophysics and Biophysical Chemistry, [‡]Department of Biology, [§]Department of Biophysics, and [∥]Department of Biomedical Engineering, Johns Hopkins University, Baltimore, Maryland 21205, United States

[⊥]Howard Hughes Medical Institute, Baltimore, Maryland 21205, United States

ABSTRACT: Molecular motors are diverse enzymes that transduce chemical energy into mechanical work and, in doing so, perform critical cellular functions such as DNA replication and transcription, DNA supercoiling, intracellular transport, and ATP synthesis. Single-molecule techniques have been extensively used to identify structural intermediates in the reaction cycles of molecular motors and to understand how substeps in energy consumption drive transitions between the intermediates. Here, we review a broad spectrum of single-molecule tools and techniques such as optical and magnetic tweezers, atomic force microscopy (AFM), single-molecule fluorescence resonance energy transfer (smFRET), nanopore tweezers, and hybrid techniques that increase the number of observables. These methods enable the manipulation of individual biomolecules via the application of forces and torques and the observation of dynamic conformational changes in single motor complexes. We also review how these techniques have been applied to study various motors such as helicases, DNA and RNA polymerases, topoisomerases, nucleosome remodelers, and motors involved in the condensation, segregation, and digestion of DNA. In-depth analysis of mechanochemical coupling in molecular motors has made the development of artificially engineered motors possible. We review techniques such as mutagenesis, chemical modifications, and optogenetics that have been used to re-engineer existing molecular motors to have, for instance, altered speed, processivity, or functionality. We also discuss how single-molecule analysis of engineered motors allows us to challenge our fundamental understanding of how molecular motors transduce energy.

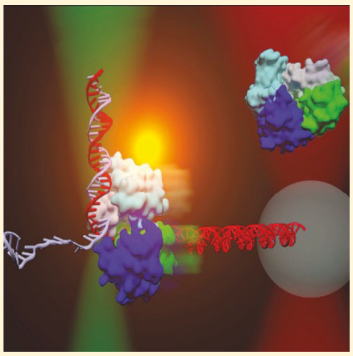

CONTENTS

Special Issue: Molecular Motors

Received: June 5, 2019
Published: October 29, 2019

DOI: 10.1021/acs.chemrev.9b00361
Chem. Rev. 2020, 120, 36−78

1. INTRODUCTION

There are two types of motion in living systems: diffusional and directional. Diffusional motion is driven by thermal energy, has no net direction, and does not require work in order to occur. The spatial extent of diffusion scales with the square root of time, rendering diffusion slow over long length scales. However, diffusion can be very rapid over short length scales and can thus significantly influence the rates of biochemical reactions. Diffusion of proteins such as transcription factors and DNA repair proteins along double-stranded (ds) DNA has been proposed to accelerate their target search by reducing the number of search dimensions.[1] Protein diffusion along single-stranded (ss) DNA also occurs and helps coordinate DNA access among proteins that function on ssDNA.[2] This review, however, is focused primarily on directional, rather than diffusional, motion along DNA. Unlike diffusion, this requires the transduction of chemical energy into mechanical work by molecular motors.

Before discussing the properties of motor proteins, it is instructive to consider the relevant physical scales involved. k_BT, where k_B is the Boltzmann constant (=1.38 × 10^{-23} J/K) and T is the absolute temperature, sets the scale of thermal energy. If the free energy change required to affect a transition is much larger than k_BT, the transition is unlikely to happen spontaneously on a biologically relevant time scale and would require acceleration by an enzyme. However, if the energy required is much less than k_BT, the transition happens constantly and reversibly and is unlikely to be of biological relevance.

At ambient temperature ($T \sim 300$ K), k_BT is approximately 2.4 kJ/mol or 0.59 kcal/mol. Per molecule, k_BT is approximately 4 × 10^{-21} J (or N m), which can be conveniently rewritten as ∼4 pN-nm, where pN stands for piconewton. As the typical length scales associated with biological macromolecules are a few nanometers, piconewton therefore emerges as a typical force scale in molecular biology. It turns out that pN scale forces can indeed modulate the functions of many motor proteins, causing them to stall, backstep, or change speed.

1.1. DNA Motor Proteins

Motor proteins can be classified based on the types of fuel and track they use, the kinds of movements they generate, and varied properties such as their directionality, assembly state, step size, speed, processivity, stall force, and coupling efficiency.

1.1.1. Fuel. DNA binding molecular motors such as helicases, topoisomerases, and chromatin remodelers transduce chemical energy from the hydrolysis of ATP into mechanical work. DNA and RNA polymerases use dNTPs and rNTPs, respectively. Exonucleases on the other hand do not use external fuel but utilize the energy released from hydrolytic cleavage of nucleic acids to power their movement along DNA.

1.1.2. Track. Double-stranded DNA is about 2 nm in diameter and is made of nucleotides (composed of adenine, guanine, thymine, and cytosine). Each strand has a polarity, running from a 5′ phosphate end to a 3′ hydroxyl end. Duplex DNA is an antiparallel assembly of the two strands running in opposite directions and is thus not polar. However, most DNA motor proteins track along a single strand of DNA and can thus be classified by polarity as either 3′ to 5′ or 5′ to 3′ motors.

1.1.3. Directionality. DNA and RNA polymerases move in the 5′ to 3′ direction relative to the newly synthesized strand. For nonpolymerizing DNA motor proteins such as helicases, both directionalities are possible. An ongoing and fundamental challenge in understanding the mechanisms of these motors involves determining the factors which dictate directionality. In the case of helicases, different translocation directionality has been achieved by walking in opposite directions despite binding to DNA with the same orientation.[3]

1.1.4. Step Size. Step size refers to the extent of the repeating physical movement of a motor protein along its track, coupled to each repeating cycle of fuel consumption. DNA and RNA polymerases extend nucleic acids one nucleotide at a time, but step sizes smaller and larger than one nucleotide may still be possible.[4] For example, a motor protein may move in smaller increments relative to DNA during each of the substeps within an ATPase cycle.[5] The ATPase cycle of a motor can be simplistically represented as

$$E \leftrightarrow T \leftrightarrow DP \leftrightarrow D \leftrightarrow E$$

Here, E denotes a motor protein in the apo state (without a bound nucleotide). T is a state with a bound ATP. DP is achieved from T via the hydrolysis of ATP into ADP and Pi. Release of Pi from DP results in the ADP-bound state D. Finally, release of ADP resets the motor. The order of release of Pi and ADP may vary between motor proteins. In addition, several single nucleotide steps may accumulate elastic energy in the complex that may be released in a single burst. Such a hierarchy of different step sizes has been observed in a number of DNA motor proteins.[6−11] DNA motors can sometimes show pausing and backstepping while moving along its track, depending on the ATP concentration and DNA sequence that it is tracking.

1.1.5. Speed. Typical motor proteins take one step once every 1−100 ms, making experimental techniques that can probe this time scale highly relevant for the study of molecular motors. One of the fastest DNA motor proteins known is FtsK, which moves at speeds as high as 7000 base pairs (bp)/s.[12] DNA synthesis in *E. coli* has been thought to occur at 1000 bp/s, but recent data suggest that the replisome can run ∼50% faster *in vitro* depending on replisome composition.[13] Earlier reports may have underestimated *in vivo* speeds due to frequent disassembly and reassembly of the replisome as it encounters transcription machinery.[14]

1.1.6. Stall Force. The stall force is the minimum external opposing force needed to halt motor movement. Experimentally, such forces can be applied using techniques such as optical and magnetic tweezers. Often, motor proteins pause temporarily before resuming movement, which is commonly referred to as a stall.

1.1.7. Processivity. This is a measure of how many times a motor protein repeats its biochemical reaction cycle before falling off the track. This has been expressed in many ways, for example, in terms of run length (the number of base pairs

DOI: 10.1021/acs.chemrev.9b00361
Chem. Rev. 2020, 120, 36−78

translocated per binding event) or the probability of dissociation of the motor from the track at every step.

1.1.8. Linear or Rotary. Any motor protein that moves on dsDNA with a single bp step size is expected to be a rotary motor, faithfully tracking the helicity of DNA. If the step size is not one base pair, there may still be a rotatory movement, but its pitch may not match the DNA periodicity.[15]

1.2. Single-Molecule Techniques and Fluorescence Primer

Several experimental techniques have been developed to directly observe the motion of individual molecular motors. Conceptually, the simplest approach is to measure the center of mass of an individual motor on a linear DNA track as a function of time. Limited spatiotemporal resolution can obscure the detection of individual motor steps but can still be useful in measuring parameters such as processivity and average speed. An added complication in the case of studying DNA motor proteins is that DNA is flexible on length scales longer than ~150 bp. Thus, in order to measure motor movements accurately, force must be applied to stretch the DNA. The position along the track can be determined by observing a probe (such as a micron sized bead, a single fluorophore, or a nanoparticle) attached to the motor. DNA stretching is not necessary if a movement on a length scale shorter than ~100 bp is probed, for example, by using fluorescence (or Förster) resonance energy transfer (FRET). In this review, we discuss various single-molecule techniques in detail, broadly categorized into fluorescence-based and mechanical-manipulation-based techniques. Here, we first provide a quick primer on fluorescence.

A fluorophore is a fluorescent dye molecule. It is made up of several aromatic rings, and the larger it is, the more red-shifted its wavelength of emission is. Typically, the size of a fluorophore is less than 1 nm, and it can be attached to a biological molecule in a specific manner at a well-defined location. With advanced microscopy and detector technologies, it is now routinely possible to detect and localize a single fluorophore.

Some Useful Facts about Fluorescence:

It Happens between Two Singlet States: These electronic states (Figure 1), called S_0 and S_1 for the ground state and the first excited state, respectively, are broadened because of additional vibrational and rotational degrees of freedom. Normally, a fluorophore is at the lowest energy level of S_0 and is excited to somewhere in the multitudes of S_1 states upon absorption of a photon with energy E_1. The molecule quickly relaxes to the lowest energy S_1 state in about a picosecond (10^{-12} s) and sits there for about a nanosecond before it transitions to somewhere in the multitudes of states in S_0 by the emission of a (fluorescence) photon with energy E_2. Then, the molecule again quickly relaxes down to the bottom of S_0 in about a picosecond, resetting the system to the original configuration.

Intersystem Crossing to the Triplet State: Once in about every 1000 excitations to S_1, a molecule can undergo "intersystem crossing" to the triplet state (T_1, Figure 1). T_1 is important despite the low frequency of visits not only because its lifetime is at least 1000 times longer than S_1 (and can even be several orders of magnitude longer in the absence of triplet state quenchers which help bring the molecule back to S_0) but also because photobleaching can occur via reaction with molecular oxygen, O_2, from T_1. O_2 is also the most effective triplet state quencher in aqueous solutions.

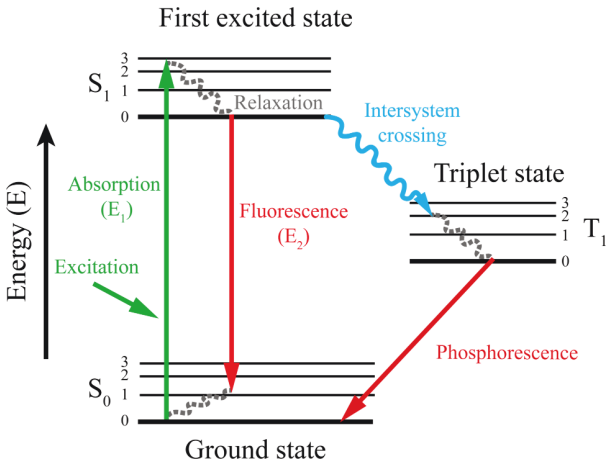

Figure 1. Jablonski diagram. When a fluorophore is excited by light, the absorbed photon with energy E_1 excites the molecule from the ground state (S_0) to the singlet excited state (S_1). The excited molecule can relax to the ground state by emission of a photon with energy E_2, which is known as fluorescence. Occasionally, the excited fluorophore can relax to a triplet state through a nonradiative process, known as intersystem crossing. This pathway leads to emission of a photon through phosphorescence.

Stokes Shift: Because of the rapid relaxation that occurs both in S_0 and in S_1, typically $E_1 > E_2$. That is, the fluorescence photon is red-shifted (lower energy) relative to the excitation photon. This is a useful feature because we can use a color-based filter to reject almost all of the excitation light and detect only the fluorescence photons. This makes fluorescence measurements nearly background free, making even single-molecule detection possible.

Nanosecond Lifetime: Unlike absorption, which is nearly instantaneous, fluorescence has a relatively long (nanosecond) lifetime. Several molecular processes can happen in one nanosecond, and thus, the local environment can greatly affect the fluorescence signal of the molecule.

Quantum Yield: Not every excitation results in a fluorescence photon (radiative decay). Sometimes, the energy is dissipated entirely as heat (nonradiative decay). The quantum yield is the fraction of excitation events that results in fluorescence emission. Typical quantum yield values for commonly used fluorophores range from about 10 to 90%.

Photobleaching: A downside of fluorescence imaging is the limited observation time, as a result of photobleaching. Photobleaching is an inherent property thought to be caused by photo-oxidation, when a fluorophore excited by photon absorption undergoes a chemical reaction with an oxygen molecule and becomes a nonfluorescent molecule (and also likely not absorbent).

Dipole Absorption and Emission: A fluorophore can be considered as an oscillating electric dipole. It preferentially absorbs light polarized along its absorption dipole, and its emission is polarized along its emission dipole. The absorption and emission dipoles are commonly collinear but not for all dyes.

Extinction Coefficient (ε) or Absorption Cross Section (σ): The extinction coefficient (ε) is a measure of how well a molecule absorbs light. ε is measured in units of M^{-1} cm^{-1}. Cy5 has the largest ε of any known fluorophore (ε = 250,000 M^{-1} cm^{-1}). Light, at a wavelength of 649 nm that matches the absorption peak, would be attenuated by a factor of $e^{-250,000}$

DOI: 10.1021/acs.chemrev.9b00361
Chem. Rev. 2020, 120, 36−78

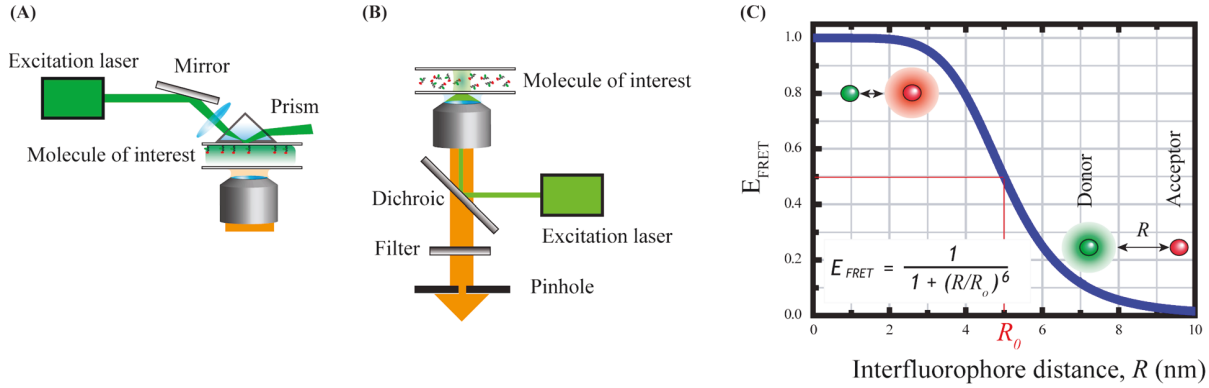

Figure 2. TIRF and confocal fluorescence microscopy can be used for smFRET imaging. Optical path of (A) the prism-type TIRF microscope and (B) the confocal fluorescence microscope. (C) FRET efficiency (E_{FRET}) is a function of the distance between the two fluorophores, donor and acceptor. Half of the donor (green) excitation events result in energy transfer to the acceptor (red), when the two dyes are separated by R_0.

after traveling through 1 cm of a 1 M solution of Cy5. However, dyes are not normally soluble at concentrations of 1 M. A more realistic concentration, 1 μM, would result in an attenuation factor of $e^{-0.25}$ = 0.78 per cm. Another way of expressing the strength of absorption is by the absorption cross section, σ. Having units of area, σ is typically a few Å^2. If laser light is focused to a very small spot (for example, 200 nm in size), only $\sigma/(200\ nm)^2$, or about 1 in a million photons of light, would be absorbed.

Reducing photobleaching as much as possible greatly enhances the ease of imaging single fluorophores. This is typically achieved by removing oxygen molecules in solution. The most popular and efficient method is to use an "oxygen scavenger system" that employs an enzymatic reaction which combines glucose with O_2. A side effect of removing oxygen molecules for single-molecule fluorescence imaging is that the triplet lifetime increases from microseconds to milliseconds. This is because O_2 is a very efficient quencher of the triplet state and, in its absence, the fluorophore spends a long time in the triplet state before relaxing to the ground state to resume the cycles of excitation and fluorescence emission. As a result, having oxygen in solution presents a problem because the light source, a single fluorophore, becomes intermittently dark. Typically, the addition of other triplet state quenchers, such as beta-mercaptoethanol or Trolox, makes the emission non-intermittent at least in the millisecond time scale.[16,17]

1.3. This Review

Due to space limitations, we will not discuss RNA motor proteins such as ribosomes, reverse transcriptases, and exoribonucleases except in passing, and instead, we recommend recent excellent reviews.[18,19] Diffusional movements of proteins on DNA will not be described either, except for cases where DNA motor proteins display such behavior, for example, RNA polymerase searching for a promoter site. Furthermore, our coverage will be biased toward more recent studies (performed in the past ~10 years) which use single-molecule methodologies to understand mechanistic details of DNA motors. We have also included a section on using various protein engineering methods to design DNA motors with desirable traits. Protein engineering can also be used in conjunction with single-molecule studies to further our understanding of DNA motors and their structure−function relationships.

2. SINGLE-MOLECULE TECHNIQUES

Single-molecule techniques bridge the gap between ensemble kinetic measurements and static structural measurements, both of which have been used for decades to understand the molecular mechanisms. While structural techniques such as X-ray crystallography and cryo-electron microscopy describe protein complexes in atomistic detail, they provide limited dynamic information. In contrast, bulk kinetic biochemical measurements measure chemical rate constants, allow for temporal ordering of substeps, and provide an understanding of how different processes are coupled. They do not, however, provide structural information about the very states and transitions they measure. Ensemble measurements such as gel electrophoresis provide information about structural intermediates but suffer from population averaging that obscures multimodal distributions which might exist in a population of molecules. Single-molecule techniques reduce the vast number of observables from static methods like X-ray crystallography to just a few, such as the position of a particular residue which has been labeled with a fluorophore. However, like kinetic measurements, single-molecule methods are also able to observe the dynamics of the variables of interest, thereby providing combined structural and kinetic information. Furthermore, unlike traditional ensemble methods, single-molecule techniques do not rely on temporal and population averaging. Instead, they collect statistics from individual molecules. Whereas biochemical methods often provide only indirect measurements of conformational dynamics, single-molecule techniques offer a quantitative, sensitive, and direct approach. They have thus developed into a powerful tool to study biological processes, deciphering the mode of action of a wide range of molecular machines involved in cell transport and motility, transcription, replication, and recombination, to name a few examples.

2.1. TIR and Confocal smFRET

Since its formulation in 1948, FRET has become one of the most popular methods to study molecular interactions in biological systems.[20] FRET refers to the excitation of an acceptor fluorophore by a donor fluorophore when they are within a distance of 2−8 nm from each other. FRET efficiency E_{FRET}, or the fraction of donor excitation events that result in energy transfer to the acceptor fluorophore, is given by

DOI: 10.1021/acs.chemrev.9b00361
Chem. Rev. 2020, 120, 36−78

$$E_{FRET} = \frac{1}{1 + \left(\frac{R}{R_0}\right)^6}$$

where R is the distance between the two fluorophores and R_0 is typically between 3 and 7 nm depending on the properties of the fluorophores (Figure 2C).

The combination of single-molecule detection and FRET (single-molecule FRET, or smFRET) allows us to study the heterogeneous behavior of molecules, as well as the dynamic behavior of single molecules.[21,22] Application of smFRET to biological systems, which often involves labeling the molecule of interest with a pair of donor and acceptor fluorophores to probe for molecular interactions, has revealed unprecedented details of biological reactions in action.[23,24]

smFRET measurements can be performed using a total internal reflection fluorescence (TIRF) microscope or a confocal microscope. Both methods can achieve good signal-to-noise ratio for single-molecule detection by reducing background. In a TIRF setup, the excitation laser intensity exponentially decays with distance from the surface; therefore, the illumination is restricted to near the slide surface and the background signal arising from fluorophores in solution is reduced (Figure 2A). In a confocal microscope, background is reduced by a pinhole that eliminates out-of-focus light (Figure 2B).

Numerous factors such as the choice of fluorophores, methods of labeling, and techniques to minimize photobleaching must be taken into account in order to image single biomolecules. Cyanine dyes and Alexa fluorophores have been commonly used for this purpose, and more recently, Janelia fluorophores have also been employed.[25] To label DNA site-specifically, *N*-hydroxysuccinimide-ester (NHS-ester) is commonly used to conjugate fluorophores to a modified DNA base that contains a terminal amino group. To label proteins, one can rely on nonspecific surface labeling using maleimide or NHS-ester conjugated dyes and restrict analysis to only those molecules that have a single donor−acceptor pair. A recent study demonstrated that one can achieve site-specific labeling by using a chemically modified NHS-ester dye to label a protein with a N-terminal cysteine.[26] An alternative strategy to label a protein site-specifically is to express the protein with a tag that can later be covalently conjugated to a fluorophore. Available systems include HaloTag (Promega) and SNAP-tag (NEB) (both of which rely on an enzymatic reaction between the reactive linker attached to a fluorescent dye and the protein tag[27,28]) or Sort tag (which utilizes the Sortase A enzyme to link a dye conjugated peptide to the protein).[29,30] Unnatural amino acids have also been used to provide a specific labeling position.[31] To be able to observe single-molecule fluorescence over longer time scales, imaging buffer containing oxygen scavenging systems and triplet state quenchers can be used to increase the photobleaching lifetime of the fluorophores,[17] in which case one needs to make sure the imaging buffer components do not interfere with the biological reaction.

To visualize fluorescence on a TIRF microscope, the molecule of interest may be tethered to the slide surface, usually via biotin−avidin interaction. For nucleic acid studies, biotinylated DNA is commercially available for immobilizing DNA. Proteins can be immobilized via a biotinylated antibody that is specific to the protein of interest.[32] It is also possible to avoid surface tethering by using an anti-Brownian electrokinetic (ABEL) trap[33,34] or detecting smFRET during a sub-millisecond passage time of a molecule through a focused laser beam.[35] For the latter, however, biochemical reactions that take longer than about a millisecond cannot be observed in real time and analysis is generally limited to population distributions, typically depicted through FRET efficiency histograms.[16]

To measure accurate FRET efficiencies, one needs to correct for several factors including background, crosstalk between different detection channels, and the gamma factor which integrates unequal detection efficiencies of the camera at different wavelengths as well as different quantum yields of the chosen fluorophores.[22,36] smFRET data are typically visualized as a histogram of the FRET efficiencies of single molecules at a certain time point or as trajectories of FRET efficiencies for single molecules over time.

Fluorophores are sensitive to their local environment, and interactions with protein or DNA can lead to significant changes in their fluorescence intensities.[37] Thus, changes in apparent FRET efficiencies could be due to changes in the local environment instead of real distance changes between the donor and acceptor fluorophores. One also needs to keep in mind that any modifications introduced for labeling could inadvertently affect the molecule of interest itself. Controls are therefore necessary to confirm that the behavior of the labeled molecule is representative of the real biological phenomena being studied.

2.2. Hydrodynamic DNA Stretching

Flow-induced DNA stretching has enabled the observation of protein−DNA interactions as a function of protein position along the DNA. Individual DNA molecules are attached on one end to the surface of a flow chamber by a biotin-based linkage, while the other end is modified for specific binding to a micron sized bead.[38,39] To prevent nonspecific interactions between the bead and the surface of the flow cell, a paramagnetic microsphere is used along with application of a small magnetic force (1 pN) by positioning a permanent magnet above the flow cell.[38,40] A laminar flow of aqueous buffer is applied above the surface to exert a drag force on the bead, which in turn causes the DNA molecules to stretch. DNA molecules are stretched by well-defined flow forces, ranging from 0.1 to 10 pN, which are proportional to the flow rate and the diameter of the bead.[39]

A dsDNA substrate with a length of 15−50 kbp is typically used.[41] Changes in the lengths of DNA molecules are determined through tracking the bead position over time via dark field microscopy. At low stretching forces (<6 pN), ssDNA coils up and is shorter than dsDNA.[38,40,42] Unwinding of dsDNA into ssDNA can be monitored by the change in DNA length at a constant force. For example, in a helicase-based unwinding assay, the number of nucleotides that are unwound can be determined using the known difference in lengths between ssDNA and dsDNA for the experimental flow conditions.

As an alternative strategy, the viscous drag of the laminar flow of buffer on the tethered DNA in the absence of any attached bead can be utilized to stretch it.[43,44] In this configuration, the stretching forces experienced by different regions of the DNA molecule segments are significantly different, and the DNA portion nearest to the point of tethering experiences the maximum stretching force. dsDNA molecules can be visualized by means of intercalating dyes such as YOYO. The flow can be continuously employed to extend

DOI: 10.1021/acs.chemrev.9b00361
Chem. Rev. 2020, 120, 36−78

DNA molecules. An advanced version of this strategy, referred to as "DNA curtains",[45] uses a combination of nanofabricated surface patterns, lipid bilayers, and hydrodynamic force to align thousands of DNA molecules into a defined pattern on a flow cell surface for single-molecule visualization. A lipid bilayer coating the surface of a microfluidic sample chamber provides an inert environment for a range of biological macromolecules. DNA molecules are tethered on one end to the bilayer via a biotin−streptavidin linkage which allows the DNA to diffuse laterally. Hydrodynamic force aligns the DNA along nanofabricated barriers that disrupt lipid diffusion. Different barrier patterns enable the DNA to be anchored in various configurations.[45−48] Singly tethered DNA curtains, such as the ones described above, require continuous buffer flow and disappear from view when the flow is turned off. An absence of constant buffer flow is preferred for experiments involving expensive reagents, protein−DNA interactions which can be perturbed by hydrodynamic force, or visualization of protein translocation along DNA. In such cases, doubly tethered DNA curtains or "DNA racks", designed for imaging DNA across its full contour length in the absence of buffer flow,[46] are useful. These "DNA racks" are accomplished by anchoring one end of the DNA through biotin−streptavidin linkage. The other end of the DNA is labeled with a different tag, typically DIG, such that it binds to antibody coated barriers on the other end of the chamber, allowing the DNA molecules to remain stretched out parallel to the surface, even when buffer flow is terminated. ssDNA curtains can also be prepared to capture molecular events in which ssDNA is a key intermediate, such as replication and DNA repair.[49−51]

Although these assays have a lower spatial resolution (on the order of 100 bp),[39] simultaneous observation of multiple reactions is feasible. The high-throughput imaging is favorable for detection of rare events associated with multicomponent protein reactions.

2.3. Single-Molecule Imaging *in Vivo*

In vivo single-molecule imaging permits the study of protein−nucleic acid interactions in a cellular environment where proteins exist in dense populations. *In vitro* single-molecule experiments have contributed significantly to our understanding of protein−DNA interactions based on detailed mechanistic studies using purified proteins and DNA oligonucleotides. However, the majority of these experiments are performed under conditions that are not representative of the physiological environment in terms of salt conditions, pH, crowding, DNA conformation, etc.; thus, *in vivo* studies must also be carried out.

The development of various super-resolution microscopy methods has enabled the imaging of subcellular spatial organization of proteins in the cell with unprecedented resolution.[52−55] The protein of interest either is labeled with photoswitchable/photoactivatable fluorescent proteins[56] or is tagged using proteins (such as Snap-Tag or Halo-Tag) which facilitate bio-orthogonal labeling with dyes added exogenously.[27,28] One has to keep in mind that such modifications to the protein could alter protein functions or cellular localization of the protein[57] and therefore appropriate control experiments are necessary. The intensity profile of the emission spot of individual fluorophores attached to the protein, known as the point spread function (PSF), is typically fit to a Gaussian function.[58] The peak position of the Gaussian profile provides the protein location with a resolution of 10−50 nm.[59] The localizations of several molecules imaged over an extended period of time can be reconstructed to obtain the spatial map of the protein. The number of "on" fluorescent molecules being imaged at any given time should ideally remain low enough to avoid overlapping PSFs and incorrect determination of protein position. Multicolor super-resolution methods have made it possible to study the spatial organization of different proteins relative to each other.[60−63] Single-molecule imaging *in vivo* can also be used to quantify the copy number of proteins within the cell.[64−69]

Single particle tracking with photoactivation localization microscopy (spt-PALM) enables the positions of molecules to be followed over several frames in order to form trajectories.[70] Trajectories of DNA binding proteins can provide direct observation of protein binding to DNA and insight into their diffusion dynamics. However, robust inference of different diffusive subpopulations from collected single-molecule trajectories is challenging. A variety of single particle tracking techniques are available that facilitate extracting desired information from these trajectories. A systematic evaluation of the performance of commonly used trajectory analysis tools is provided by Hansen et al.[71] and Chenouard et al.,[72] allowing users to decide the tool which is appropriate for their experimental conditions. The dwell times of proteins on DNA obtained from the trajectories can be used to estimate the rates of enzymatic reaction between the protein and DNA. The rates of DNA binding can also shed light on the different mechanisms by which proteins find their targets in the nucleoid region.

The usage of *in vivo* single particle tracking for studying spatial organization and diffusion dynamics of DNA motors has been limited. We have included relevant examples of such studies in the following sections. For readers interested in learning more about super-resolution imaging *in vivo*, a recent review article by Sahl et al. is a useful resource.[73]

2.4. Tethered Particle Motion

Tethered particle motion (TPM) is a single-molecule technique measuring the amplitude changes of two-dimensional Brownian motion of a bead in solution, tethered to a surface via nucleic acids. The changes in the effective length of nucleic acids (the tether), caused by protein−nucleic acid interactions, would lead to corresponding proportional changes in the amplitude of the Brownian motion of the tethered bead. The amplitude changes of the tethered bead are calculated by the root-mean-square of the two-dimensional projection of the bead positions with respect to the tethered point (ρ_{RMS}), as shown below

$$\rho_{RMS} = \sqrt{\langle (X - \overline{X_t})^2 + (Y - \overline{Y_t})^2 \rangle}$$

where X and Y are the coordinates of the tethered bead center at each frame and $\overline{X_t}$ and $\overline{Y_t}$ are the average of X and Y within a time interval, t. When the bead is tethered with a linear polymer such as DNA, the value of ρ_{RMS} proportionally increases with increasing length of the attached polymer. With precalibration of the system, one can extract the increase or decrease in effective lengths of nucleic acid, mediated by DNA motor proteins.

The experimental schemes of TPM are varied and depend on the studied system. For example, the DNA motor of interest can be specifically tethered to the bead through antibody−antigen interaction, while the nucleic acid substrate is immobilized through biotin−avidin interactions. TPM can be

DOI: 10.1021/acs.chemrev.9b00361
Chem. Rev. 2020, 120, 36−78

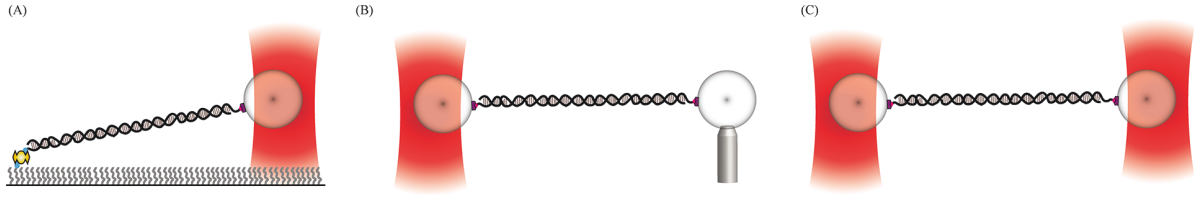

Figure 3. Different optical tweezers configurations used in single-molecule studies. (A) Single-trap configuration: one end of the tether is attached to a dielectric bead through a linker or a handle. The other end of the tether is anchored onto the polymer-passivated surface. (B) Single-trap configuration: Unlike the configuration in part A, the other tethered end is linked to another dielectric bead which is held by a glass micropipette. (C) Dual-trap configuration: two dielectric beads are trapped by two trapping laser beams.

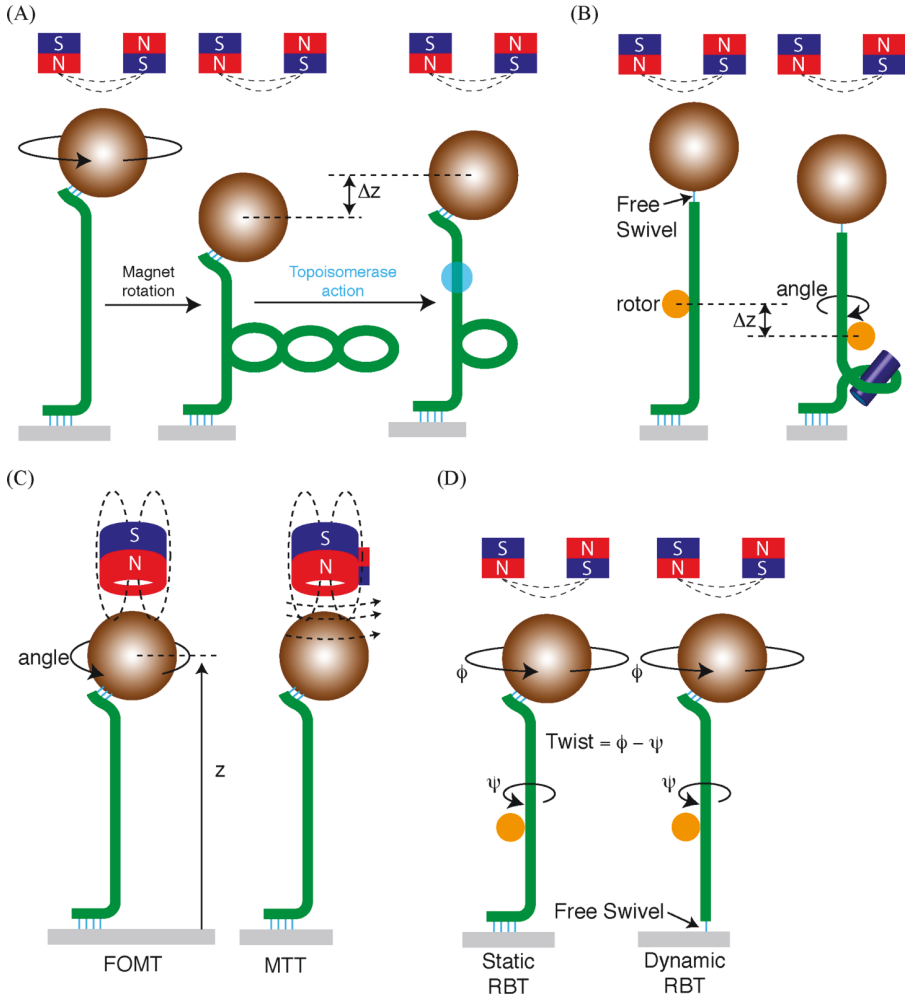

Figure 4. (A) In conventional MTs, magnetic field lines are perpendicular to the DNA axis. This tightly constrains the angular rotations of the bead while exerting an upward pulling force. Rotating the magnets introduces torque. When torque buildup is greater than the bucking torque, plectonemed structures form that lead to the bead being pulled toward the coverslip. Enzyme action, such as the action of topoisomerases or polymerases, can relax or further supercoil the DNA, leading to changes in the bead height. Height changes can be calibrated to reflect ΔLk introduced into the DNA by enzyme action. (B) In RBT, rotations and extensions of DNA produced by the action of DNA binding proteins (blue cylinder) can be decoupled. A free swivel allows for the relaxation of writhe, while direct 3D tracking of the rotor permits independent measurements of extension and angle. (C) In FOMTs, the field lines are parallel to the DNA axis, thereby permitting free rotation of the magnetic bead about the DNA axis. Addition of a weak horizontal component to the field via permanent magnets in MTTs or electromagnets in EMTTs leads to a soft angular constraint while maintaining the strong upward pulling force. The weak angular constraint allows for reasonably large angular deflections that can be measured to calibrate torque. (d) In static RBT, torque is directly introduced via the rotation of the magnetic bead and calculated based on precalibration of the DNA segment between the rotor and the magnetic bead. In dynamic RBT, the magnetic bead is spun and a feedback algorithm maintains a fixed twist in the upper DNA segment. Hydrodynamic drag on the rotor generates torque, which can be calibrated by measuring its angular velocity.

used to study a wide range of biological interactions that involve changes in the end-to-end length of a tethered nucleic acid substrate, such as DNA binding and looping with transcription factors,[74−76] protein synthesis,[77] DNA super-

DOI: 10.1021/acs.chemrev.9b00361
Chem. Rev. 2020, 120, 36−78

coiling by gyrase,[78] recombinase activities,[79−81] transcription by RNA polymerase,[82] and helicase-catalyzed DNA unwinding and translocation.[83,84] Recent developments on TPM by Plénat et al. have increased the throughput of the assay, up to hundreds of single molecules in a single field of view.[85] Moreover, combining TPM with other imaging techniques (fluorescence and TIRF microscopies) to expand its applications has been demonstrated.[86,87] Generally speaking, TPM has a spatial resolution of 10−15 nm (60−70 bp) and is sensitive to the tether length changes when the immobilized tethers are between 100 and 4000 bp.[88] The main limitation in the temporal resolution of TPM arises from the time required for a tethered bead to adequately explore the available hemisphere of motion. Hence, the size of the used bead and the length of the immobilized tether affect the temporal resolution.[89]

2.5. Optical Tweezers

Ashkin first demonstrated single-beam optical tweezers (or optical trap) in 1986 which became an enormously successful and popular technique for various biological and soft condensed matter physics studies. Optical tweezers can trap a small particle, typically close to the wavelength of the light used, near the center of a sharply focused laser beam.[90] There are two components to the force exerted by a focused laser light on a trapped bead. The scattering force (owing to light absorption and reflection) is in the direction of propagation of the laser and pushes the bead away from the focus. The gradient force (due to refraction) pulls the bead toward the region of strong electric field (i.e., focus) and is proportional to the gradient of the electric field and the polarizability of the bead.

An external electric field $\boldsymbol{E}$ induces a dipole moment $\boldsymbol{\mu} = a\boldsymbol{E}$ on a dielectric particle with polarizability a. This dipole experiences a force given by $\boldsymbol{F}_{\text{gradient}} = -\nabla U = -\nabla(-\boldsymbol{\mu}\cdot\boldsymbol{E}) = -\nabla(-a\boldsymbol{E}^2) = a\nabla|\boldsymbol{E}|^2$, where U is the potential energy of the dipole. This force is called the gradient force, and as it is directed to the region of the space that has the highest electric field magnitude, it tends to draw the particle into the center of the focused laser beam. In order to trap the bead, the gradient force along the axial direction must be large enough to equal the scattering force. This requires a fairly high gradient, possible only when light is tightly focused using a high-NA (numerical aperture) objective. If an external force is applied to the bead, it will be displaced from the trap center until the external force cancels out the restoring force of the trap. For small displacements, the optical trap can be considered as a Hookean spring, in that the restoring force $\boldsymbol{F}$ is linearly proportional to the displacement Δx, $\boldsymbol{F} = -k\Delta x$, where k is the spring constant or stiffness of the trap, often expressed in units of pN/nm. As a result, by measuring Δx, one can obtain the trapping force $\boldsymbol{F}$ as well.

Optical tweezers have been widely used to reveal biophysical properties and provide mechanistic insights into DNA−protein interactions such as the wrapping of DNA around histones.[91−95] In a typical optical trapping experiment, one end of the molecule of interest is attached through a linker or a handle to a dielectric bead which is trapped by a high-power laser beam. A near-infrared wavelength (830, 980, 1064 nm) laser source is used to minimize heating and reduce laser-induced damage to the trapped biomolecule. The other end of the molecule of interest is anchored onto a glass slide/coverslip surface (single-trap configuration, Figure 3A) or attached to another dielectric bead held in a micropipette (single-trap configuration, Figure 3B) or a second trapping laser beam (dual-trap configuration, Figure 3C). By gradually moving the surface (single-beam configuration) or one of the trapped beads (dual-beam configuration) away from the other trapped bead, increasing tension can be applied to the nucleoprotein complex. State-of-the-art optical trapping provides a spatio-temporal resolution down to 0.1 nm on the second time scale.[96−98] The combination of optical trapping with fluorescence microscopy has added an extra layer of molecular information (see section 2.9, Hybrid Single-Molecule Techniques, below). The high sensitivity in force and displacement measurements and the versatility of coupling it with other detection modalities have made optical tweezers a powerful platform to study molecular mechanisms. However, one of the major limitations of this assay is its low throughput.

2.6. Magnetic Tweezers

Magnetic tweezers (MTs) employ magnets to apply forces and torques on biomolecules tethered to magnetic particles in various geometries.[99] Conventional MTs apply tension on tethered molecules such as DNA while constraining the angle of the magnetic bead. Z-Tracking of the magnetic bead reports changes in DNA extension. Rotations introduced into torsionally constrained DNA are partitioned into twist and writhe, the latter being coupled to extension changes (Figure 4A). For example, this coupling has been exploited by Koster et al. to study DNA relaxation by topoisomerases[100] and by Strick and co-workers to study DNA scrunching by RNA polymerase.[101] Two recent improvements—enhanced rotor bead tracking (RBT) and freely orbiting magnetic tweezers (FOMTs)[102,103]—decouple extension changes from rotations. In RBT (Figure 4B), a large magnetic bead applies tension to torsionally unconstrained DNA, while evanescent darkfield 3D tracking of a separate, smaller bead (or an even smaller gold particle in AuRBT[104]) attached off center to the side of the stretched DNA molecule serves as a direct readout of extension and rotation. The small size of the rotor allows for high spatiotemporal resolution. RBT has been used to map out the mechanochemical pathway of DNA gyrase and to study how ATPase substeps drive specific structural changes.[103,105] In FOMTs (Figure 4C), the magnetic field is aligned parallel to the DNA axis, thereby permitting free rotation of the magnetic bead. Force application, as well as readouts of 3D position, are relegated to the single, large magnetic bead, at the cost of reduced spatiotemporal resolution. FOMTs have been used to measure the torsional stiffness of DNA by observing angular fluctuations at various tensions and to follow the assembly of RecA filaments on DNA.[102]

MTs, along with optical tweezers, have also made possible the application and measurements of torque on single biological molecules. The large torsional stiffness of conventional MTs makes it impractical to measure tiny angular displacements of the bead and thus to measure torque. Magnetic torque tweezers (MTTs) (Figure 4C)[106] and electromagnetic torque tweezers (EMTTs)[107] use magnetic fields aligned parallel to the DNA axis to provide a large pulling force but also incorporate a soft component perpendicular to the DNA axis in order to measure torques. Static and dynamic RBT (Figure 4D) rely on measuring torque by observing the angular position or velocity, respectively, of the off-center rotor bead.[108]

DOI: 10.1021/acs.chemrev.9b00361
Chem. Rev. 2020, 120, 36−78

MTs have also been successfully combined with other orthogonal techniques to increase the number of observables in single-molecule experiments. Conventional MTs have been combined with total internal reflection fluorescence (TIRF) microscopy to provide simultaneous single-molecule visualization and mechanical manipulation,[109−113] while fluorescence-RBT (FluoRBT) combines RBT with smFRET, in order to correlate DNA extension and compaction with structural changes.[114]

As the magnetic field is uniform over a large area, MTs can be successfully implemented in high-throughput single-molecule methods. De Vlaminck et al. have recently developed a highly parallel MT instrument to pull on a tethered array of hundreds of DNA molecules.[115] Basu et al. recently applied MTs to simultaneously pull on hundreds of mechanotransduction ion channels in the entire sacculus from the inner ear of bullfrogs.[116] By combining it with electrical measurements of ion flow through the tissue, they showed direct evidence for a long-standing hypothesis in the field of hearing—that tension on specific protein filaments, called tip-links, gates the opening of mechanotransduction ion channels in hair cells of the inner ear.

2.7. Atomic Force Microscopy (AFM)

AFM is another useful technique for single-molecule imaging and manipulation. An atomically sharp tip is attached to a cantilever to measure the surface topography of a sample. Due to the high stiffness of the cantilever, AFM is suitable for applications where forces range from 10 to 10,000 pN.

For protein−DNA interactions and other biological studies, AFM imaging is typically performed in the "tapping mode" where a probe tip at the end of an oscillating cantilever scans the surface.[117,118] In addition to measuring surface interactions with increased sensitivity, tapping mode causes less damage to the biological sample and allows for longer duration visualizations.[119] The development of reliable methods for imaging DNA has led to the application of AFM to study protein−DNA interactions. Protein binding can induce DNA bending or other structural changes in DNA. AFM images can distinguish different DNA structures through their twists and linking number.[120−123] Images of protein−DNA complexes appear as blobs and have been characterized by AFM in terms of DNA bending.[124−128] Single-stranded and double-stranded DNA can be distinguished by their imaging height which allows for visualization of unwinding products of helicases.[129] AFM can also report on the oligomeric state of a protein−DNA complex. The approximate molecular masses of protein complexes can be determined from the measured volume of the generated three-dimensional topological images, by calibrating them against proteins of known molecular mass.[130]

The last few decades have seen major developments in this technique such as the introduction of smaller cantilevers and improvements in image acquisition rate.[131] High-speed AFM offers time resolutions on the orders of seconds to subseconds which have been used to follow DNA−protein interactions.[132] Different modes of target search such as sliding, hopping, and intersegmental transfer, adopted by DNA binding proteins, have been visualized using high-speed AFM.[133−135] Specific target sites such as lesions or bubbles can be introduced into DNA fragments to study protein−DNA interactions necessary for DNA repair.[136]

In addition to its high (subnanometer) resolution, AFM involves relatively simple and fast sample preparation. The technique is however limited in terms of its throughput and force resolution. The range of biological questions that can be answered with this technique is also limited, due to the associated difficulty of studying real-time enzyme kinetics.

2.8. Nanopore Tweezers

Another class of single-molecule measurement technologies that predates all techniques discussed so far is electronic recording, initially pioneered for studying ion channels. When a channel protein in a membrane opens, ions flow through the channel's pore under the influence of an external electric field. If a membrane protein with a large pore is chosen, single-stranded DNA can be selectively induced to go through the pore, thereby blocking ion currents. The magnitude of ion current through the pore changes in a manner dependent on the sequence of DNA at the narrowest region of the pore. Sequencing of DNA by measuring the ion current as it traverses such a nanopore has been sought after since the 1990s. Early attempts used α-hemolysin as the pore-forming protein, but its narrowest constriction spans about a dozen nucleotides in length, making it unsuitable for obtaining sequence information at single nucleotide resolution.[137−139] A different pore-forming protein, called MspA, has a short, narrower constriction of about 2−3 nucleotides long and finally enabled DNA sequencing.[140,141] Another important innovation was the use of a DNA motor protein to feed DNA at a measured pace, typically hundreds of nucleotides per second. Without a motor protein, a DNA molecule goes through the nanopore too quickly to yield meaningful sequence information. Earlier efforts used DNA polymerases as motor proteins, but their frequent backsteps due to their exonuclease activity prevented accurate DNA sequencing.[142,143] Instead, DNA helicases are widely used for nanopore sequencing.[5] The exquisite temporal and subnucleotide spatial resolution of nanopore sequencing makes it suitable to use single nanopore recordings to study the biophysics of motor proteins themselves, as we will discuss in the SF2 helicase section (section 3.1) below. Nanopore tweezers experiments can be performed with an inexpensive hardware setup while monitoring the passage of DNA through motor proteins with a spatial resolution of ∼40 pm. The interpretation of data obtained from the nanopore setup is often the most challenging part.

2.9. Hybrid Single-Molecule Techniques

Single-molecule experiments typically only measure one dynamic observable such as the distance between two points in smFRET or DNA extension in optical tweezers. As we study more complex systems with multiple components to better mimic physiological conditions, it is no longer sufficient to measure just one observable. smFRET can be extended to three[144] and four colors[145] to obtain information on three and six sets of distances, respectively. Colocalization of fluorescently labeled proteins on DNA using multicolor imaging reveals factor-dependent transcription dynamics and replication initiation.[146,147] Instruments that combine fluorescence measurements and mechanical manipulations can be used to probe single-molecule conformational changes using smFRET, as a function of force applied via optical tweezers or magnetic tweezers.[91,148−153] Such "*fl*eezers = *fl*uorescence + tweezers" experiments can be extended to ultrahigh resolution by employing dual optical traps for mechanical measurements of DNA−helicase interactions at the single base pair resolution (Figure 5).[154−158] Magnetic tweezers have also been combined

DOI: 10.1021/acs.chemrev.9b00361
Chem. Rev. 2020, 120, 36−78

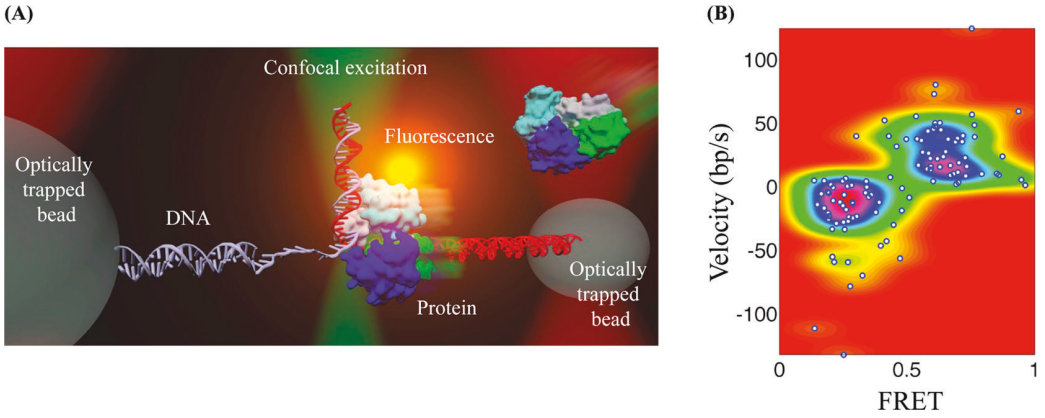

Figure 5. Ultrahigh-resolution optical tweezers with single fluorophore sensitivity. (A) Dual optical traps apply forces to a DNA connecting the beads and detect DNA length changes induced by the enzymatic activity of DNA unzipping by a protein at ~0.1 nm resolution. At the same time, confocal fluorescence excitation and detection can measure the protein's structural changes. (B) Correlation between DNA unzipping activity, measured by optical tweezers and expressed in reaction velocity (bp/s), and protein structural changes, measured by smFRET. Adapted with permission from ref 155. Copyright 2015 The American Association for the Advancement of Science.

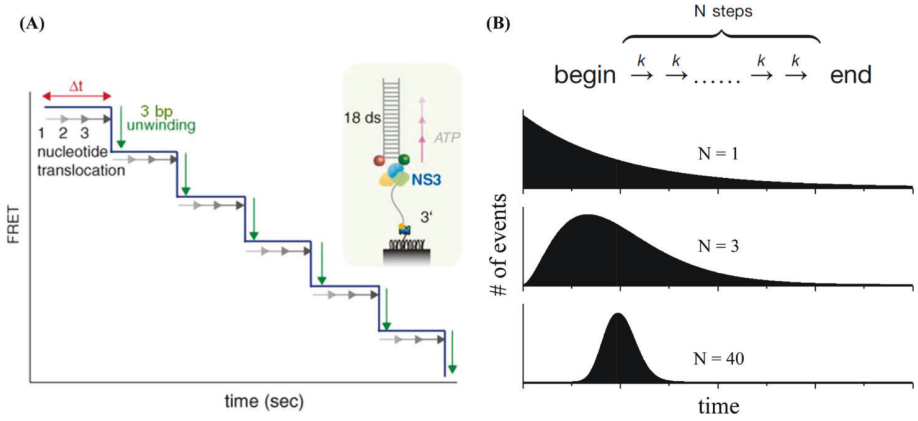

Figure 6. (A) Schematics of NS3 helicase unwinding in 3 bp steps measured via smFRET. As the helicase unwinds the DNA, the donor and the acceptor, green and red spheres in the inset, become further separated, giving rise to stepwise decreases in FRET efficiency. Each dwell appears to consist of three hidden steps. (B) If each step is made of N hidden steps with equal stepping rates of k, the dwell time histogram for these steps should follow a gamma distribution. Three examples of N = 1, 3, and 40 are shown.

with TIRF (MT-TIRF)[110] to enable mechanical manipulation and fluorescence detection. Rotor bead tracking (RBT), which permits direct observation of DNA twisting and extension by observing the angular and z positions of a probe attached to the side of a magnetically stretched DNA molecule, has also been combined with smFRET (fluo-RBT[114]). Fluo-RBT can report on protein conformations together with DNA rotation and extension measurements and manipulations in nucleoprotein complexes. If the density of fluorescently labeled proteins on DNA is too high for single-molecule detection, stimulated emission depletion microscopy can be combined with DNA mechanical manipulation.[159]

3. DNA MOTOR PROTEINS

3.1. Helicases

Helicases are motor proteins that unwind double-stranded nucleic acids. For genome duplication or mismatch repairs to occur, double-stranded DNA (dsDNA) formed via Watson–Crick base pairing must be separated into single strands. Similarly, double-stranded RNA is frequently separated into single strands for transcription, splicing, ribosome biogenesis, and translation. Such nucleic acid unwinding should not occur indiscriminately, and our genome encodes more than 200 helicases that function in highly specialized pathways. Defects in helicases or their misregulation can cause serious human genetic diseases including cancer and premature aging. Helicase-catalyzed unwinding produces a transient intermediate of single strands that become substrates for a variety of metabolic processes. Traditional biochemical assays that examine all-or-none reaction outcomes are blind to these critical intermediates. In addition, many of the said reactions cannot be easily synchronized, making ensemble kinetic analysis inapplicable. However, single-molecule measurements can detect rare intermediates and multiple reaction pathways. Before we discuss specific helicases, we first highlight some of the most generalizable characteristics of helicases that were revealed by single-molecule studies.

3.1.1. Passive vs Active Helicases. The helix–coil transition from dsDNA to entropically disordered ssDNA can be achieved through thermal fluctuations alone if the temperature is sufficiently high. Even at ambient temperatures, terminal base pairs in a duplex DNA can melt spontaneously and reform. Based on the ability of helicases to exploit such fluctuations, they can be classified as passive vs active.[160] A

DOI: 10.1021/acs.chemrev.9b00361
Chem. Rev. 2020, 120, 36–78

purely passive helicase would wait until thermal fluctuations melt base pairs at the ss−dsDNA (single-stranded−double-stranded DNA) junction and then translocate forward to capture one of the unwound strands. In contrast, a purely active helicase would melt the duplex at its own rate and would unwind DNA at the same speed as its translocation on ssDNA. Generally speaking, a passive helicase would slow down if the GC content is high or speed up if an external force is applied to favor the unzipped.

3.1.2. Hierarchy of Steps. It is widely accepted that nonhexameric helicases moving along single-stranded DNA consume one ATP per nucleotide translocated.[161] A prior model, based in part on structural analysis, posited that one base pair of DNA is unwound each time a helicase translocates by one nucleotide.[162,163] This model was challenged by single-molecule data showing that hepatitis C virus NS3 helicase unwinds DNA in 3 bp steps[6] (Figure 6A). The histogram of the dwell time Δt of these steps was not exponentially distributed, as would be expected if there is a single rate-limiting step for 3 bp unwinding. Instead, the data could be best described using a gamma distribution $\Delta t^{N-1}e^{-k\Delta t}$ with a defined stepping rate of k where $N = 3$, suggesting that there are irreversible hidden steps before 3 bp unwinding, likely due to 1 bp movement per ATP consumed (Figure 6B). Subsequent single-molecule experiments provided evidence that T7 gp4 helicase unwinds DNA in 2−3 bp steps[7] and that yeast Rrp44 exoribonuclease unwinds RNA duplex in about 4 bp steps, despite the fact that it digests RNA in single nucleotide steps.[8] Most recently, the Chemla group has also obtained evidence that *E. coli* UvrD helicase unwinds DNA in 3−4 bp steps[9] and the Joo lab showed that CRISPR/Cas3 helicase unwinds DNA in 3 bp bursts which contain three hidden steps.[10] Together with 2.5 and 10 bp steps observed in viral DNA packaging by the Bustamante lab,[11] these results showed a surprisingly complex picture where a protein can accumulate elastic energy from multiple reactions and release the energy in a large burst once a threshold is exceeded. Such a mechanism may allow helicases to overcome a large energetic barrier, for example, a protein roadblock on DNA, which cannot be overcome using the chemical energy of one ATP hydrolysis event alone.

3.1.3. Regulation Mechanisms. If helicases unwind every nucleic acid they encounter, unregulated generation of single strands can be toxic to the cell. How is the unwinding activity regulated? Can we unleash potent helicase activities that are normally suppressed based on our understanding of helicase regulation? In an attempt to identify the functionally active conformation of *E. coli* Rep helicase, it was discovered that once it is intramolecularly cross-linked in a closed conformation—termed "Rep-X"—it becomes a "superhelicase" that unwinds thousands of base pairs without falling off, even against strong opposing forces.[164] In contrast, a wild type Rep monomer has undetectable unwinding activity. Why, then, does the open conformation exist? Using ultrahigh-resolution optical trapping combined with single fluorophore sensitivity[154] and doubly labeled UvrD, a related helicase, to distinguish between different conformations through FRET,[165] it was shown that UvrD adopts a closed form during unwinding but, after unwinding about a dozen base pairs, switches to the open conformation and reverses direction to allow DNA rezipping in its wake.[155] Overall, these studies revealed a novel mechanism of helicase regulation.

3.1.4. Other Activities of Helicases. In addition to unwinding double-stranded DNA, helicases show a variety of activities that may be important for their function in DNA repair and replication. These include DNA rewinding,[166] unwinding of G-quadruplexes,[167−169] branch migration of the four-way DNA (Holliday) junctions,[166,170−172] and slippage.[173−175] Single-molecule force measurements identified active, i.e., not due to passive reannealing, rewinding properties of RecG and UvsW helicases that help overcome stalled replication forks when combined with DNA unwinding and protein displacement.[166] Double-stranded DNA translocation activities of helicases and helicase-like enzymes can drive directional branch migration of the Holliday junction,[176−178] likely through rectifying spontaneous branch migration that has been detected at single base pair resolution.[166,170−172,179] While unwinding dsDNA, helicases can sometimes lose grip and slide backward which is termed as "slippage".[180] Single-molecule studies on T7 helicase unwinding showed that processive unwinding is interspersed with repeated slippage events.[173] Effects of slippage of replicative helicases from T7 and T4 phages on DNA replication have also been studied using magnetic and optical tweezers.[174,175]

Below, we describe some of the recent single-molecule studies of representative helicases from different superfamilies (SFs). SF1 and SF2 are monomeric, but some require more than one protein molecule (dimer or more) for detectable nucleic acid unwinding activity. SF3, SF4, SF5, and SF6 are ring-shaped enzymes that are typically hexameric.

3.1.5. Superfamily 1 (SF1). Members of the SF1 helicase family share a common structural organization consisting of four subdomains: two highly conserved RecA-like motor subdomains, 1A and 2A, and the accessory domains, 1B and 2B.[162,163,181−183] SF1A helicases translocate and unwind dsDNA in the 3′−5′ direction, whereas SF1B helicases such as Upf1[184,185] have the opposite directionality.

Rep. In *E. coli*, Rep is involved in DNA repair, DNA replication, and alleviating stalled replication.[186−188] *In vivo* single-molecule imaging of Rep has shown that it colocalizes with nearly 70% of all replication forks in *E. coli*.[189] Like other SF1 helicases, it is composed of four subdomains: 1A, 1B, 2A, and 2B. The 2B subdomain can swivel about a hinge connecting the 2A and 2B subdomains to transition between two extreme conformations, the "open" and "closed" states.[182,190] Rep is monomeric in solution and can serve as a processive ssDNA translocase with no detectable unwinding activity.[191−194] Processive unwinding activity is demonstrated by Rep, only as dimers/oligomers.[191,193,194] Previous studies have implicated the 2B subdomain as a regulatory domain for unwinding activity.[191,192] The 2B domain deleted variant, RepΔ2B, primarily exists as a monomer and is a faster ssDNA translocase and helicase compared to wild type Rep.[156,191,192] Arslan et al. engineered a Rep variant where intramolecular cross-linking of the 2B subdomain locks the helicase in a closed state which turns out to be the unwinding active form.[164] They used smFRET and optical tweezers assays to show that this superhelicase version of Rep, termed "Rep-X", is capable of unwinding thousands of base pairs with very high processivity as a monomer.[164] In contrast, cross-linked Rep in an open state exhibited little unwinding activity, comparable to wild type.[164] As a whole, these studies suggest that the activity of Rep is determined by its conformational state, mediated by the rotation of the 2B subdomain. The closed state activates Rep

DOI: 10.1021/acs.chemrev.9b00361
Chem. Rev. 2020, 120, 36−78

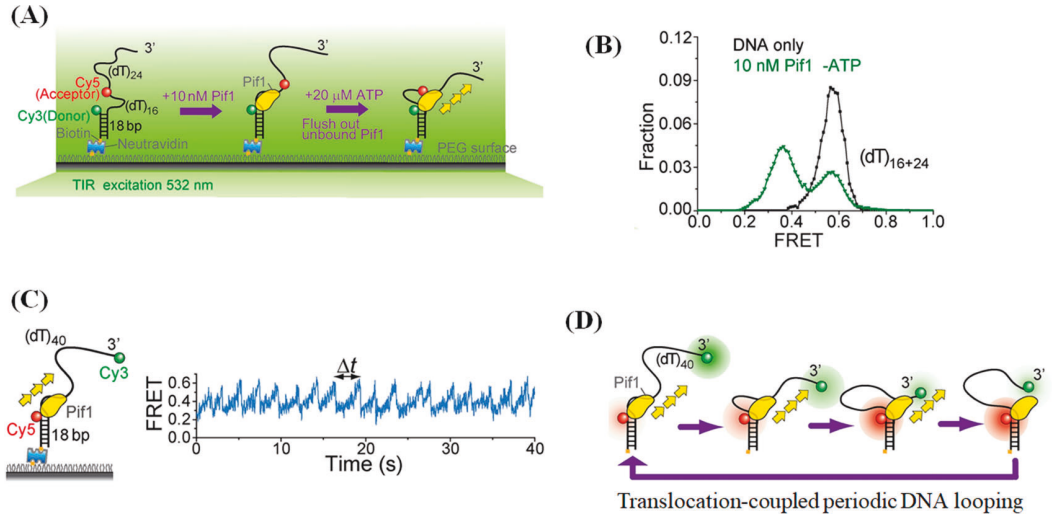

Figure 7. Repetitive ssDNA looping of Pif1 monomer.[167] (A) A cartoon representation of experimental conditions for smFRET measurements of monomeric Pif1. (B) In the absence of ATP, monomeric Pif1 binds to DNA, which is observed by the appearance of a lower FRET peak. (C) Representative smFRET trace showing repetitive ssDNA looping induced by a single molecule of Pif1. Δt denotes the time interval of each looping cycle, which is dependent on ATP concentration. Note: The labeling positions in part C are different than those in parts A and B. (D) Proposed mechanism of how a Pif1 monomer stations itself at the 3′ ss−dsDNA junction and uses its ssDNA translocation activity to repetitively reel in the 3′ ssDNA overhang.

for processive unwinding, while the open state has negligible unwinding properties.

Recent studies using an optical tweezers assay showed that the unwinding activity of both RepΔ2B and wild type Rep, however, is limited by strand switching, during which Rep alternately switches between constituent strands of the duplex. Their measurements showed that the 2B domain is not essential for strand switching.[156] Apart from functioning as a helicase, Rep can remove proteins from DNA and this protein displacement activity requires the 2B subdomain.[186] smFRET studies have shown ATP-dependent pushing of SSB proteins on ssDNA by Rep.[195]

UvrD. UvrD is primarily involved in nucleotide excision repair and mismatch repair in *E. coli*.[196,197] Like the structurally similar Rep, UvrD translocates in the 3′ to 5′ direction on ssDNA as a monomer and unwinds dsDNA as a dimer.[161,198−202] Its ATP-dependent activities also include displacing RecA filaments from ssDNA[203,204] and pushing proteins along ssDNA.[195] The 2B domain of UvrD can exhibit "open" and "closed" conformations with respect to other domains.[162,165] Dual-labeling of UvrD enabled identification of different rotational conformers of UvrD and measurement of their interconversion rates.[205] It was found that the 2B domain of the UvrD monomer can populate two additional rotational conformations, between an extreme open and closed conformation. UvrD monomer displays helicase activity with very low processivity, unwinding only 10 base pairs or so.[155] The binding of a second UvrD to a UvrD monomer switches the 2B conformation of the incumbent UvrD to a more closed state, that promotes its helicase activity.[205] These results suggest that the closed conformation of UvrD is the helicase active state. During dsDNA unwinding, the 2B subdomain of UvrD is predominantly in a closed conformation, whereas, after unwinding a few base pairs, it changes to an open conformation and at the same time switches strands, translocating on the opposite strand and letting the DNA rezip in its wake.[155] This is consistent with a strand switching model proposed earlier.[206]

PcrA. B. stearothermophilus PcrA is another SF1 helicase that translocates with 3′−5′ directionality along ssDNA.[193,207,208] PcrA can unwind a duplex DNA that possesses a 3′ single-stranded tail. Monomeric PcrA translocates in the 3′ to 5′ direction on a DNA with a 5′ ssDNA tail while positioning itself on the ss−dsDNA junction, thereby repetitively reeling in the 5′ ssDNA tail.[209] This behavior was observed by repetitive cycles of a gradual increase in FRET as the donor and acceptor fluorophores on the ssDNA approach each other, followed by a decrease in FRET. A translocation step of 1 nt per ATP hydrolyzed has been measured for PcrA using biochemical studies[207] and confirmed later by single-molecule studies.[209]

As a nonreplicative helicase, roles of PcrA are not completely understood. Helicases translocating on ssDNA can serve to remove unwanted bound proteins. One of the possible functions of PcrA is the removal of RecA filaments at the replication fork as an anti-recombinase. smFRET showed that the repetitive reeling in activity of PcrA could induce displacement of preformed RecA filament from the 5′ tail, similar to UvrD.[204,209] PcrA's conformation during DNA looping was also determined using a dual labeled PcrA. PcrA monomer changes its conformation from closed to open state upon DNA binding and continues in an open conformation during ssDNA translocation while looping.[209] The unwinding activity of PcrA requires the formation of a closed conformation upon dimerization or oligomerization. PcrA could also be converted to a superhelicase, PcrA-X, through cross-linking into the closed conformation.[164]

Srs2. Srs2 is a SF1A helicase in *S. cerevisiae* that prevents homologous recombination by dismantling filaments of a recombinase protein called Rad51.[210,211] Recent single-molecule fluorescence studies shed light on the molecular mechanism by which Srs2 accomplishes this task. smFRET studies have shown that Srs2 undergoes repetitive translocation on short ssDNA near the ssDNA−duplex DNA junction.[212]

DOI: 10.1021/acs.chemrev.9b00361
Chem. Rev. 2020, 120, 36−78

This behavior may enable Srs2 to repeatedly remove Rad51 filaments. Single-molecule DNA curtain studies have shown that Srs2 loads itself onto DNA via replication protein A (RPA) clusters present at the ends of Rad51 filaments and forms a complex with RPA clusters to displace Rad51 from ssDNA.[213] Dismantling Rad51 filaments creates short tracts of naked ssDNA that are then filled by RPA. Srs2 translocates more rapidly on both naked ssDNA and RPA-coated ssDNA, exhibiting velocities of ∼460 and ∼170−190 nt/s, respectively, compared to the slower velocity seen on Rad51-coated ssDNA.[213,214] In combination, these studies propose a mechanism through which ATP-dependent translocase activity of Srs2 facilitates its role as an anti-recombinase.

Pif1. Helicases of the Pif1 family are multifunctional SF1B helicases, conserved from bacteria to humans.[215,216] Apart from unwinding double-stranded DNA, Pif1 plays critical roles in protein displacement from nucleic acids, unwinding of G-quadruplexes, chromatin remodeling, and inhibiting telomerase activity at telomeres.[161,183,216−221] Zhou et al. used smFRET techniques to extend our understanding of the DNA binding and unwinding properties of Pif1 (Figure 7). *S. cerevisiae* Pif1 monomer was shown to bind preferentially to 3′ ss−dsDNA junctions. Once bound, Pif1 monomer displays ATP-dependent repetitive DNA looping. Pif1 monomer unwinds RNA−DNA hybrids, but unwinding dsDNA requires multiple Pif1 units. The study characterized the unwinding properties of Pif1 with different DNA substrates including G-quadruplex and R-loops.[167] Pif1 unwinds G-quadruplexes in two to three distinct steps, consistent with intermediate structures made of two and three G-rich repeats.[167,222] Interestingly, Pif1 unfolds a G4 structure as a monomer but cannot do so for DNA duplexes.[167,222] smFRET studies have also revealed ATP-dependent protein displacement by Pif1. Translocating Pif1 pushes SSB toward the 3′ ssDNA end, followed by SSB dissociation from DNA.[195]

RecBCD. *E. coli* RecBCD is a dual helicase/nuclease necessary for recombinational repair of dsDNA breaks. It consists of two ATP-dependent helicase motors with opposite polarities: RecB translocating in the 3′−5′ direction on one strand and RecD translocating in the opposite direction on the other strand. Overall, the holoenzyme moves in the same direction along the dsDNA. RecC holds the complex together and recognizes the recombination hotspot, χ.[223] Upon encountering a χ recombination hotspot, RecBCD undergoes a conformational change resulting in decreased helicase activity and production of a long 3′ ssDNA for loading of RecA recombinase for homologous recombination.[224−227] RecBCD was the first helicase studied at the single-molecule level.[83,228] Earlier single-molecule studies using fluorescence microscopy enabled visualization of single RecBCD unwinding and degrading a single molecule of λ DNA that is optically trapped.[228] RecBCD is one of the fastest known helicases, unwinding DNA with an average velocity of ∼1500 bp/s.[229] Recent real-time imaging of RecBCD in live *E. coli* cells showed that RecBCD degrades DNA at a rate of ∼1600 bp/s, in strong agreement with *in vitro* measurements.[230] Although the unwinding speed was constant for each RecBCD molecule, the speed was highly heterogeneous among molecules in a population.[228] Liu et al. sought to understand this heterogeneity in unwinding rates in depth. Unwinding activity of individual RecBCD was halted temporarily by depletion of Mg^{2+}-ATP. The new distribution of rates upon reintroduction of Mg^{2+}-ATP recapitulated the original distribution of the entire population prior to depletion. Their study suggested that each RecBCD enzyme is capable of switching into different microstates that determine its unwinding rates.[229]

In vivo, RecBCD is expected to collide with other DNA binding proteins such as actively transcribing RNA polymerase, transcription factors, etc. Using DNA curtain assay, RecBCD was challenged with molecular roadblocks such as RNAP, EcoRI, lac repressor, and nucleosomes.[231] It was shown that, when RecBCD collided with the RNAP elongation complexes, RecBCD pushed most complexes away except for a small minority of cases where RecBCD was stalled or ejected. Similar observations were made for EcoRI and lac repressor.[231] How molecular crowding influences removal of tightly bound protein obstacles was also studied using DNA curtains. The translocation of RecBCD causes collision of each DNA-bound protein with its nearest neighboring bound protein, followed by the eviction of bound proteins.[232] RecBCD is able to displace protein-bound complexes, suggesting that it generates high forces. A recent optical tweezers assay measured the forces generated by RecBCD and its subunits as 25−40 pN as they translocate on the DNA.[233]

3.1.6. Superfamily 2 (SF2). SF2 helicases are similar to SF1s in that their core is composed of two RecA-like domains.[234] Most members of SF2 are however RNA helicases which are beyond the scope of this review. We nevertheless note that some of the SF2 RNA helicases do not function as a motor and instead work like a switch to melt short RNA duplexes through a single cycle of ATP hydrolysis.[235] RecQ family helicases are the most extensively studied SF2 DNA helicases at the single-molecule level[169,172,236−245] likely because mutations in human RecQ helicases such as BLM and WRN cause severe genetic diseases.[246] Other disease-linked human SF2 DNA helicases such as FANCJ and XPD have also been examined at the single-molecule level,[247−249] although they most likely exist as part of a large complex. Here, we highlight nanopore tweezers studies of Hel308 which represent the highest resolution measurements of any helicases thus far, revealing subnucleotide steps, and hepatitis C virus NS3 helicase studies that revealed a hierarchical stepping mechanism.

Hel308. In order to fully understand how helicases convert the chemical energy stored in ATP into mechanical energy, we need to detect the protein movement with sufficient spatial and temporal resolution to reveal all of the reaction intermediates. Although DNA unwinding has been measured down to single base pair resolution,[248,250] individual steps of ATP binding, hydrolysis, and productive release and how these individual chemical steps are coupled to the mechanical process of DNA translocation and unwinding are poorly understood. The Gundlach laboratory refined the nanopore technology, originally developed for single-molecule DNA sequencing, to improve its position accuracy down to about 50 pm (or 0.05 nm) for determining where single-stranded DNA (ssDNA) is relative to the pore of an engineered pore-forming protein MspA.[5] Because single-stranded DNA, fully stretched, would span about 0.65 nm per nucleotide, this approach, called SPRNT (single-molecule picometer-resolution nanopore tweezers), can in principle detect down to about 0.1 nm movement. In the initial application of SPRNT, it was discovered that Hel308, an SF2 helicase that translocates DNA in the 3′ to 5′ direction, moves two steps per nucleotide, one step having a duration independent of ATP concentration and the other ATP-dependent (Figure 8).[5] They then

DOI: 10.1021/acs.chemrev.9b00361
Chem. Rev. 2020, 120, 36−78

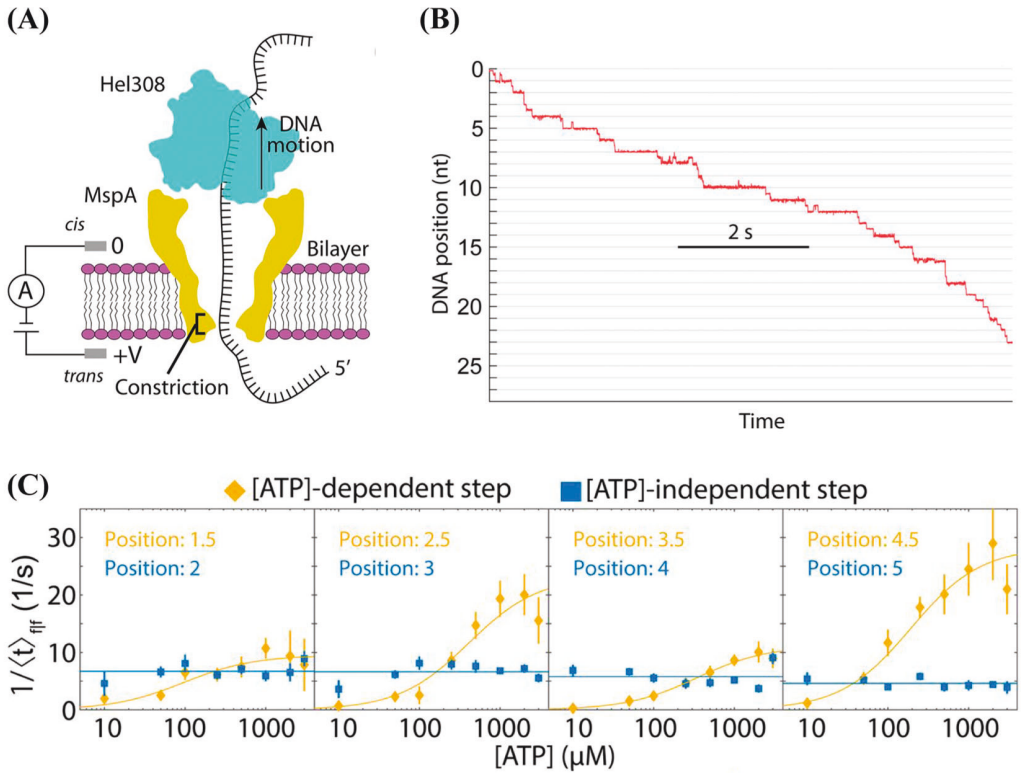

Figure 8. (A) Schematics of Hel308 helicase pulling ssDNA out of a nanopore using its 3′ to 5′ ssDNA translocation activity.[251] Voltage applied across the membrane induces ionic current through the pore, which is blocked to different degrees depending on the DNA sequence in the narrowest constriction in the pore. (B) DNA position in the pore as a function of time determined using SPRNT analysis. Two steps are observed per nucleotide. (C) Forward stepping rate as a function of ATP concentration for ATP-dependent and ATP-independent steps and their Michaelis−Menten fits. $\langle t \rangle_{flf}$ denotes the average dwell time before a forward step if the previous step was also a forward step. Data for four different DNA positions are shown with dramatically different Michaelis−Menten parameters.

measured the dwell times in the ATP-dependent and -independent steps as a function of Hel308 position on DNA and concentrations of ATP and ADP and discovered that the ATP-independent step is composed of additional hidden steps through gamma distribution analysis (see Figure 8).[251] In addition, maximum velocity and K_M were determined from the Michaelis−Menten kinetics fit. [ATP] dependence of apparent translocation rates varied up to an order of magnitude for different locations on the DNA (Figure 8C), suggesting that DNA sequence can have a profound impact on Hel308's motor function. Finally, pervasive backsteps were observed which also showed sequence dependence. Because SPRNT detects the sequences within the pore and in order to identify sequence features responsible for altered kinetics of helicase, the spacing between the pore and the relevant DNA section needs to be determined. A more recent study found that the nucleotides relevant to the sequence-dependent kinetics of Hel308 are located at 17 and 20 nucleotides relative to that of the nanopore constriction. Cytosine at the 20th position reduces backsteps, whereas an adenine at the same position increases backsteps.[252]

SPRNT has not been used for DNA unwinding studies because Hel308 is not very active in DNA unwinding, and future studies using highly active helicases such as engineered superhelicases Rep-X and PcrA-X may shed light on coupling mechanisms between DNA translocation and unwinding. Will unwinding occur with the same step size as translocation, or would multiple translocation steps be necessary before unwinding multiple base pairs in a burst? The same question may be addressed for hexameric helicases because coordination between different subunits within a ring helicase has not been studied in real time at high resolution. Another important question is how mechanical forces affect translocation and unwinding as well as backsteps and sequence dependence. DNA *in vivo* is likely under varying amounts of transient tension. Thus, in order to fully comprehend the mechano-chemical coupling between ATP hydrolysis and helicase movement on DNA, we need to measure these reaction rates as a function of force. It will also be exciting to combine SPRNT with single-molecule fluorescence detection so that the assembly state of the motor and its interaction partner proteins as well as their conformational changes can be measured simultaneously.

Hepatitis C Virus Nonstructural Protein 3 (HCV NS3, SF2). NS3 protein is a bifunctional enzyme encoded in the genome of HCV and a potential antiviral target in drug design against hepatitis C.[253,254] The N-terminal region of NS3 contributes to its protease activity when in complex with NS4A cofactor. The ATPase domain with 3′−5′ helicase activity is located at the C-terminal region of NS3, and the helicase activity can be modulated by the protease domain.[255,256] Like many other SF1 and SF2 helicases, the oligomerization of NS3 increases the unwinding processivity but a monomer of NS3 is sufficient to unwind double-stranded nucleic acids (dsNAs).[257,258] The helicase and serine protease activity are both vital to the replication and the assembly of HCV.[259] Besides being a

DOI: 10.1021/acs.chemrev.9b00361
Chem. Rev. 2020, 120, 36−78

valuable therapeutic target, NS3 helicase (NS3h) is also well-characterized and serves as a model helicase of SF2. As a member of the NS3/NPH-II family,[260] NS3h is composed of three domains, two Rec-A-like domains which provide the ATPase activity and an α-helical domain. Structural studies have shown that NS3h binds nucleic acids mostly through their phosphodiester backbones, which allow interaction with DNA or RNA substrate in a highly similar structural conformation but with different kinetic parameters.[261−263] NS3h translocates 3 times faster on ssRNA compared to ssDNA.[264] Single-molecule approaches have been used to study the unwinding activity of NS3h on DNA and RNA. A spring-loaded mechanism has been proposed based on smFRET analysis. In this model, NS3 unwinds dsDNA in 3 bp increments with three 1 bp hidden steps. The mechanical energy accumulated from several 1 nt per ATP steps triggers the NS3−DNA complex to unwind periodically in 3 bp bursts.[6] Repetitive unwinding is observed with a short dsDNA substrate. For dsRNA, NS3 has been observed to unwind 1 bp per ATP through optical trapping experiments.[250]

3.1.7. Superfamily 3−6 (SF3−6). Three of the superfamilies (SF3−6) are composed of ring-shaped hexameric DNA helicases, including SF3 (eukaryotic), DnaB-like SF4 (bacterial), and AAA+-like (ATPase associated with a variety of activities) SF6 (eukaryotic) helicases. In general, DNA ring-shaped hexameric helicases function at the replication fork and adopt either a RecA-like (SF4) or an AAA+ (SF3, SF6) fold in their monomeric structure.[265] The ring-shaped hexameric complex includes two facets, the N and C tiers. The N tier side is defined by the assembly of the N-terminal of monomeric subunits. The N tier can be facing the front and the rear during the movement on DNA. Besides the difference in translocation directionality (5′−3′ for RecA-like and 3′−5′ for AAA+ fold), the orientation of individual monomers within the quaternary structure of hexamers is different between the two types of ATPase folds.[266] The NTP binding sites are located at the interface between monomers, and the structural conformation of adjacent monomer modulates the NTPase activity of hexameric helicases. DNA binds to the central pore of hexameric helicases, most notably through the DNA binding loop.[267,268] Here are some examples of hexameric DNA helicases characterized by single-molecule assays:

Bovine Papillomavirus (BPV) E1 Helicase (SF3). The hexameric E1 helicase is the most conserved protein across the members of papillomavirus.[269] It recognizes and binds to the origin of DNA replication (ori) in a sequence-specific manner through the N-terminal dsDNA binding domain (DBD).[270] E1 travels from 3′ to 5′ with its N tier facing the direction of translocation. The current working model "staircase" based on an E1−ssDNA complex's crystal structure describes the translocation of E1 on ssDNA.[271] Sequential ATP hydrolysis around the staircase formed by six subunits leads to the detachment of the bottom subunit from DNA and rebinding to the topmost position which is six nucleotides away. Single-molecule studies have revealed the highly heterogeneous unwinding patterns by the E1 helicase core.[272] A repetitive unwinding pattern was also reported where E1 unwinds, backtracks, and then unwinds the same dsDNA repetitively. The presence of DBD made the unwinding reaction more monotonic and less heterogeneous.

T7 gp4 Helicase-Primase (SF4). The full-length bacteriophage T7 gp4 (gp4A) protein is a bifunctional enzyme which contains helicase and primase domains.[273] During the replication of bacteriophage T7, the gp4A proteins assemble as a ring-shaped hexamer on the lagging strand template and translocate in the 5′ to 3′ direction to unwind the parental DNA, fueled by deoxythymidine triphosphate (dTTP) which is preferred over ATP *in vitro*.[274] The T7 helicase unwinds DNA by strand-exclusion; only the lagging strand template can enter the helicase's central pore, and during its movement, the leading strand template is excluded, resulting in DNA unwinding.[275]

DNA unwinding speed was measured using optical tweezers in the presence of force applied in the unzipping direction.[173,276] The speed increased with increasing force or with decreasing GC content, both being a hallmark of a passive helicase. Comparison of the data to a mathematical model led to the proposed unwinding step size of about 2 base pairs,[276] which is consistent with the structures of gp40 and DnaB showing that each subunit contacts two nucleotides.[277,278] smFRET unwinding experiments detected step sizes of 2−3 base pairs, but dwell times in each step followed a gamma distribution with 2−3 hidden steps, therefore suggesting that the elementary unwinding step size of gp4 may be one base pair.[7] A related SF4 helicase DnaB was also proposed to take single base pair unwinding steps based on smFRET unwinding experiments.[279] How helicase translocation is coupled to DNA unwinding and what the coupling efficiency is are still unresolved questions that demand investigation with higher spatiotemporal resolution, possibly using the nanopore technique.

Cdc45-Mcm-GINS (SF6). Unlike other hexameric DNA helicases, the eukaryotic nuclear helicase is a heterohexamer composed of Mcm2-7 (minichromosome maintenance) with 3′−5′ helicase activity.[280,281] To better study the structure and biochemical activity of eukaryotic nuclear helicase, one commonly used protein expression system is budding yeast. During protein purification, the Mcm2-7 complex is pulled down by GINS-tag. Cdc45 is also pulled down along with the Mcm2-7 complex, which indicates the critical role of Cdc45 within the complex.[282,283] EM structures of Cdc45-Mcm2-7-GINS (CMG)[284−286] suggested that the N tier leads the C tier when CMG translocates on the fork DNA substrate. Moreover, GINS, Cdc45, and three other accessory factors bind to the side of the Mcm2-7 two-tiered ring to keep the CMG complex in an active state.[285] Although the translocation mechanism remains to be investigated, several cryo-EM studies[285,287,288] have proposed the "inchworm" model based on the observations of structural changes on the CMG-ssDNA complex at the N tier side and the CMG itself at the C tier side. Furthermore, the mutation study shows that the Drosophila CMG loses only 50% unwinding activity if any one of its ATP active sites is mutated.[283] Together, it is more likely that the CMG translocates DNA using a different mechanism than the "staircase" model. Recent studies using single-molecule approaches have shown sequential loading and cooperative binding of Mcm2-7 to form the double-hexamer at the ori.[146] A Brownian ratchet mechanism is proposed based on the real-time detection of CMG unwinding.[289] The loading process can be modulated by Cdc6, Cdt1, and the origin recognition complex (ORC).[146] During replication, CMG excludes the lagging strand away from its central channel.[290] When the replisome stalls because of a lesion, CMG could uncouple from the DNA polymerase, which will result in the CMG−Mcm10 complex's transition into a faster diffusive model such that it diffuses on the dsDNA.[291] Once, the

DOI: 10.1021/acs.chemrev.9b00361
Chem. Rev. 2020, 120, 36−78

CMG−Mcm10 complex encounters another replication fork, it can transition back to ssDNA from dsDNA and restore the fork to resume replication.

Archaeal MCM Helicase (SF6). Similar to the eukaryotic CMG helicase, its archaeal homologue, hexameric MCM helicase, is also a 3′−5′ unwinding helicase fueled by ATP hydrolysis and involved in the replication process coupled with the replisome.[292] However, instead of the heterohexamer configuration of CMG, the archaeal hexameric MCM helicases are homohexamers composed of an Mcm2-7 archaeal homologue. A single-molecule study indicates that the MCM helicase unwinds dsDNA by strand-exclusion with ∼4000 bp processivity and a 50 bp s^{-1} unwinding rate.[293] Structural studies indicate that MCM interacts with DNA and assembles into a hexamer through its N-terminal domain.[294−296] Deletion of the winged-helix domain (WHD) at the C-terminal enhances MCM helicase unwinding activity.[297,298] Considering the highly conserved nature of the WHD from archaea to most eukaryotic Mcm2-7 subunits,[299] it is believed that WHD regulates the helicase activity and the loading of MCM complexes onto DNA through protein−protein interactions with accessory proteins or initiators.

3.2. DNA Polymerases

DNA polymerases use single-stranded genomic DNA as a template to synthesize the complementary sequence. Although there is a diversity in the structures and functions of different DNA polymerases, they adopt a general mechanism of action. They utilize the energy released from hydrolytic cleavage of dNTPs to translocate along DNA. So far, all known DNA polymerases catalyze the incorporation of nucleotides into the newly synthesized DNA in a 5′ to 3′ direction.

Most DNA polymerases are involved in genomic DNA replication. The process of replication has been and continues to be studied through different biochemical approaches. Recent developments in the field of single-molecule biophysics have led to the study of this dynamic process, at a single-molecule level. This has contributed to our current understanding of the mechanistic details, identification of rare intermediate species, and kinetics of individual steps of replication, across different organisms. The replication machineries of bacteriophages T4 and T7 and *E. coli* are some of the most well-studied systems using single-molecule tools. An excellent review by Stratmann et al. summarizes different single-molecule studies on DNA replication machinery, both *in vivo* and *in vitro*.[300]

The coordination between lagging and leading strand synthesis is a necessity for efficient replication and transmission of genetic information by all replisomes. Different single-molecule studies have investigated the synchronization between lagging and leading strand polymerases.[301,302] A recent study using real-time single-molecule visualization of the replication process challenged the widely accepted semi-discontinuous model of replication which predicts that the leading strand is continuously synthesized, whereas the lagging strand is replicated in a discontinuous manner.[303] A rolling circle assay that can differentiate lagging and leading strand DNA strand synthesis was used. A template DNA is immobilized on the glass surface. The *E. coli* replisome complex along with other necessary ingredients for replication are added to initiate synthesis of DNA. The newly replicated DNA strands are visualized using SYTOX Orange. The leading and lagging strand synthesis occurs independently with similar synthesis rates. Contrary to popular belief, leading strand synthesis was shown to occur sporadically and stalled stochastically during replication. *In vitro* studies on the replication machinery have generally shown that dsDNA synthesis occurs processively and that the replisome is a stable protein complex.[304,305] *In vivo*, the replisome is a more dynamic system with multiple interacting partners. The stability of replisome in live *E. coli* cells was investigated using single particle tracking and FRAP (fluorescence recovery after photobleaching).[306] The bound times for different replisome subunits except β were measured to be ∼10 s using both FRAP and sptPALM,[70] suggesting frequent exchange of subunits in the active replisome. The authors proposed a mechanism in which both leading and lagging strand replication is discontinuous, in line with previous *in vitro* measurements by Graham et al.[303]

Recent single-molecule studies of replication have also focused on the coordination between different components of the replication machinery. During replication, the polymerase often faces obstacles in the form of DNA binding proteins, transcribing RNA polymerases that also use DNA as their template, DNA supercoils and lesions. In eukaryotes, nucleosomes pose as additional roadblocks. A recent review[307] summarizes the interaction between replisomes and roadblocks and how replication bypasses these roadblocks.

Cells use specialized translesion DNA polymerases to overcome DNA lesions. Our understanding of how translesion synthesis (TLS) DNA polymerases access the target DNA selectively and how the action of replicative polymerase is coordinated with translesion DNA polymerase is limited. Single-molecule *in vitro* studies of these TLS polymerases have been reviewed recently.[308] Single particle tracking of *E. coli* Pol IV in live cells revealed static Pol IV molecules at replication sites upon DNA damage. The mechanism of recruitment of Pol IV to DNA damage sites was shown to be dependent on the type of DNA damage.[309] The cooperation between replicative polymerase Pol III and translesion polymerases Pol II and Pol IV was followed using colocalization single-molecule spectroscopy.[310,311] In the majority of cases, alternate binding of Pol III and Pol IV to DNA was observed by virtue of competitive binding. In a few cases, Pol III and Pol IV colocalized on the DNA. Three different DNA types—matched, mismatched, and lesioned DNA—were tested in this study. Interestingly, the binding preference between the replicative polymerase and translesion polymerases was unaffected by the type of DNA. This suggested that the exchange between replicative and translesion polymerases is dynamic and determined by the concentration of individual species.

3.3. RNA Polymerases

Transcription is the process by which RNA polymerase (RNAP) synthesizes RNA using genomic DNA as its template. RNA polymerases are multisubunit enzymes that motor along the template DNA using energy released from nucleotide polymerization and folding of the transcribed RNA. Transcription is a complex, multistep process, broadly divided into initiation, elongation, and termination. Single-molecule methods have revealed rich details about all three phases of transcription in both bacteria and eukaryotes (reviewed in refs 312−315).

During bacterial transcription initiation, the core polymerase must assemble into a holoenzyme by binding to a σ factor, which specifies the types of promoters to which the RNAP

DOI: 10.1021/acs.chemrev.9b00361
Chem. Rev. 2020, 120, 36−78

holoenzyme binds. How RNAP searches for its target promoter sequences has been studied extensively using various single-molecule tools.[316] Friedman et al. used colocalization single-molecule fluorescent spectroscopy (CosMoS) to assess the contribution of facilitated diffusion to promoter search by σ^{54} RNAP holoenzyme.[317] σ^{54} is a noncanonical σ factor, as opposed to the canonical σ^{70}. DNA templates, with and without a promoter sequence, were labeled with different fluorophores and immobilized on a surface. The RNAP holoenzyme was labeled with a third fluorophore and added into the chamber with immobilized DNA templates. If the holoenzyme appears on the same location as a surface-tethered DNA for 0.2 s or longer, it is identified as a binding event. To determine if 1D sliding or hopping have an effect on promoter search, the length of the DNA segment flanking a promoter site was varied. The length of the flanking DNA (up to 3000 bp) had no observable effect on the promoter binding rate. It was concluded that the facilitated diffusion mechanism over distances up to 3000 bp is negligible for the noncanonical σ^{54} RNAP's promoter search, favoring instead 3D diffusion as the major promoter search mechanism.[317] In another study, quantum-dot-labeled σ^{70} holoenzymes were followed in real time as they searched for promoters on doubly tethered double-stranded DNA curtains. They concluded that 3D diffusion is the major mechanism of promoter search for the canonical σ^{70} holoenzyme.[318] However, the spatial resolution of DNA curtain assay is at best about 200 bp, so 1D diffusion on a shorter length scale may have been missed. In fact, DNA curtain studies of Cas9 binding to its target could not see evidence of 1D sliding,[319] but smFRET studies showed that Cas9 does undergo 1D sliding during its target search, likely as a result of superior distance resolution.[320] smFRET has also been used to detect 1D sliding of RecA filaments on DNA[321] and argonaut−microRNA complexes on mRNA.[322]

After binding to a promoter, the RNAP holoenzyme forms a promoter closed complex (RPc). RNAP then unwinds ∼14 bp of DNA, creating a transcription bubble enclosed inside the RNAP core. Subsequently, it undergoes conformational changes to form the catalytically active open complex (RPo).[323] For σ^{54}-holoenzyme transcription initiation, two distinct types of closed complexes were observed:[147] a long-lived RPc and a precursor that is shorter-lived. Both types of closed complexes are formed multiple times before the open complex is formed, indicating that σ^{54}-holoenzyme experiences multiple bindings to the promoter before transcription is initiated. After promoter opening, RNAP synthesizes short transcripts (2−12 nucleotides) without losing its contact with the promoter during which the downstream DNA is scrunched in. smFRET and magnetic tweezers studies have detected such DNA conformational changes, like DNA opening and scrunching, during initiation.[324−327]

For a complete description of transcription mechanisms, we need information on the structural changes of the RNAP itself during transcription. RNAP has a claw-like structure that surrounds the active site to which DNA binds. One of the two pincers of the claw is called the clamp. Crystal structures have shown the clamps exist in two different conformations, open and closed. Using smFRET, Chakraborty et al. observed three different clamp conformations in solution and quantified their population changes through the transcription cycle.[328] Analysis of both σ^{70} RNAP holoenzyme and σ^{54} RNAP holoenzyme in the absence of DNA revealed pincer conformations consistent with a clamp open form (dominant population) and a closed form (a minority population). A novel collapsed state was also observed. The clamp is primarily open in free RNAP and RPc and is in a closed state during transcription initiation and elongation. Overall, this study showed that functionally important conformations already exist even for the holoenzyme or RNAP core alone. However, because smFRET measurements were performed on freely diffusing molecules in solution, real-time conformational changes could not be observed.

Koh et al. monitored conformational changes of T7 RNAP and its interactions with a surface-tethered DNA using a combination of approaches such as protein-induced fluorescence enhancement, fluorescence lifetime measurements, and FRET.[329] They were able to detect a transient closed complex state on the way to promoter opening and record transcription initiation with near base resolution, revealing the kinetic rate of each RNA lengthening step. Premature release of short transcripts, known as abortive initiation, was directly detected and correlated with the ultimate outcome of whether the RNAP enters the elongation phase. Quite unexpectedly, most of the RNAP molecules that successfully transit to the elongation phase did not produce any abortive transcripts. Another approach to correlate RNAP−DNA interaction with transcription is to perform multicolor colocalization.[330]

Transcription is interspersed with pausing. Single-molecule measurements provide direct quantification of pausing frequency and duration, whereas ensemble measurements cannot tell if a strongly pausing sequence is due to high probability of pausing or long duration of the paused state. Using high-resolution optical tweezers and accurate registration of pausing site at ∼100 ms, Gabizon et al.[331] were able to determine the position of RNAP on pause sites with an accuracy of ±3 bp. Pausing was observed to be sequence specific. The authors also studied the effect of nascent RNA transcripts on pausing durations. Upon adding RNase A which degraded RNA, they noticed a significant decrease in pause durations, which suggested that nascent RNA transcripts modulate transcriptional pausing. Earlier studies by Dalal et al.[332] had observed no effect of nascent RNA on pausing, possibly due to averaging over multiple pausing sites in the absence of a pausing analysis with high spatiotemporal resolution. The mechanism of transcription termination as a function of various termination sequences found in nascent transcripts can also be studied using optical tweezers.[333]

As RNAP tracks along the DNA, it generates positive and negative DNA supercoils ahead and behind, respectively. These supercoils can pose as barriers to RNAP motion along DNA, causing RNAP to stall, backtrack, or undergo transcriptional pausing, in the absence of proper regulatory mechanisms. Utilizing an angular optical trap[334] and a novel supercoiling assay, the effects of DNA supercoiling on transcription have been investigated. Supercoiling was shown to stall RNAP, with a stall torque of ∼11 pN·nm.[335] Extensive backtracking was observed when RNAP worked against the resisting torque of DNA. Transcriptional factors such as GreB enhance the torsional capacity of RNAP to overcome the resisting torques and decrease backtracking.[336]

RNA polymerases *in vivo* exist in different states, some freely diffusing in cytoplasm, some searching for its promoter in nonspecific sequences, and yet others relatively immobile due to stable interaction with promoter or their transcriptional activities. Live cell single-molecule tracking of RNAPs using Spt-PALM showed that there are multiple species that differ in

DOI: 10.1021/acs.chemrev.9b00361
Chem. Rev. 2020, 120, 36−78

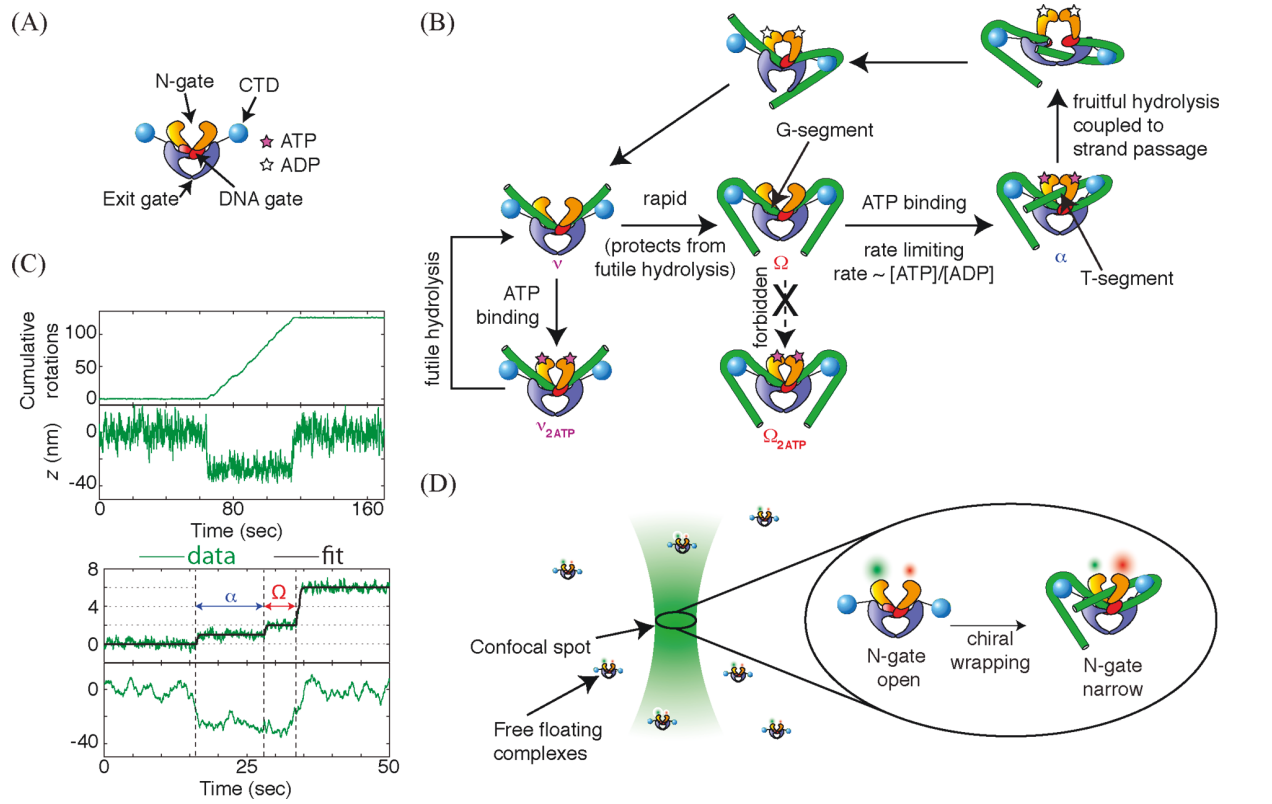

Figure 9. (A) The gyrase holoenzyme comprises a heterotetramer containing two copies of two subunits: GyrA and GyrB. The complex involves three protein−protein interfaces called the N-gate, the DNA gate, and the Exit gate. A specialized C-terminal domain of the GyrA subunit (CTD) can chirally wrap DNA in a positive superhelical fashion. (B) Details of the mechanochemical cycle of DNA gyrase that have been worked out on the basis of RBT experiments have been highlighted here. The Ω configuration involves extensive DNA:CTD contacts, with a DNA segment (the G-segment) captured within the DNA gate. Upon ATP binding, a rate limiting remodeling transition results in the formation of the α state where DNA is chirally wrapped around at least one CTD and another DNA segment in cis (the T-segment) is trapped within the N-gate cavity. ATP binding drives closure of the N-gate. Subsequent hydrolysis accelerated opening of the DNA gate and passage of the T-segment through a transient break in the G-segment. After expulsion of the passed T-segment via the Exit gate, DNA is released from the enzyme, resulting in the ν configuration. ν rapidly converts to Ω but, if stabilized, can bind ATP, leading to closure of the N-gate in the absence of a trapped T-segment. The enzyme must then undergo futile hydrolysis to reset. (C) Top panel: Simultaneous measurements of angle and z as a function of time during a single processive burst of activity, as measured by RBT at 1 mM ATP. Rotations introduced into DNA are relaxed at the free swivel (Figure 9B). Gyrase processively introduces several rounds of two rotations. Bottom panel: At 75 μM ATP, long dwells in Ω and α can be discerned—both states are contracted in z, indicating extensive sequestering of DNA. However, while Ω lies at the ~0 rotation mark, α is rotated by ~1 rotation, consistent with chiral wrapping of DNA in α. (D) Schematic of the confocal smFRET experimental geometry used to study nucleoprotein conformations in *B. subtilis* DNA gyrase. smFRET from complexes freely diffusing into the confocal volume of the excitation laser is detected. By controlling solution concentrations of DNA and nucleotides, conformations stabilized by particular substrates can be detected. For instance, in the absence of DNA or nucleotides, the N-gate remains in a largely open conformation, indicated by low FRET, whereas, in the presence of DNA, high FRET is observed, indicating a narrowing of the N-gate. Adapted with permission from ref 105. Copyright 2018 Springer Nature.

their diffusional properties.[337−339] In *E. coli*, RNAP spends 85% of its time in nonspecific associations with DNA.[339] In mammalian cells, RNAP forms transient clusters that correlate with transcription, leading to a model where a high concentration of RNAP near a promoter facilitates the launching of one or several RNAP molecules, which represents only a small fraction of RNAPs in the cluster.[340,341]

In the past decade, single-molecule measurements *in vitro* have begun to address questions pertaining to eukaryotic transcription.[342−352] In eukaryotes, RNAP encounters nucleosomes during transcription. Optical tweezers have been used to investigate how Pol II, eukaryotic RNAP responsible for mRNA transcription Pol II RNAP and *E. coli* RNAP negotiates with nucleosomes.[92,348,353,354] Most recently, Pol I, which is responsible for transcribing rRNA, has been studied using optical tweezers[345] and tethered particle motion.[355]

3.4. Topoisomerases and DNA Gyrase

Topoisomerases are enzymes that have evolved to solve the topological problems associated with accessing and replicating closed circular or otherwise topologically constrained DNA.[356−358] These enzymes function by changing the number of times one strand of DNA wraps around the other, known as the linking number (Lk). They do so via cleavage and relegation of single or double strands of DNA. Topoisomerases can relax positive or negative supercoils to facilitate replication and transcription elongation and to decatenate DNA molecules to unlink daughters after replication. Topoisomerases can also introduce negative supercoils to counter positive supercoiling generated downstream of replication and transcription and to maintain the genome at a global level of negative supercoiling.

Topoisomerases are broadly classified into two types—I and II. Type I topoisomerases cleave a single strand of DNA and

DOI: 10.1021/acs.chemrev.9b00361
Chem. Rev. 2020, 120, 36−78

either pass another strand through it, thereby changing *Lk* in units of ±1 (type IA), or permit free rotations about the nick (type IB). They do not consume ATP and so can only relax DNA toward equilibrium. Type II topoisomerases cleave a DNA duplex and pass another duplex through it, thereby changing *Lk* in units of ±2. They consume ATP and achieve a distribution of topoisomers tighter than thermal distribution.

As topoisomerase action leads to changes in *Lk* in DNA, single-molecule methods that can track Δ*Lk* in DNA, such as magnetic tweezers, have extensively been used to study them. Using magnetic tweezers, Koster et al. measured supercoiling relaxation by topoisomerase IB[100] (Figure 9A). They determined that the number of supercoils relaxed per event is exponentially distributed and that the rate and extent of relaxation depend on torque. They concluded that rotation of DNA around the transient nick is hindered by rotational friction within the enzyme. Linking number changes introduced by type IA topoisomerases have also been observed using magnetic tweezers. Gunn et al. have recently developed a TIRF microscope capable of combined protein-induced fluorescence enhancement (PIFE) detection with magnetic tweezing to simultaneously follow changes in *Lk* and conformational changes in the nucleoprotein complex.[110] They find that *E. coli* topoisomerase I samples multiple conformations when attempting to change DNA topology but succeeds sparingly. Type II topoisomerases have also been studied using magnetic tweezers, by observing the relaxation of plectonemes and the subsequent changes in extension. Strick et al. first used this approach to demonstrate that the action of type II topoisomerase on DNA changes *Lk* in units of ±2.[359]

Among type II topoisomerases, the bacterial enzyme DNA gyrase can directionally introduce negative supercoils and is thus a molecular motor. Directionality is ensured by chiral wrapping of DNA in a positive superhelical fashion around a specialized C-terminal domain (CTD) of the enzyme.[360] This creates a chiral DNA duplex crossing, where one strand of DNA (the G-segment) is captured by a protein−protein interface known as the DNA-gate, while another segment of DNA called the T-segment is captured within a closed "N-gate" (Figure 9A,B). Opening of the DNA-gate results in strand passage of the T-segment through a transient break in the G-segment, thereby introducing two negative supercoils.[361] Negative supercoiling by gyrase facilitates chromosome compaction, initiation and elongation of replication, and transcription[362] and is a regulator of gene expression programs.[363,364]

Rotor bead tracking (RBT) and conventional magnetic tweezers have been extensively used to study DNA gyrase.[103−105,365,366] In RBT, the two rotations introduced into DNA per cycle are fully relaxed by a free swivel, preventing the permanent accumulation of torque (Figure 9B). Angular dwells are representative of structural intermediates. Simultaneous tracking of the height of the rotor can differentiate structural intermediates at the same angle coordinate.

RBT measurements have uncovered several structural intermediates in the mechanochemical cycle of DNA gyrase and showed how nucleotide states and tension on the DNA alter their distribution and interconversion dynamics (Figure 9B,C). It paints a picture of loosely coupled mechanochemical transitions funneling the motor toward productive energy transduction, quite distinct from the tightly coupled landscape of P-loop NTPases such as myosins and F1 ATPase.[103,105] RBT studies identified an intermediate called the Ω state, where DNA makes extensive contacts with the CTD but is not chirally wrapped.[103] ATP is exchanged for ADP in driving a rate-limiting remodeling of the complex, resulting in conversion of Ω to α—a state where DNA is chirally wrapped around the CTD.[103,105] Subsequent hydrolysis was shown to accelerate strand passage of the T-segment through a transient break in the G-segment and to be required to reset the enzyme, confirming earlier bulk measurements.[105] RBT measurements also showed that, between cycles, gyrase passes through a configuration called the ν state, where DNA is transiently released from the complex.[104] ν, like Ω, can bind ATP. However, ATP binding to ν leads to closure of the N-gate in the absence of a trapped T-segment and requires futile hydrolysis to reset the enzyme.[105]

RBT measurements have shed light on how gyrase might mechanistically serve as a link between cellular metabolism and gene expression.[105] The rate-limiting Ω-to-α transition was shown to depend on the [ADP]/[ATP] ratio. In turn, it suggests how gyrase might throttle its supercoiling rate in response to environmental changes that alter the state of cellular metabolism and thus the intracellular [ADP]/[ATP] ratio. Global levels of negative supercoiling set by gyrase in turn control gene expression programs[363] that may enable cells to cope with the changing environmental conditions.

RBT measurements also uncovered a possible unique gyrase adaptation to ensure tight coupling between ATP consumption and supercoil introduction.[105] Mechanically stabilizing the otherwise transient ν state shows that, while in ν, the enzyme is susceptible to futile rounds of ATP hydrolysis decoupled from supercoil introduction. The authors proposed a model where the properties of the Ω state prevent futile ATP hydrolysis, and thus, the rapid ν-to-Ω transition is a unique gyrase adaptation to ensure tight coupling between ATP hydrolysis and supercoil introduction. The authors contrast gyrase with yeast topo II, which lacks CTDs and hence an Ω state, and point out that yeast topo II has been shown to undergo futile hydrolysis in the presence of abundant ATP.

Gyrase configurations have also been studied by observing FRET within individual molecules as they transiently float through a confocal volume. These experiments provide valuable snapshots of gyrase conformations and have been used to study how nucleotides and DNA alter their distributions (Figure 9C). These experiments make possible the observations of degrees of freedom associated with the protein itself, which is impossible to observe in RBT or other DNA-manipulation-based techniques that essentially measure conformations of the DNA alone. A FRET pair placed on the N-gate of *B. subtilis* gyrase shows an open N-gate in the apo state, a closed gate in the presence of AMP-PNP, and, surprisingly, a narrowed N-gate in the presence of DNA wrapped around the CTDs without ATP.[367] It suggests coordination between chiral wrapping around the CTD and the dynamics of the N-gate—an idea later also confirmed via RBT experiments. Similar experimental designs have also revealed dynamic movements of the CTDs coupled to DNA wrapping—CTDs are initially in a lower configuration near the exit gate and move upward toward the N-gate upon DNA binding.[368] These experiments help dispel an earlier notion that the CTDs might be acting as static and passive elements around which DNA wraps chirally. Instead, they support the idea that CTDs are dynamic and that chiral wrapping of DNA

DOI: 10.1021/acs.chemrev.9b00361
Chem. Rev. 2020, 120, 36−78

around them is coordinated with large-scale and long-range nucleoprotein rearrangements.

While structural studies provide atomistic detail regarding the geometry of the gyrase:DNA complex,[360,369,370] they fail to capture any dynamics. Single-molecule experiments on the other hand explore the rich ATP-coupled dynamics via the observations of a few degrees of freedom such as FRET or the extension and rotation of DNA. It is likely that, as hybrid techniques such as FluoRBT[114] or MT-TIRF[110] are developed and applied to studying gyrase, added degrees of freedom will create a more complete picture of coordination between conformations of the nucleoprotein complex and substeps in the ATPase cycle.

3.5. Chromatin Remodelers

In eukaryotes, DNA is packaged into chromatin in units of nucleosomes. A nucleosome is made up of about 150 base pairs of DNA wrapped 1.7 times around an octamer of histone proteins, which is composed of two copies each of H2A, H2B, H3, and H4 histones.[372] Compared to linker DNA, which bridges two adjacent nucleosomes, nucleosomal DNA is generally less accessible to sequence specific factors.[373,374] Thus, the positioning of nucleosomes with respect to regulatory sequence elements such as transcription factor binding sites has significant implications for gene regulation.[375] Native nucleosome positions cannot be fully recapitulated by DNA sequence alone and require the activities of ATP-dependent chromatin remodeling complexes.[376] There are four families of ATP-dependent chromatin remodelers, ISWI, CHD, SWI/SNF, and INO80, all of which share RecA-like ATPase domains (Figure 10A). Unlike helicases, these RecA-like domains lack the "pin" motifs which are necessary for DNA strand separation and are therefore able to translocate on DNA without unzipping the two DNA strands. The different families of chromatin remodelers have distinct but overlapping functions, including sliding histone octamers along the DNA[377−379] (often referred to as nucleosome sliding), exchanging histones for noncanonical variants,[380] removing the histone octamer from DNA,[381−385] or other alterations of nucleosome structure.[386,387] These reactions are often strictly dependent on ATP hydrolysis because the intermediates that form during these processes are energetically unfavorable and require breaking multiple, if not all, histone−DNA contacts within a nucleosome. The ATPase motors of chromatin remodeling complexes are highly regulated by their substrates and accessory subunits and, as we will discuss here, contribute to the specific recognition of target nucleosomes and the defined mechanism that leads to the remodeled nucleosome.

Earlier footprinting and structural evidence revealed that most ATP-dependent chromatin remodelers function by translocating DNA from an internal nucleosomal site,[388−392] but how the translocation activity leads to different remodeled products and how this process is regulated across different remodeling enzymes remained elusive. In the past decade, single-molecule studies sought to answer these questions by providing near base pair resolution details of intermediates and dynamics during chromatin remodeling. One representative example is nucleosome sliding, a process defined by the relative movement of the histone octamer relative to the DNA without loss of histones. Blosser et al. used smFRET to monitor the position of the histone octamer relative to the DNA by placing a FRET donor on a histone residue and a FRET acceptor on a DNA base[393] (Figure 10C). By monitoring nucleosome sliding

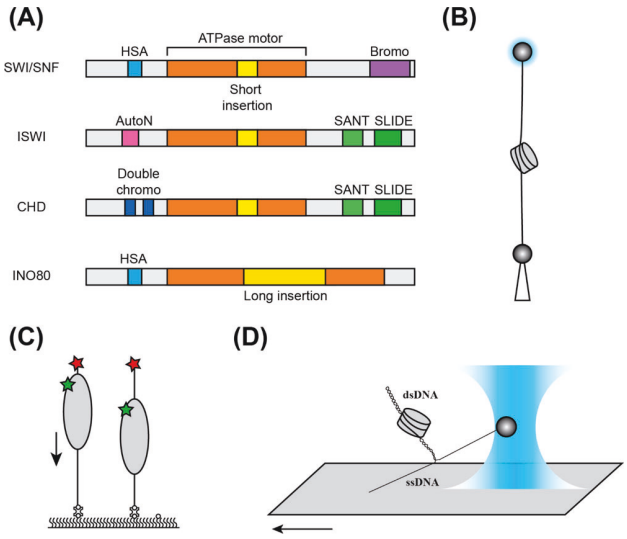

Figure 10. ATPase motors of chromatin remodeling complexes are studied with various single-molecule methods. (A) ATPase domain architecture of four major chromatin remodeler families.[371] (B) In an optical trap experiment, nucleosomal DNA is tethered on both ends with an optical trap on one end and a micropipette on the other. (C) In a typical single-molecule FRET assay to monitor nucleosome sliding, the histone octamer is labeled with a donor fluorophore (green) and the DNA end is labeled with an acceptor fluorophore (red). Movement of the histone octamer along the DNA is reported through changes in FRET efficiency. (D) In a DNA unzipping experiment, two single strands of nucleosomal DNA are tethered to the trapped bead and the slide. As the slide moves relative to the bead, the nucleosomal DNA is unzipped into two single strands. The strength of interaction between the DNA-bound proteins (histone or transcription factor, for example) can be probed by the force required to unzip DNA base pairs where the protein is bound.

in real time, they observed that ACF, an ISWI family enzyme that can regularly space nucleosome arrays, takes well-defined pauses after an initial 7 bp slide and subsequent 3−4 bp movements. The duration of pauses depends on the ATP concentration, suggesting that sliding activity is coupled to ATP hydrolysis. The ATPase subunits of the ISWI family share a conserved AutoN domain which can compete with the H4 tail for binding to the catalytic site and inhibit ATPase activity. As investigated in a later study, this autoinhibition mechanism is utilized by ACF to sense linker DNA lengths through the accessory subunit Acf1 which associates with the H4 tail.[394] During the pause phase between translocation steps, Acf1 preferentially binds to long linker DNA, releasing the H4 tail to compete with AutoN for the motor domains. As a result, the ATPase activity is derepressed when long linker DNA is present. Regularly spaced nucleosomes are often found on silenced chromatin,[395] and these studies provide an intriguing model for how they can be generated.

Like other well-characterized SF2 helicases such as NS3, the RecA-like motors of chromatin remodelers can translocate on DNA strands in the 3′ to 5′ direction.[261] Due to the symmetry of a canonical nucleosome structure, there are two possible locations for the ATPase of remodeling enzymes to engage that will lead to opposite remodeling outcomes. Bidirectional sliding has been observed in ISWI, CHD, and SWI/SNF families on the single-molecule level. In the case of ISWI, two ACF complexes can bind to one nucleosome[396] and are inferred to be responsible for carrying out bidirectional

DOI: 10.1021/acs.chemrev.9b00361
Chem. Rev. 2020, 120, 36−78

translocation on a centered nucleosome.[393] ACF functions optimally as a dimer, for which coordination can be achieved through a recently proposed allosteric regulation through a distorted octamer structure.[396−398] Chd1 resembles ISWI in the ATPase domain architecture (Figure 10A) and has also been observed to carry out bidirectional nucleosome sliding. Unlike ACF, Chd1 dimer has not been observed to coexist on a nucleosome, and in fact, single-molecule studies suggest a different mechanism where Chd1 monomers are sufficient to slide nucleosomes back-and-forth.[399] The authors proposed that bidirectional sliding by a single ATPase can be achieved if the ATPase domain is able to swing to the opposite superhelical location 2 (SHL2) or to the SHL6 on the adjacent gyre, a location utilized by INO80.[400] Despite the differences in stoichiometry, both ACF and Chd1 are sensitive to DNA linker lengths. Given an end-positioned nucleosome, they will unidirectionally move the nucleosome toward the center. In contrast, SWI/SNF is not regulated by flanking DNA lengths and, given an end-positioned nucleosome, can move the octamer off the DNA end as far as 50 bp past the edge of the nucleosome.[401−403] Indeed, smFRET studies suggested that RSC, a member of the SWI/SNF family, does not have a strong bias for sliding an end-positioned nucleosome toward either direction.[404]

One long-standing question for nucleosome sliding is how local DNA movement generated by the ATPase motors is propagated on the nucleosome surface to result in a net movement of the histone octamer with respect to the DNA. Recently, researchers used three-color FRET to observe the coordinated movement of DNA on both sides of the nucleosome. They found that Chd1 and SNF2h, the ATPase subunit of ISWI, pull in DNA from the entry side first before the DNA emerges on the exit side.[405] In an earlier study where entry and exit side movements were probed in two separate FRET experiments, the researchers found that the lag time for ISWI to start shifting the exit side DNA is shorter than the time needed to start shifting the entry side DNA. After converting FRET efficiency to distance, it was inferred that ISWI pushes 7 base pairs of DNA out of the nucleosome before DNA enters in 3 base pair increments from the other side.[406] While the two studies appear to reach conflicting results, one possible explanation is that, in the initial two-color experiments, the entry and exit side movements were not directly measured on the same nucleosome, and the differences in lag time can be explained by the asymmetry of the artificial "601" DNA that was used to reconstitute these nucleosomes.[91] The order of DNA movement where the entry side precedes the exit side is also supported by recent cryo-EM structures of Snf2, the ATPase subunit of yeast SWI/SNF, bound to a nucleosome in the presence of ADP or ADP-BeF_3.[407] In this study, researchers observed that Snf2 stabilizes a 1 base pair bulge near SHL2 in the apo or ADP-bound state. This results in a 1 bp shift of the proximal linker DNA onto the nucleosome up to where ATPase engages, while re-establishing most of the histone−DNA contacts. When bound to ADP-BeF_3, a mimic for prehydrolysis ATP, the ATPase motors are in a closed conformation, indicating ATP binding may allow the 1 bp bulge to relax and propagate toward the exit side. Subsequent ATP hydrolysis may initiate another cycle of 1 bp translocation. These studies suggest that DNA on the entry and exit side of the nucleosome is shifted in a highly coordinated manner during nucleosome sliding.

It has been proposed that chromatin remodelers can generate large DNA loops on the nucleosome surface during remodeling,[408] which cannot be explained by these highly coordinated movements of DNA on the entry and exit side of the nucleosome. By tethering nucleosomal DNA on both ends using an optical trap, researchers observed 25 bp DNA shortening events during nucleosome remodeling by SWI/SNF, although movements smaller than 25 bp could be beyond the detection limit (Figure 10B).[408−410] Harada et al. applied similar smFRET assays discussed above[393,406] to RSC and found that RSC translocates nucleosomal DNA in 2 bp increments, to a similar degree as ISWI and Chd1.[404]

The INO80 family chromatin remodelers, INO80 and SWR1, are distinct from other families in having a long insertion that splits their ATPase into two segments (Figure 10A). While the INO80 complex has diverse functions including DNA repair, transcription, and replication,[411−413] INO80 can slide mononucleosomes on DNA and its sliding activity is regulated by linker DNA lengths.[414] The other family member SWR1 is specialized in exchanging H2A−H2B dimer in a nucleosome for the variant H2A.Z−H2B dimer.[380] The ATPase motors of SWR1 interact with the nucleosome near SHL2,[415,416] similar to most other chromatin remodelers,[389,407,417] whereas INO80 motor domains are located across SHL-6 to -7.[400] Like other helicases, both SWR1 and INO80 ATPase domains adopt a "closed" conformation in the ADP-BeF_3-bound state. The motor domains of the Swr1 subunit stabilize a 1 bp bulge at SHL2, while two other SWR1 subunits stabilize 25 bp nucleosomal DNA at the ATPase-proximal entry/exit site in a significantly unwrapped conformation, suggesting that the proximal H2A−H2B dimer is poised to be evicted. In the INO80-bound nucleosome, DNA is unwrapped to a smaller degree, but the DNA is lifted away from the histone surface, with potential implications for histone octamer sliding and reported,[418] but unconfirmed,[419,420] histone exchange activity. smFRET assays have been applied to both remodelers to monitor histone exchange through loss or gain of labeled histones. In the case of SWR1, the FRET donor and acceptor were placed on histone H2A and DNA, respectively, to monitor H2A eviction. SWR1 has been shown to be recruited by long linker DNA,[421] but it is not known whether exchange can be biased toward one H2A−H2B dimer when linker DNA lengths are asymmetric. Using FRET efficiency as a reporter for the remaining H2A location, Willhoft et al. saw no preference for evicting the linker-proximal or linker-distal H2A−H2B dimer, even though the linkers were of different lengths, indicating that SWR1 ATPase engages with either side of the nucleosome with equal probability.[415] The histone exchange activity of INO80 has been probed using a single-molecule assay by performing the reaction in bulk and then capturing them to an imaging surface to score the loss and gain of fluorescently labeled H2A.Z and H2A.[422]

Many ATP-dependent chromatin remodelers are recruited to chromatin by other chromatin factors, such as transcription factors (TFs),[423,424] and the impact of such nonhistone DNA binding proteins on remodeling outcomes has been the subject of many studies.[425,426] DNA unzipping is advantageous in looking at the outcome of individual remodeling events because it allows detection of nucleosome positions beyond the dynamic range of FRET, making it possible to record the outcomes of remodeling reactions at near base pair resolution[427] (Figure 10D). Li et al. applied DNA unzipping

DOI: 10.1021/acs.chemrev.9b00361
Chem. Rev. 2020, 120, 36−78

to study the interaction between SWI/SNF and ISWI with the DNA binding domain of Gal4 (Gal4-DBD), a well-characterized transcription factor.[428] They found that Gal4-DBD acts as a barrier to ISWI remodeling, where ISWI cannot slide nucleosomes past the Gal4-DBD. SWI/SNF, on the other hand, is able to displace the Gal4-DBD and reposition the nucleosome past the Gal4-DBD binding site. Such studies not only provide insight on what happens when a chromatin remodeler encounters a TF but also provide the mechanistic basis for engineering chromatin remodelers to manipulate nucleosome positions *in vivo* in a sequence specific manner, as reviewed in section 4.1. DNA unzipping to map the nucleosome position has also been used to examine how histone variants such as H2A.Z can modulate nucleosome stability and motility on native genomic sequences[429] instead of the artificial "601" sequence that has been used in the vast majority of biophysical studies due to its ability to form a nucleosome at a single defined location. Interplay between nucleosome mobility and transcription factors has also been studied through DNA unzipping.[430]

3.6. Other DNA Motors

There are miscellaneous DNA motors that do not quite fit into the categories described so far. For example, Rad54[431,432] and Mfd[111,112,433] are dsDNA translocases that possess helicase-like motifs but do not have any detectable DNA unwinding activity. Here, we discuss ring-shaped dsDNA translocating systems: a viral packaging motor, one loop-extrusion complex, a DNA translocase, and one processive DNA degradation machinery.

3.6.1. Viral DNA Packaging Motor. During self-assembly, double-stranded DNA (dsDNA) viruses employ a ring-shaped motor to package the viral genome into a preformed protein capsid (prohead). The packaging process is often divided into initiation, translocation, and completion phases.

Optical tweezers are a popular tool to investigate the packaging kinetics of these motors in real time. Single-molecule optical trap assay allowed accurate characterizations of viral packaging by bacteriophages φ29, T4, and λ.[434−437] Generally, the prohead and the end of the DNA awaiting packaging are attached to the trapped microsphere and the other microsphere, respectively. The packaging of DNA can be visualized in real time, enabling measurements of packaging rates and forces generated by the packaging motor. Two different approaches are typically employed to prepare the DNA-packaging motor complex for single-molecule studies: (1) A single DNA molecule can be fed to a preassembled prohead−motor complex to initiate packaging. (2) The packaging of DNA can also be initiated in the bulk and then stalled by addition of non-hydrolyzable ATP. A single stalled complex can then be studied with optical tweezers. The progress of packaging is monitored by measuring the decrease in DNA tether length under constant force or by measuring the increase in force while the distance between the microspheres is kept constant.

The φ29 motor complex consists of a homopentameric ATPase that generates mechanical force for genome packaging.[438,439] Initial studies of the φ29 motor using a stalled complex have shown that the motor is highly processive and can package the entire 19.3 kbp genome, even against high opposing forces (~60 pN).[437] Since then, methods have been improved to be able to follow packaging from initiation to completion.[440] The φ29 motor translocates with an average speed of 145 bp/s, which varied depending on the salt conditions.[440] A series of high-resolution optical tweezers studies from the Bustamante lab has revealed a complicated and coordinated packaging procedure in which each packaging cycle is composed of a dwell phase and a burst phase.[11,434,441,442] During the dwell phase, pentameric ATPase subunits release ADP and load ATP sequentially. During the burst phase, rapid sequential ATP hydrolysis results in the translocation of 10 bp of DNA in four 2.5 bp steps. The pentameric ATPase subunits in the motor must coordinate their enzymatic activity to accomplish the task. Using targeted mutagenesis, it was shown that the arginine fingers are crucial for nucleotide exchange promotion and activating ATP hydrolysis.[443] As the prohead is filled beyond half of its capacity, an intracapsid pressure of 60 atm builds up, due to DNA jamming in the prohead. An estimated force of ~80 pN is required to drive the remaining DNA into the capsid.[437] Recent studies on the physical behavior of packaging DNA suggest that long time scales of DNA relaxation and jamming of DNA inside the viral head during packaging necessitate the regulation of packaging rates.[444]

Other packaging motors such as those from T4 and λ phages have been investigated using similar assays.[435,436] The average motor velocities for T4 and λ packaging motors were measured to be 590 and 770 bp/s, respectively, at a 5 pN load. A single-molecule fluorescence assay detected long pausing events during T4 DNA packaging initiation reactions that were not previously observed with bulk measurements.[445] A recent study determined how interactions between the T4 motor and DNA substrate is modulated by nucleotide binding. The ATP-bound T4 motor grips DNA strongly, intermittent gripping strength is observed in the ADP-bound state, while no significant gripping was observed in the apo state.[446]

3.6.2. Condensin. Genomic DNA is organized in a way such that it fits inside the cells and is accessible to enable various cellular processes. Members of the SMC (structural maintenance of chromosomes) family are important players in the macroscale organization of chromosomes and are conserved from bacteria to humans. How SMC complexes participate in these processes is not completely understood. Eukaryotic condensin is so far the only SMC complex whose motor activity has been reported.[447]

Condensin consists of two SMC proteins, Smc2 and Smc4, which form ~45 nm antiparallel coiled coils that dimerize at a central hinge.[448] High-speed AFM revealed flexible Smc2−Smc4 complexes that switch conformations.[449] Magnetic tweezers have been the technique of choice to measure changes in the end-to-end distance of DNA upon compaction by SMC complexes. Initial single-molecule studies on condensin from *X. laevis* showed that the binding of condensin to DNA occurred in an ATP-independent manner. However, ATP was essential for condensin mediated DNA compaction. Compaction and decompaction of DNA occurred with a mean step size of ~80 nm.[450] Similar findings were obtained from recent magnetic tweezers studies on condensin complexes from *S. cerevisiae*. The DNA compaction was proposed to occur in two steps: Initiation of compaction occurs by binding of condensin to DNA through electrostatic interactions before ATP hydrolysis, followed by irreversible compaction requiring ATP hydrolysis.[451]

DNA−condensin interactions can be visualized using fluorescence-based imaging approaches in which both the DNA and the protein of interest are labeled. Using the DNA

DOI: 10.1021/acs.chemrev.9b00361
Chem. Rev. 2020, 120, 36−78

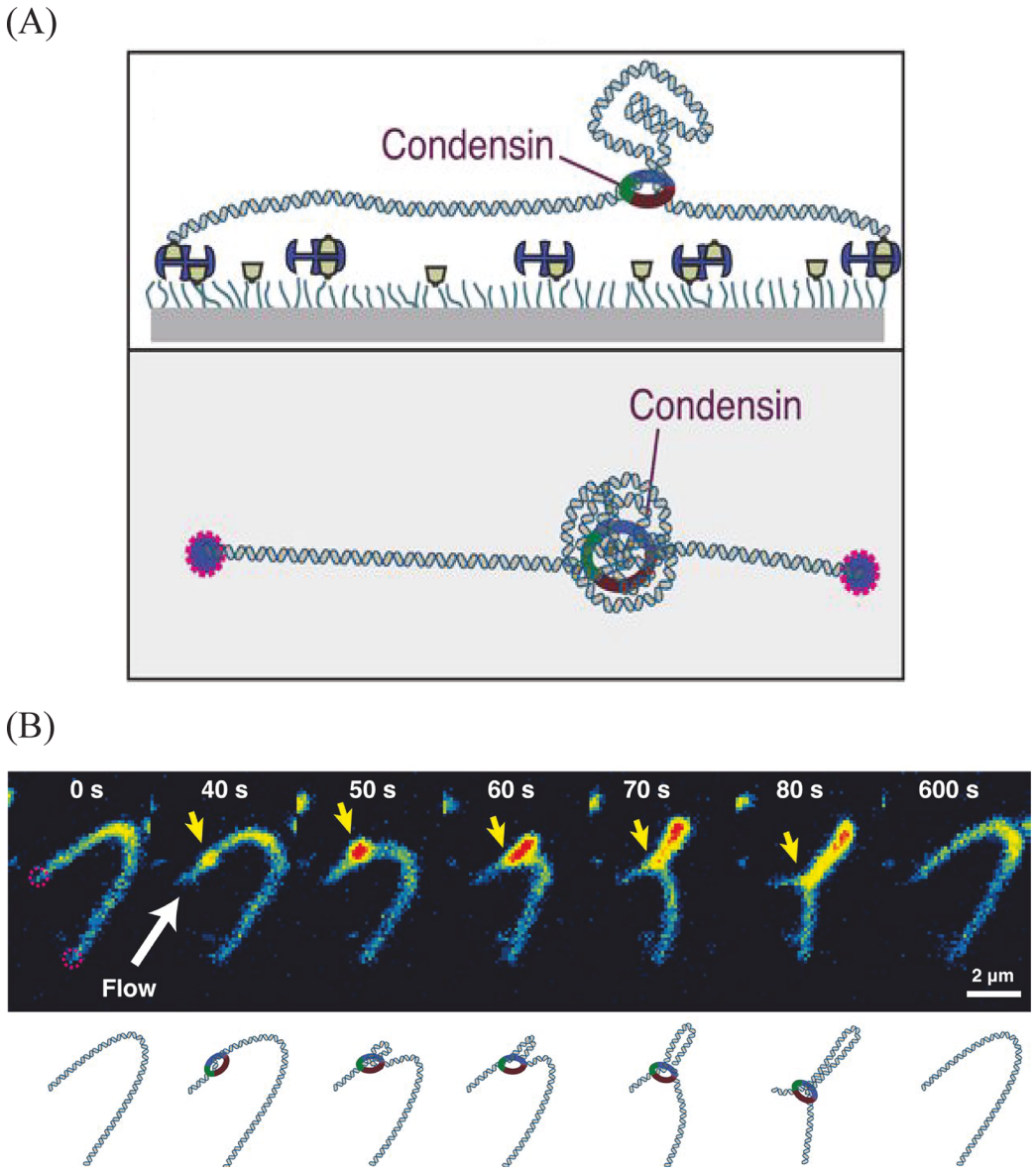

Figure 11. Single-molecule fluorescence imaging of condensin-induced DNA loop extrusion. (A) Schematic representation of the experimental setup for visualization of condensin-induced loop extrusion. (B) Snapshots showing DNA loop extrusion intermediates stained by SYTOX Orange. Adapted with permission from ref 452. Copyright 2018 The American Association for the Advancement of Science.

curtain assay described earlier, motor properties of *S. cerevisiae* condensin along DNA were examined. Condensin molecules translocate at a velocity of 60 bp/s in an ATP-dependent manner for very long distances (>10 kbp). The ATPase deficient variant of condensin exhibited no ATP hydrolysis or DNA compaction activity. This study provided the first direct evidence of ATP powered translocation of condensin. Additionally, it was shown that condensin is able to transport a second DNA molecule along the DNA.[447] The observation suggested the involvement of condensin in DNA compaction through mechanisms such as loop extrusion. The formation of DNA loops by condensin complexes was visualized by staining doubly tethered stretched DNA molecules with SYTOX Orange (Figure 11). By monitoring the fluorescence intensities, condensin-induced gradual extrusion of DNA was visualized in real time. This loop extrusion required ATP hydrolysis and occurred asymmetrically with an average rate of 0.6 kbp/s.[452]

3.6.3. SpoIIIE/FtsK Family. The SpoIIIE/FtsK family of hexameric DNA translocases segregates DNA prior to cell division. During the *B. subtilis* sporulation lifecycle, SpoIIIE translocates the DNA from the mother cell into the forespore. The *E. coli* homologue FtsK is recruited to the division septum and coordinates circular chromosome segregation with cell division. Among ring ATPases, SpoIIIE and FtsK are the fastest known DNA translocases, with a rate of 4000−7000 bp/s.[453−455] Both FtsK and SpoIIIE possess an N-terminal integral transmembrane domain that enables septum localization.[456] The C-terminal is a Rec-A-like motor domain consisting of three subdomains: α, β, and γ.[456] The α and β domains contain ATP binding and hydrolysis motifs, while the γ domain imparts translocation directionality that depends on 8-mer DNA recognition sequences[453,454,457−460] named KOPS

DOI: 10.1021/acs.chemrev.9b00361
Chem. Rev. 2020, 120, 36−78

(FtsK orienting polar sequences) for FtsK[461,462] and SRS (SpoIIIE recognition sequences) for SpoIIIE.[454]

How FtsK recognizes the KOPS sequence and how the recognition facilitates the directionality of FtsK translocation has been widely debated.[460−465] To shed light on FtsK−KOPS interaction and translocation mechanisms, quantum dot labeled FtsK molecules were visualized on doubly tethered DNA curtains.[453] The authors used a linked trimeric version of the FtsK motor, which forms a hexamer upon dimerization. FtsK locates the KOPS sequence in the DNA through 3D diffusion and binds to the KOPS sequence specifically in the presence of non-hydrolyzable ATP variants like ADP, AMP-PNP, and ATPγS. The initial translocation directionality was determined by the orientation of KOPS. Encounters of an already translocating FtsK with KOPS sequence do not have any effect on its translocation directionality. FtsK can pause and switch directions while translocating along naked DNA, independent of KOPS.[453] Two color labeling was used to study protein−protein collisions on DNA with FtsK. FtsK was labeled with quantum dots, while the protein roadblocks were labeled with a differently colored quantum dot. Depending on the affinity of the bound roadblock proteins, FtsK could either push, evict, or bypass them.[466]

Liu et al. used optical tweezers to study the interaction of SpoIIIE with DNA.[467] DNA constructs with a 30 base pair modified neutral insert containing double-stranded methyl phosphonate (Me-P) were used to investigate how SpoIIIE interacts with DNA substrates. SpoIIIE failed in translocating the neutral segment, suggesting that interactions with negatively charged phosphates are crucial to SpoIIIE translocation. ssMe-P (single-stranded Me-P) inserts in either the 3′−5′ strand or the 5′−3′ strand were used to reveal the translocation directionality of SpoIIIE. The majority of the SpoIIIE molecules were able to traverse the insert if Me-P was on the 3′−5′ strand, while fewer molecules traversed when the insert was on the 5′−3′ strand.[467] This indicated that SpoIIIE translocates on the 5′−3′ strand. A step size of 2 base pairs was inferred from DNA constructs with two neutral Me-P inserts separated by a single charged base pair. Similar to other DNA translocases, SpoIIIE can operate against forces of ∼50 pN.[468] Translocation of SpoIIIE was monitored using optical tweezers in a passive mode. At sufficiently high opposing forces (20−40 pN), translocation of SpoIIIE is interrupted by slipping. At low concentrations of ATP, spontaneous pausing events are detected. The authors suggest that an ultrafast translocase, SpoIIIE, adopts these mechanisms in order to adapt to various cellular conditions and molecular roadblocks. This might explain why *in vivo* translocation rates of SpoIIIE (1000−2000 bp/s)[469] are lower than that observed *in vitro*.[454]

3.6.4. Lambda Exonuclease. DNA exonucleases are involved in various cellular processes such as DNA repair, recombination, and replication. λ exonuclease from bacteriophage λ is a 5′−3′ exonuclease that is crucial to homologous recombination.[470] It converts the energy from hydrolytic cleavage of phosphodiester bonds to translocate for processive degradation. λ exonuclease processively degrades linear double-stranded DNA with a 5′−3′ directionality, generating 3′ single-stranded overhangs.

DNA degradation by λ exonuclease was shown to be comprised of three distinct phases: initiation, distributive, and processive phases.[471] The initiation phase refers to the protein binding stage, which is dependent on protein concentration. The phosphate group at the 5′ end of double-stranded DNA helps in the formation of an enzymatically active exonuclease complex.[472] During the distributive phase, there are multiple rounds of short degradation events interspersed with frequent protein dissociation. It has been proposed that these initial degradation steps lead to generation of ssDNA overhang, long enough to allow stable protein binding and processive degradation. The rate of degradation slows down in the presence of multiple mismatches in DNA, due to poor DNA helicity.[472] Using high-resolution optical trapping assay, the enzyme was also shown to exhibit sequence-dependent pausing behavior.[473] smFRET in combination with molecular dynamics simulation and kinetic modeling of Mg^{2+}-dependent DNA degradation was used to probe the magnesium-concentration-dependent activity of λ exonuclease.[474] At physiological concentrations of Mg^{2+}, processive degradation occurs. When the Mg^{2+} concentration is lowered, occasional dissociation of exonuclease results in pauses during processive degradation.[474]

4. PROTEIN ENGINEERING

One of the goals of mechanistic studies of protein dynamics and function is to engineer proteins with novel activities, based on the knowledge gained. Altered optimal pH conditions for protein functioning or improved thermal stability, better enzymatic activity, and better substrate specificity are some of the traits that could be imparted to an engineered protein. In addition, protein engineering could serve as a tool to progress our understanding of the structure−function relationship of a protein of interest. Progress in genetic engineering, structural biology, computational protein design, bioinformatics, and synthetic biology has fueled the application of protein engineering to a wide range of proteins. With the introduction of optogenetics tools, it is now possible to regulate protein function spatiotemporally *in vivo*. Computational tools play an important role in the *de novo* design of proteins. Using structure-based design principles, it is possible to enhance or modulate different properties of DNA motors. Below, we describe some of the commonly used tools in protein engineering. Since the number of examples of engineered DNA motors are limited, we will discuss existing protein engineering strategies in the context of DNA motors.

4.1. Mutagenesis

A crude way of modifying protein function is through altering a specific amino acid residue or a stretch of residues in a protein sequence. This process is tedious, and the outcome is hard to predict. In order to make the process efficient, precise information on the structure of the target protein as well as an understanding of the catalytic domains of the protein, the location of the active site of the protein, and the substrate binding site is helpful.

In studies performed two decades ago, 18,000 individual colonies carrying mutagenized *uvrD* plasmids were tested to isolate a mutant UvrD (D403AD404A) which exhibited increased unwinding activity.[475] The increased unwinding activity was due to increased processivity of the unwinding reaction.[476] A computational technique combining atomic level free energy calculations with structural bioinformatics approaches provided a molecular explanation for the hyperhelicase activity of UvrD (D403AD404A).[477] The study suggested that mutating the two charged aspartic acid residues into hydrophobic alanine residues makes the interactions between 1B and 2B domains stronger, favoring a more closed UvrD (D403AD404A) state and processive unwinding, in

DOI: 10.1021/acs.chemrev.9b00361
Chem. Rev. 2020, 120, 36−78

agreement with previous studies by Comstock et al.[155] Mutagenesis studies performed on the structurally similar Rep protein have contributed to our understanding of the role of the 2B domain in the functionality of Rep. The 2B domain of Rep has been deemed the regulatory domain controlling the unwinding activity of Rep. The 2B domain deleted Rep variant, RepΔ2B, was shown to have a faster unwinding rate than that of wild type Rep,[192] suggesting that the 2B domain of Rep is not essential for the unwinding activity of Rep. These early studies fueled a series of single-molecule experiments (section 3.1) aimed toward investigating the role of the 2B domain of Rep in its various functions. RepΔ2B was, however, deficient in protein displacement from DNA.[186] This suggested that the 2B domain is necessary for protein displacement by Rep and that translocation is not enough for protein displacement.

Altering protein activity through mutagenesis is not limited to helicases, such as Rep and UvrD. SpoIIIE, another DNA motor (section 3.6.3), was mutagenized to transport chromosomes slower than the wild type. Screening several mutants in and around the ATPase motifs of SpoIIIE led to a mutant (D584A) that transported chromosomes at a rate lower than that of the wild type SpoIIIE.[469] Guided by structural and genetic analysis, Lin et al. generated variants of T4 viral packaging motors with altered packaging velocity and ATP hydrolysis rates.[478] Such mutagenized variants could also further our understanding of evolutionary selection of optimal motors for the survival of an organism.

Another protein engineering approach is to introduce domains in proteins that can impart novel functions to the proteins. Multidomain proteins can either be created by linking the proteins end to end or by domain insertion. A bifunctional protein named "helimerase" was engineered by linking UvrD with a DNA polymerase using a coiled coil.[479] This engineered helimerase could amplify significantly longer fragments in helicase-dependent amplification (HDA)[480] reactions, in comparison to nonlinked UvrD and DNA polymerase proteins added to the reaction. A similar strategy was used to impart sequence specificity onto a monomeric chromatin remodeler, Chd1. It has been demonstrated *in vitro* that the direction in which Chd1 slides nucleosome along DNA can be predictably altered by replacing the DNA binding domain of Chd1 with that of transcription factors such as AraC or engrailed.[426] Extensions of such a strategy, such as targeting chromatin remodeler with a dCas9 fusion, can be used to program nucleosome positions *in vivo*.[481,482]

4.2. Chemical Modifications

Proteins are biological machines that switch between different conformational states to regulate their functions. Conformational control of proteins through different chemical methods can provide functional insights and enable the design of proteins with novel activities. Knowledge of protein structures aided with computational predictions can assist in designing a protein that is capable of on-demand conformational transitions. Chemical transformations of proteins include various strategies such as protein cross-linking, introduction of ligands and effector molecules that alter interactions between different protein domains, and covalent modifications that change protein−protein interactions.

Arslan et al. engineered variants of Rep protein that were intramolecularly cross-linked to constrain the 2B domain in closed (Rep-X) or open conformations (Rep-Y)[164] (Figure 12A). Double cysteine Rep mutants were cross-linked with bis-

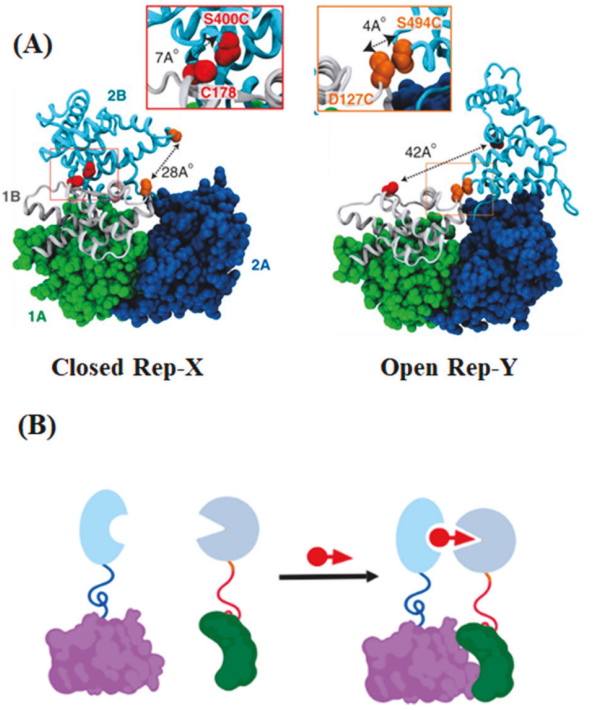

Figure 12. Chemical control of protein functions (A): (left) superhelicase Rep-X obtained by cross-linking the 2B domain in the closed conformation; (right) open Rep-Y is obtained by locking the 2B domain in the open conformation. Adapted with permission from ref 164. Copyright 2015 The American Association for the Advancement of Science. (B) Schematics of chemical-induced protein dimerization. Protein domains linked to chemical dimerization systems can form heterodimers in the presence of a ligand molecule (red).

maleimide cross-linkers (BMOE). The length of the cross-linker was chosen based on the distance between the two cysteine positions being cross-linked. Intramolecular cross-linking locks Rep-X in a closed conformation that is capable of unwinding thousands of base pairs processively with a speed of 136 bp/s. In contrast, Rep-Y displayed unwinding rates similar to that of wild type Rep. Thus, the closed form of Rep was identified as its functionally active form. Another member of the same helicase family, PcrA, could also be cross-linked in its closed conformation, PcrA-X. PcrA-X unwinds DNA in a highly processive manner, though not as fast as Rep-X. The engineering of a monomeric superhelicase opens the door to several biotechnological applications. One of them is co-transcriptional RNA folding studies. It was shown that Rep-X processively unwinds RNA/DNA heteroduplexes with a 3′ ssDNA tail. As Rep-X unwinds the RNA/DNA heteroduplex, the 5′ end of the RNA strand is gradually revealed to the solution for folding. The folding of fluorescently labeled 5′ RNA emerging behind Rep-X as the unwinding proceeds, mimics co-transcriptional folding which can be measured using smFRET.[483,484]

Chemically inducible dimerization methods can be used to investigate the roles of protein−protein interactions or interactions between different protein domains as well as to manipulate cellular functions.[485] The FRB−FKBP−rapamycin heterodimer formation system is one of the most widely used dimerization systems.[485,486] Rapamycin simultaneously binds to FRB and FKBP domains and facilitates formation of a tight

DOI: 10.1021/acs.chemrev.9b00361
Chem. Rev. 2020, 120, 36−78

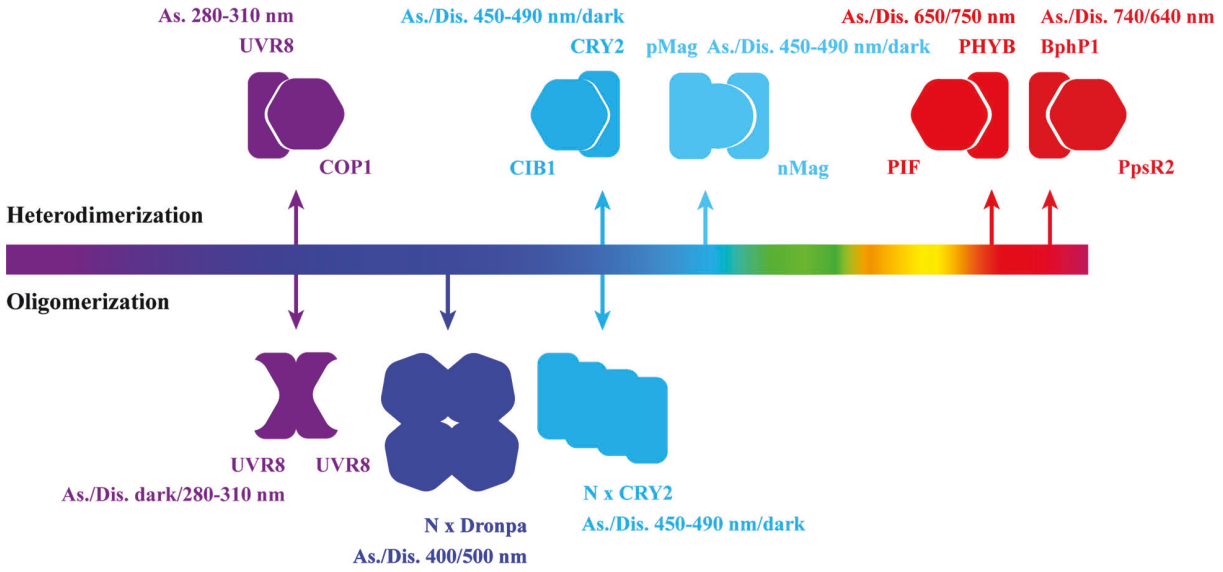

Figure 13. Toolbox of light-sensitive motifs and associated light-induced conformational changes. As./Dis. represent the wavelengths of light used to drive the heterodimerization/oligomerization (association) and dissociation, respectively, of a given photosensitive motif. Some photosensitive motifs do not require light stimulus to initiate the association or dissociation (dark). The color bar in the center shows the wavelengths of light that trigger the light-induced conformational changes. The upper part of the figure shows proteins that display light-induced heterodimerization (UVR8/COP1, CRY2/CIB1, pMag/nMag, PHYB/PIF, and BphP1/PpsR2). The proteins below the color bar demonstrate light-induced oligomerization (UVR8, dimer; Dronpa, $4 \leq N$; CRY2, $N > 1$).

heterodimer system[487,488] (Figure 12B). A photocaged version of rapamycin (pRap) in combination with an engineered rapamycin binding domain (iFKBP) allows for light-induced heterodimerization of domains.[489] Dagliyan et al. designed a unimolecular rapamycin regulatable (uniRapR) domain which is a fusion of iFKBP and FRB.[490] Inserting uniRapR domains into proteins could allosterically regulate their active sites in response to a chemical ligand, rapamycin. Using pRap could potentially transform uniRapR into a tool that offers spatial and temporal control of protein activity. Effective sites for protein insertion could be predicted through an automated approach developed by Dagliyan et al. using a scoring function termed "split energy".[491] SF1 helicases described here do not unwind dsDNA in their monomeric state but work as dimers or oligomers. Chemically inducible dimerization might help us in artificially controlling the oligomerization of such proteins on demand and to regulate their unwinding activity.

All ATPase DNA motor proteins use ATP to power their movement along DNA. Chemical tools can be employed to advance our understanding of the ATPase activity of DNA motors. In the past, several analogues of ATP such as caged ATP[492] and reversible photocontrolled ATP[493] have been synthesized. These ATP analogues have been utilized to understand the motility of individual kinesin molecules.[493] One could use these ATP analogues for artificial control and investigation of ATPase activities.

4.3. Optogenetics

Optogenetics, or more generally optobiology, aims at engineering light-controllable proteins to investigate protein−protein and protein−nucleic acid interactions within physiological contexts or for therapeutic purposes. An ideal optogenetics approach allows one to modulate the function of molecules of interest, both spatially and temporally, with minimal perturbation to the intrinsic biological behavior. Earlier applications of optogenetics have focused on areas such as the interrogation of cell-type-specific neuronal activity,[494] the connection between various molecular mechanisms, and brain circuits underlying specific organism behaviors.[495,496] Well-developed light-sensitive ion channels (channelrhodopsin), pumps (halorhodopsin, bacteriorhodopsin), and chimera enzymes (vertebrate opsins engineered with specific G-protein-coupled receptors)[497] have been used extensively to explore the molecular physiology of the central nervous system (CNS), as well as in numerous clinical applications.[498,499] The fast-growing array of light-sensitive proteins offers a wide range of usable wavelengths of light, allowing researchers to design molecules of interest with suitable light stimuli and avoiding cross-talk with their favorite fluorescent signals (Figure 13).[500,501] These tools are being employed to control gene expression,[502−504] intracellular signaling,[505−508] neuronal activity,[509] cellular cycle,[510] differentiation,[511] migration,[512] and even the behavior of organisms.[513,514] Since the commonly used light-sensitive motifs have been reviewed[497,515−517] extensively (light−oxygen−voltage, cryptochrome, and phytochrome) with a focus on their structures and photochemical properties, the following paragraphs mainly highlight the strategies for engineering light-activated recombinant proteins: (1) spatial control by oligomerization; (2) manipulating the conformation of the engineered recombinant proteins.

4.3.1. Controlling the Spatial Distribution of Engineered Proteins by Oligomerization. Controlling the localization of engineered recombinant proteins within the cell is the most commonly used strategy in designing light-mediated protein systems. There are two kinds of molecular design to achieve spatial confinement of engineered proteins in the cell: heterodimerization and oligomerization. There are two components in the heterodimerization system, the light-sensitive motif and its binding partner protein. The development of pair systems has received much attention in the past decades owing to the diversified needs of engineering proteins with a choice of excitation wavelengths, binding kinetics, and

DOI: 10.1021/acs.chemrev.9b00361
Chem. Rev. 2020, 120, 36−78

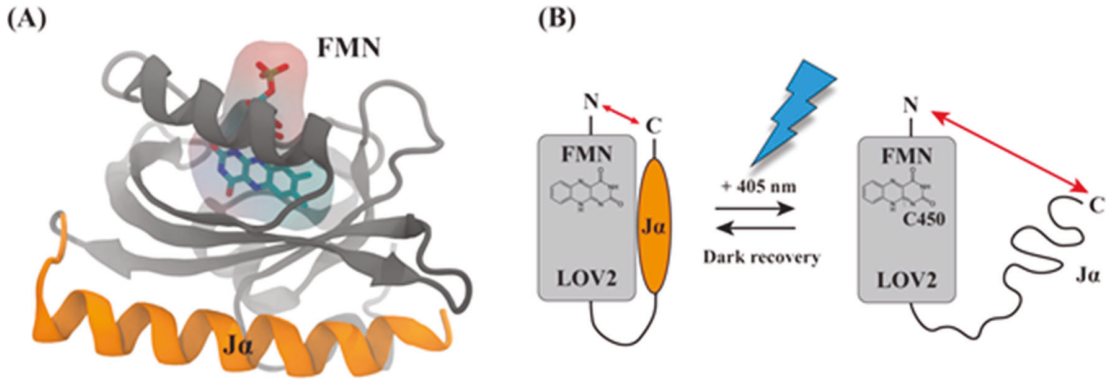

Figure 14. Mechanism of light-induced conformational change of *A. sativa* LOV2. (A) Crystal structure of *A. sativa* LOV2 (PDB: 2V1A[520]). The Jα helix is shown in orange, and the five-stranded antiparallel β-sheet is in gray. The cofactor, FMN (shown in CPK format), binds to LOV2 through the five-stranded antiparallel β-sheet. (B) Mechanism of photoreaction dynamics of LOV2. When LOV2 binds to FMN and is illuminated by blue light (~405 nm), the formation of a flavin-cysteinyl adduct leads to the partial unfolding of the Jα helix and increases the spacing between its two termini. The Jα helix folds back when the blue-light stimulus is turned off; therefore, the distance between the two termini recovered to its original length.

reversibility. The following are some of the most well-studied and widely used pairs: UV response locus 8 and constitutively photomorphogenic 1 (UVR8/COP1), engineered fungal photoreceptor VVD (nMag/pMag), cryptochrome 2 and CIB1 protein (Cry2/CIB1), phytochrome B and phytochrome-interacting factor (PhyB/Pif), and engineered bacterial phytochrome with its partner (BphP1/PpsR2).[497] Based on one's needs, the caged protein can either localize to the nucleus or the cytoplasm. The heterodimerization between the light-sensitive motif and its effector molecule limits the spatial distribution of the engineered protein. When the system is illuminated with appropriate wavelengths of light, light-triggered dissociation releases the heterodimer and allows the engineered protein to redistribute in the cell. Baumschlager et al.[518] introduced a blue-light-triggered gene expression system by engineering T7 RNA polymerase with the VVD system in *Escherichia coli*. The T7 RNA polymerase is split into two fragments (N- and C-terminal domain). The individual fragments are fused with nMag (N-terminal domain fragment) and pMag (C-terminal domain fragment), respectively. Their results showed high gene expression contrast between the cases with and without blue-light stimulus and fast response to the off-expression state upon turning off the light. Another example that used the LOV2 caging strategy is the light-controlled proteasomal degradation tag.[519] Renicke et al. fused the ubiquitin-independent proteasomal degradation motif with the Jα helix. The uncaging of the degron sequence by blue light triggers the degradation of the whole recombinant protein. Such an optogenetic tool allows one to control cellular functions temporally.

Light-controlled nuclear transportation (import and export) systems are reported by Niopek et al. and Yumerefendi et al. independently using similar designing strategies involving LOV2 caging.[521,522] LOV2 (light−oxygen−voltage), a widely used caging domain, is originally isolated from the non-phototropic hypocotyl 1-1 (NPH1-1) gene of *Avena sativa* (Figure 14A).[523] In the dark state, the Jα helix binds to the core domain of LOV2. With blue-light excitation, its local structural rearrangement increases the spacing between its two termini and displaces the Jα helix away from the protein core (Figure 14B).[524] The displacement releases the Jα helix, which leads to the uncaging of the effector domain, since the effector domain is fused with the Jα helix.[525] In the mammalian cell, the binding of the NES motif (nuclear export signal peptide) and CRM1 (nuclear export receptor) leads to the NES-protein exportation from the nucleus to the cytoplasm. In the 2016 study reported by Niopek et al.,[521] the nuclear export signal (NES) is fused with the Jα helix within the LOV2 domain (AsLOV2-caged NES), and the recombinant protein contains histone H2B and AsLOV2-caged NES. When blue light is introduced to the system, the uncaged Jα-NES sequesters CRM1 and inhibits nuclear export. Similarly, Yumerefendi et al. demonstrated light-mediated regulation of histone H2B monoubiquitylation in yeast using the LOV2 caging strategy.[522]

The spatial confinement of engineered proteins can also be controlled by the oligomerization of light-sensitive motifs (Cry2, PhyB).[510,526,527] Either clustering or the sequestration effect by light-induced oligomerization provides the ability to spatially control the concentration of the engineered proteins. The activation or inhibition of a specific cellular activity by light-induced oligomerization has great potential, since it requires only one species of protein to be engineered and less prior structure−function relationship knowledge is needed. The position of insertion of light-sensitive motifs is often treated as the fusion of fluorescent proteins either placed on the N- or C-terminal of the target protein. Light-controlled transcription,[527] granule formation,[528,529] suborganelle assembly/disassembly,[510] and cellular structure formation[530] are some of the applications of the oligomerization strategy.

4.3.2. Manipulating the Conformation of Engineered Proteins. In addition to the methods that control cellular localization, our knowledge of the protein structure−function relationship can guide the modulation of protein function through conformational control. This has been demonstrated for protein phosphorylating enzymes, either by using a small molecule or light as an external control.[531] For example, insertion of the LOV2 domain[532] or FRB-FKBP fusion[490] to a loop allosterically connected to the active site of a kinase can control the kinase activity using light or rapamycin, respectively. Engineered proteins have also been introduced into multicellular organisms and are employed to control cell migration *in vivo*.[533,534] Light-dependent dimerization of engineered Dronpa fluorescent proteins[535] has also been

DOI: 10.1021/acs.chemrev.9b00361
Chem. Rev. 2020, 120, 36−78

reported. Insertion of the Dronpa variant into the N- and C-termini of a kinase hinders binding of kinase substrates at the active site, due to dimerization of Dronpa in the dark. Upon illumination, the dimer dissociates, opening up the binding site for substrate phosphorylation. These approaches, however, require prior knowledge of the structure−function relationship and may suffer from unpredictable protein folding and conformational changes caused by the insertion of control elements. Alternatively, an active site residue may be modified with a "caged" amino acid residue and subsequently uncaged with light on demand, as has been shown for a helicase *in vitro*.[536]

A challenge associated with engineering light-controllable proteins is that prior knowledge of the structure−function relationship of the target protein is required. Without high-resolution protein structures, rational protein design is hard to achieve. Therefore, fewer tools have been developed based on this approach, and to our knowledge, none of them have been applied to DNA motor proteins. Due to the need to finely control DNA motor activity (for example, in helicase and polymerase) to maintain cellular functions, some DNA motors contain an autoinhibitory domain to attenuate their monomer activity. The autoinhibition can be relieved if the DNA motor protein self-oligomerizes or interacts with accessory proteins. If a high-resolution structure is not available for the motor of interest, controlling its activity through the autoinhibitory domain serves as an alternative. This can be achieved via, for instance, light-induced unfolding of the autoinhibitory domain. Modifying the protein with the LOV2 domain is particularly attractive because LOV2 (1) can undergo light-induced end-to-end distance changes (Figure 14B), (2) does not need a partner protein, (3) and has a wide range of mutants available with different photochemical properties.[537] A LOV2 domain can also be inserted into a loop which is located within the autoinhibitory domain of a target protein.[531] Blue light induces unfolding of the LOV2 domain and subsequent partial unfolding of the autoinhibitory domain. The activity of the engineered protein is thus enhanced in the presence of blue light and is attenuated in the dark.

5. CONCLUDING REMARKS AND OUTLOOK

DNA motors are involved in a wide variety of cellular processes such as replication, transcription, DNA segregation, and DNA repair, to name a few. The last two decades have seen the emergence of a plethora of single-molecule techniques, and their applications have provided mechanistic insights into the intricate workings of DNA motors. How DNA motors bind their substrate DNA and translocate directionally, what determines their translocation step size, speed, processivity, and rate of energy consumption, and how they stall, interact with other protein road-blocks, undergo conformational changes upon substrate binding, and cooperate with each other while sharing DNA as their common template are some of the questions pertaining to DNA motors whose answers have been sought using single-molecule methods. An increasing number of cryo-EM structures are now available for a variety of DNA motors. These structures provide a snapshot of the structural intermediates of proteins. With this information in hand, researchers can now design better single-molecule experiments to track the transitions between different structural intermediates in real time. The advent of hybrid single-molecule techniques described earlier has also made it possible to investigate the interactions between different DNA motors in order to obtain a more wholesome, physiologically relevant picture. Most single-molecule measurements of DNA motors are performed with naked oligonucleotides, but recent developments in single-molecule *in vivo* imaging can be applied to DNA motors to study their heterogeneous behavior and their interactions with chromosomal DNA. Single-molecule studies have also focused on understanding the coordination between different DNA motors.

Thus far, single-molecule studies have provided us with a detailed molecular picture of the interactions of DNA motors with their templates, as well as insights into their internal mechanisms. Improvements in structural methods, genetic engineering, and computational tools, in combination with single-molecule techniques, can aid in the engineering of DNA motors to suit various requirements. The tool box of chemical and optogenetics modifications is rapidly evolving, allowing for the design of controllable artificial motors with the ability to function on demand or to perform novel functions, and with customized processivities, speeds, or other parameters. So far, applications of this tool box in the context of DNA motors have been limited. In the future, engineered DNA motors can enhance our current understanding of the causal connections between structures and functions and of the external factors in the environment of an organism that impact the evolution of diverse molecular motors and substrates. It is also likely that these engineered motors will aid in the development of novel biotechnological and therapeutic applications.

AUTHOR INFORMATION

Corresponding Author

*E-mail: tjha@jhu.edu.

ORCID

Taekjip Ha: 0000-0003-2195-6258

Notes

The authors declare no competing financial interest.

Biographies

Sonisilpa Mohapatra received her Masters in Chemistry from National Institute of Science Education and Research (NISER), Bhubaneswar, India. She moved to the U.S. to pursue a Ph.D. in Chemistry at the University of Wisconsin—Madison under the supervision of Prof. James C. Weisshaar. Her thesis research was focused on investigating intracellular spatiotemporal organization of translation and ribosome binding dynamics of translation factors in *E. coli* using super-resolution fluorescence imaging. She is currently a postdoctoral research fellow with Prof. Taekjip Ha in the department of Biophysics and Biophysical Chemistry, Johns Hopkins School of Medicine.

Chang-Ting Lin received his M.Sc. in Biophotonics Engineering from the National Yang-Ming University in Taiwan, where he studied how ionic strength regulates the structural diversity of G-quadruplexes. He then came to the U.S. to pursue his Ph.D. in Biophysics and Biophysical Chemistry at the Johns Hopkins University School of Medicine under the supervision of Dr. Taekjip Ha. His Ph.D. research mainly focused on using optical trapping and protein engineering as tools to investigate protein−nucleic acid interactions.

Xinyu A. Feng received her B.S. in Chemical Biology and B.A. in Computer Science from the University of California, Berkeley. She studied the molecular basis of cyanobacterial photoprotection using X-ray radiolytic labeling in the Lawrence Berkeley National

DOI: 10.1021/acs.chemrev.9b00361
Chem. Rev. 2020, 120, 36−78

Laboratory and the structural basis of gene silencing using cryo-electron microscopy in the Nogales Lab. She is currently pursuing a Ph.D. in Biology at the Johns Hopkins University under the co-mentorship of Dr. Taekjip Ha and Dr. Carl Wu. Her research mainly focuses on mechanisms of chromatin remodeling.

Aakash Basu received a Ph.D. in Applied Physics from Stanford University, where he worked in the laboratory of his thesis advisor Prof. Zev Bryant. He built high-resolution single-molecule instruments to dissect the mechanochemical cycle of the topoisomerase DNA gyrase. Subsequently, he was a postdoctoral researcher in Prof. A. James Hudspeth's laboratory at The Rockefeller University. He combined electrical measurements with high-throughput magnetic tweezing to apply controlled molecular-scale forces on mechanically gated inner-ear ion channels on a tissue-wide scale. He directly established the role of cadherin proteins in channel gating. He is currently a postdoctoral researcher in Prof. Taekjip Ha's laboratory at Johns Hopkins University, where he is continuing work on developing hybrid single-molecule techniques. He is addressing the question of how the sequence dependence of the physical properties of DNA affects downstream biological processes.

Taekjip Ha is a Bloomberg Distinguished Professor of Biophysics and Biomedical Engineering at Johns Hopkins University. He is also an investigator with the Howard Hughes Medical Institute. He uses sophisticated physical techniques to manipulate and visualize the movements of single molecules to understand basic biological processes involving DNA and other molecules. His research pushes the limits of single-molecule detection methods to study protein–nucleic acid and protein–protein complexes and the mechanical regulation of their functions. He received his undergraduate degree in Physics from Seoul National University in 1990 and his Physics Ph.D from University of California at Berkeley in 1996. After postdoctoral training at Stanford University, he was a Physics professor at University of Illinois at Urbana–Champaign until 2015.

ACKNOWLEDGMENTS

The authors acknowledge Dr. Carl Wu, Brian Y. Soong, Jasmin Zarb, Wesley Yon, and Vinu Harihar for helpful suggestions and critical reading of the manuscript. Research in the Ha laboratory is funded by the grants from the National Science Foundation (PHY 1430124, EFMA 1933303, and EF 1934864) and the National Institutes of Health (GM 112659, GM 122569). T.H. is an investigator of the Howard Hughes Medical Institute.

REFERENCES

(1) Mirny, L.; Slutsky, M.; Wunderlich, Z.; Tafvizi, A.; Leith, J.; Kosmrlj, A. How a Protein Searches for Its Site on DNA: The Mechanism of Facilitated Diffusion. *J. Phys. A: Math. Theor.* **2009**, *42*, 434013.

(2) Ha, T.; Kozlov, A. G.; Lohman, T. M. Single-Molecule Views of Protein Movement on Single-Stranded DNA. *Annu. Rev. Biophys.* **2012**, *41*, 295–319.

(3) Saikrishnan, K.; Powell, B.; Cook, N. J.; Webb, M. R.; Wigley, D. B. Mechanistic Basis of 5′-3′ Translocation in Sf1b Helicases. *Cell* **2009**, *137*, 849–59.

(4) Wuite, G. J. L.; Smith, S. B.; Young, M.; Keller, D.; Bustamante, C. Single-Molecule Studies of the Effect of Template Tension on T7 DNA Polymerase Activity. *Nature* **2000**, *404*, 103–106.

(5) Derrington, I. M.; Craig, J. M.; Stava, E.; Laszlo, A. H.; Ross, B. C.; Brinkerhoff, H.; Nova, I. C.; Doering, K.; Tickman, B. I.; Ronaghi, M.; Mandell, J. G.; Gunderson, K. L.; Gundlach, J. H. Subangstrom Single-Molecule Measurements of Motor Proteins Using a Nanopore. *Nat. Biotechnol.* **2015**, *33*, 1073–5.

(6) Myong, S.; Bruno, M. M.; Pyle, A. M.; Ha, T. Spring-Loaded Mechanism of DNA Unwinding by Hepatitis C Virus Ns3 Helicase. *Science* **2007**, *317*, 513–6.

(7) Syed, S.; Pandey, M.; Patel, S. S.; Ha, T. Single-Molecule Fluorescence Reveals the Unwinding Stepping Mechanism of Replicative Helicase. *Cell Rep.* **2014**, *6*, 1037–45.

(8) Lee, G.; Bratkowski, M. A.; Ding, F.; Ke, A.; Ha, T. Elastic Coupling between RNA Degradation and Unwinding by an Exoribonuclease. *Science* **2012**, *336*, 1726–9.

(9) Whitley, K. D.; Comstock, M. J.; Jia, H.; Lohman, T. M.; Chemla, Y. R. Direct Observation of the Stepping Behavior of E. Coli Uvrd Helicase. *Biophys. J.* **2016**, *110*, 561a.

(10) Loeff, L.; Brouns, S. J. J.; Joo, C. Repetitive DNA Reeling by the Cascade-Cas3 Complex in Nucleotide Unwinding Steps. *Mol. Cell* **2018**, *70*, 385–394.e3.

(11) Moffitt, J. R.; Chemla, Y. R.; Aathavan, K.; Grimes, S.; Jardine, P. J.; Anderson, D. L.; Bustamante, C. Intersubunit Coordination in a Homomeric Ring Atpase. *Nature* **2009**, *457*, 446–50.

(12) Saleh, O. A.; Perals, C.; Barre, F. X.; Allemand, J. F. Fast, DNA-Sequence Independent Translocation by Ftsk in a Single-Molecule Experiment. *EMBO J.* **2004**, *23*, 2430–9.

(13) Elshenawy, M. M.; Jergic, S.; Xu, Z. Q.; Sobhy, M. A.; Takahashi, M.; Oakley, A. J.; Dixon, N. E.; Hamdan, S. M. Replisome Speed Determines the Efficiency of the Tus-Ter Replication Termination Barrier. *Nature* **2015**, *525*, 394–8.

(14) Mangiameli, S. M.; Merrikh, C. N.; Wiggins, P. A.; Merrikh, H. Transcription Leads to Pervasive Replisome Instability in Bacteria. *eLife* **2017**, *6*, No. e19848.

(15) Liu, S.; Chistol, G.; Hetherington, C. L.; Tafoya, S.; Aathavan, K.; Schnitzbauer, J.; Grimes, S.; Jardine, P. J.; Bustamante, C. A Viral Packaging Motor Varies Its DNA Rotation and Step Size to Preserve Subunit Coordination as the Capsid Fills. *Cell* **2014**, *157*, 702–713.

(16) Rasnik, I.; McKinney, S. A.; Ha, T. Nonblinking and Long-Lasting Single-Molecule Fluorescence Imaging. *Nat. Methods* **2006**, *3*, 891–3.

(17) Ha, T.; Tinnefeld, P. Photophysics of Fluorescent Probes for Single-Molecule Biophysics and Super-Resolution Imaging. *Annu. Rev. Phys. Chem.* **2012**, *63*, 595–617.

(18) Prabhakar, A.; Choi, J.; Wang, J.; Petrov, A.; Puglisi, J. D. Dynamic Basis of Fidelity and Speed in Translation: Coordinated Multistep Mechanisms of Elongation and Termination. *Protein Sci.* **2017**, *26*, 1352–1362.

(19) Perez, C. E.; Gonzalez, R. L., Jr. In Vitro and in Vivo Single-Molecule Fluorescence Imaging of Ribosome-Catalyzed Protein Synthesis. *Curr. Opin. Chem. Biol.* **2011**, *15*, 853–63.

(20) Forster, T. Zwischenmolekulare Energiewanderung Und Fluoreszenz. *Ann. Phys.* **1948**, *437*, 55–75.

(21) Ha, T.; Enderle, T.; Ogletree, D. F.; Chemla, D. S.; Selvin, P. R.; Weiss, S. Probing the Interaction between Two Single Molecules: Fluorescence Resonance Energy Transfer between a Single Donor and a Single Acceptor. *Proc. Natl. Acad. Sci. U. S. A.* **1996**, *93*, 6264–8.

(22) Roy, R.; Hohng, S.; Ha, T. A Practical Guide to Single-Molecule Fret. *Nat. Methods* **2008**, *5*, 507–16.

(23) Lerner, E.; Cordes, T.; Ingargiola, A.; Alhadid, Y.; Chung, S.; Michalet, X.; Weiss, S. Toward Dynamic Structural Biology: Two Decades of Single-Molecule Forster Resonance Energy Transfer. *Science* **2018**, *359*, eaan1133.

(24) Dimura, M.; Peulen, T. O.; Hanke, C. A.; Prakash, A.; Gohlke, H.; Seidel, C. A. Quantitative Fret Studies and Integrative Modeling Unravel the Structure and Dynamics of Biomolecular Systems. *Curr. Opin. Struct. Biol.* **2016**, *40*, 163–185.

(25) Grimm, J. B.; Muthusamy, A. K.; Liang, Y.; Brown, T. A.; Lemon, W. C.; Patel, R.; Lu, R.; Macklin, J. J.; Keller, P. J.; Ji, N.; Lavis, L. D. A General Method to Fine-Tune Fluorophores for Live-Cell and in Vivo Imaging. *Nat. Methods* **2017**, *14*, 987–994.

(26) Dempsey, D. R.; Jiang, H.; Kalin, J. H.; Chen, Z.; Cole, P. A. Site-Specific Protein Labeling with N-Hydroxysuccinimide-Esters and the Analysis of Ubiquitin Ligase Mechanisms. *J. Am. Chem. Soc.* **2018**, *140*, 9374–9378.

DOI: 10.1021/acs.chemrev.9b00361
Chem. Rev. 2020, 120, 36–78

(27) Keppler, A.; Gendreizig, S.; Gronemeyer, T.; Pick, H.; Vogel, H.; Johnsson, K. A General Method for the Covalent Labeling of Fusion Proteins with Small Molecules *in vivo*. *Nat. Biotechnol.* **2003**, *21*, 86−9.
(28) Los, G. V.; Encell, L. P.; McDougall, M. G.; Hartzell, D. D.; Karassina, N.; Zimprich, C.; Wood, M. G.; Learish, R.; Ohana, R. F.; Urh, M.; Simpson, D.; Mendez, J.; Zimmerman, K.; Otto, P.; Vidugiris, G.; Zhu, J.; Darzins, A.; Klaubert, D. H.; Bulleit, R. F.; Wood, K. V. Halotag: A Novel Protein Labeling Technology for Cell Imaging and Protein Analysis. *ACS Chem. Biol.* **2008**, *3*, 373−82.
(29) Theile, C. S.; Witte, M. D.; Blom, A. E.; Kundrat, L.; Ploegh, H. L.; Guimaraes, C. P. Site-Specific N-Terminal Labeling of Proteins Using Sortase-Mediated Reactions. *Nat. Protoc.* **2013**, *8*, 1800−7.
(30) Guimaraes, C. P.; Witte, M. D.; Theile, C. S.; Bozkurt, G.; Kundrat, L.; Blom, A. E.; Ploegh, H. L. Site-Specific C-Terminal and Internal Loop Labeling of Proteins Using Sortase-Mediated Reactions. *Nat. Protoc.* **2013**, *8*, 1787−99.
(31) Wang, K.; Sachdeva, A.; Cox, D. J.; Wilf, N. M.; Lang, K.; Wallace, S.; Mehl, R. A.; Chin, J. W. Optimized Orthogonal Translation of Unnatural Amino Acids Enables Spontaneous Protein Double-Labelling and Fret. *Nat. Chem.* **2014**, *6*, 393−403.
(32) Jain, A.; Liu, R.; Ramani, B.; Arauz, E.; Ishitsuka, Y.; Ragunathan, K.; Park, J.; Chen, J.; Xiang, Y. K.; Ha, T. Probing Cellular Protein Complexes Using Single-Molecule Pull-Down. *Nature* **2011**, *473*, 484−8.
(33) Wang, Q.; Moerner, W. E. Single-Molecule Motions Enable Direct Visualization of Biomolecular Interactions in Solution. *Nat. Methods* **2014**, *11*, 555−8.
(34) Wilson, H.; Windeler, R. S.; Wang, Q.; Gregor, I.; Gryczynski, Z. K.; Koberling, F. Tetherless, Precise and Extended Observation of Single-Molecule Fret in an Anti-Brownian Trap. *Single Molecule Spectroscopy and Superresolution Imaging XII*; 2019.
(35) Deniz, A. A.; Laurence, T. A.; Dahan, M.; Chemla, D. S.; Schultz, P. G.; Weiss, S. Ratiometric Single-Molecule Studies of Freely Diffusing Biomolecules. *Annu. Rev. Phys. Chem.* **2001**, *52*, 233−53.
(36) Ha, T.; Ting, A. Y.; Liang, J.; Caldwell, W. B.; Deniz, A. A.; Chemla, D. S.; Schultz, P. G.; Weiss, S. Single-Molecule Fluorescence Spectroscopy of Enzyme Conformational Dynamics and Cleavage Mechanism. *Proc. Natl. Acad. Sci. U. S. A.* **1999**, *96*, 893−8.
(37) Hwang, H.; Kim, H.; Myong, S. Protein Induced Fluorescence Enhancement as a Single Molecule Assay with Short Distance Sensitivity. *Proc. Natl. Acad. Sci. U. S. A.* **2011**, *108*, 7414−8.
(38) Lee, J.-B.; Hite, R. K.; Hamdan, S. M.; Sunney Xie, X.; Richardson, C. C.; van Oijen, A. M. DNA Primase Acts as a Molecular Brake in DNA Replication. *Nature* **2006**, *439*, 621−624.
(39) van Oijen, A. M.; Blainey, P. C.; Crampton, D. J.; Richardson, C. C.; Ellenberger, T.; Xie, X. S. Single-Molecule Kinetics of λ Exonuclease Reveal Base Dependence and Dynamic Disorder. *Science* **2003**, *301*, 1235.
(40) Hamdan, S. M.; Loparo, J. J.; Takahashi, M.; Richardson, C. C.; van Oijen, A. M. Dynamics of DNA replication loops reveal temporal control of lagging-strand synthesis. *Nature* **2009**, *457*, 336−9.
(41) Yodh, J. G.; Schlierf, M.; Ha, T. Insight into Helicase Mechanism and Function Revealed through Single-Molecule Approaches. *Q. Rev. Biophys.* **2010**, *43*, 185−217.
(42) Hamdan, S. M.; Johnson, D. E.; Tanner, N. A.; Lee, J.-B.; Qimron, U.; Tabor, S.; van Oijen, A. M.; Richardson, C. C. Dynamic DNA Helicase-DNA Polymerase Interactions Assure Processive Replication Fork Movement. *Mol. Cell* **2007**, *27*, 539−549.
(43) Blainey, P. C.; van Oijen, A. M.; Banerjee, A.; Verdine, G. L.; Xie, X. S. A Base-Excision DNA-Repair Protein Finds Intrahelical Lesion Bases by Fast Sliding in Contact with DNA. *Proc. Natl. Acad. Sci. U. S. A.* **2006**, *103*, 5752.
(44) Doyle, P. S.; Ladoux, B.; Viovy, J.-L. Dynamics of a Tethered Polymer in Shear Flow. *Phys. Rev. Lett.* **2000**, *84*, 4769−4772.
(45) Fazio, T.; Visnapuu, M.-L.; Wind, S.; Greene, E. C. DNA Curtains and Nanoscale Curtain Rods: High-Throughput Tools for Single Molecule Imaging. *Langmuir* **2008**, *24*, 10524−10531.
(46) Gorman, J.; Fazio, T.; Wang, F.; Wind, S.; Greene, E. C. Nanofabricated Racks of Aligned and Anchored DNA Substrates for Single-Molecule Imaging. *Langmuir* **2010**, *26*, 1372−1379.
(47) Granéli, A.; Yeykal, C. C.; Prasad, T. K.; Greene, E. C. Organized Arrays of Individual DNA Molecules Tethered to Supported Lipid Bilayers. *Langmuir* **2006**, *22*, 292−299.
(48) Visnapuu, M.-L.; Fazio, T.; Wind, S.; Greene, E. C. Parallel Arrays of Geometric Nanowells for Assembling Curtains of DNA with Controlled Lateral Dispersion. *Langmuir* **2008**, *24*, 11293−11299.
(49) Gibb, B.; Silverstein, T. D.; Finkelstein, I. J.; Greene, E. C. Single-Stranded DNA Curtains for Real-Time Single-Molecule Visualization of Protein−Nucleic Acid Interactions. *Anal. Chem.* **2012**, *84*, 7607−7612.
(50) Ma, C. J.; Gibb, B.; Kwon, Y.; Sung, P.; Greene, E. C. Protein Dynamics of Human Rpa and Rad51 on Ssdna During Assembly and Disassembly of the Rad51 Filament. *Nucleic Acids Res.* **2017**, *45*, 749−761.
(51) Gibb, B.; Ye, L. F.; Kwon, Y.; Niu, H.; Sung, P.; Greene, E. C. Protein Dynamics During Presynaptic-Complex Assembly on Individual Single-Stranded DNA Molecules. *Nat. Struct. Mol. Biol.* **2014**, *21*, 893−900.
(52) Betzig, E.; Patterson, G. H.; Sougrat, R.; Lindwasser, O. W.; Olenych, S.; Bonifacino, J. S.; Davidson, M. W.; Lippincott-Schwartz, J.; Hess, H. F. Imaging Intracellular Fluorescent Proteins at Nanometer Resolution. *Science* **2006**, *313*, 1642.
(53) Hess, S. T.; Girirajan, T. P. K.; Mason, M. D. Ultra-High Resolution Imaging by Fluorescence Photoactivation Localization Microscopy. *Biophys. J.* **2006**, *91*, 4258−4272.
(54) Rust, M. J.; Bates, M.; Zhuang, X. Sub-Diffraction-Limit Imaging by Stochastic Optical Reconstruction Microscopy (Storm). *Nat. Methods* **2006**, *3*, 793−795.
(55) Klar, T. A.; Jakobs, S.; Dyba, M.; Egner, A.; Hell, S. W. Fluorescence Microscopy with Diffraction Resolution Barrier Broken by Stimulated Emission. *Proc. Natl. Acad. Sci. U. S. A.* **2000**, *97*, 8206.
(56) Chozinski, T. J.; Gagnon, L. A.; Vaughan, J. C. Twinkle, Twinkle Little Star: Photoswitchable Fluorophores for Super-Resolution Imaging. *FEBS Lett.* **2014**, *588*, 3603−3612.
(57) Landgraf, D.; Okumus, B.; Chien, P.; Baker, T. A.; Paulsson, J. Segregation of Molecules at Cell Division Reveals Native Protein Localization. *Nat. Methods* **2012**, *9*, 480.
(58) Thompson, R. E.; Larson, D. R.; Webb, W. W. Precise Nanometer Localization Analysis for Individual Fluorescent Probes. *Biophys. J.* **2002**, *82*, 2775−2783.
(59) Smith, C. S.; Joseph, N.; Rieger, B.; Lidke, K. A. Fast, Single-Molecule Localization That Achieves Theoretically Minimum Uncertainty. *Nat. Methods* **2010**, *7*, 373.
(60) Winter, F. R.; Loidolt, M.; Westphal, V.; Butkevich, A. N.; Gregor, C.; Sahl, S. J.; Hell, S. W. Multicolour Nanoscopy of Fixed and Living Cells with a Single Sted Beam and Hyperspectral Detection. *Sci. Rep.* **2017**, *7*, 46492.
(61) Valm, A. M.; Cohen, S.; Legant, W. R.; Melunis, J.; Hershberg, U.; Wait, E.; Cohen, A. R.; Davidson, M. W.; Betzig, E.; Lippincott-Schwartz, J. Applying Systems-Level Spectral Imaging and Analysis to Reveal the Organelle Interactome. *Nature* **2017**, *546*, 162−167.
(62) Bates, M.; Huang, B.; Dempsey, G. T.; Zhuang, X. Multicolor Super-Resolution Imaging with Photo-Switchable Fluorescent Probes. *Science* **2007**, *317*, 1749.
(63) Mohapatra, S.; Weisshaar, J. C. Modified Pearson Correlation Coefficient for Two-Color Imaging in Spherocylindrical Cells. *BMC Bioinf.* **2018**, *19*, 428.
(64) Ehmann, N.; van de Linde, S.; Alon, A.; Ljaschenko, D.; Keung, X. Z.; Holm, T.; Rings, A.; DiAntonio, A.; Hallermann, S.; Ashery, U.; Heckmann, M.; Sauer, M.; Kittel, R. J. Quantitative Super-Resolution Imaging of Bruchpilot Distinguishes Active Zone States. *Nat. Commun.* **2014**, *5*, 4650.
(65) Lee, S.-H.; Shin, J. Y.; Lee, A.; Bustamante, C. Counting Single Photoactivatable Fluorescent Molecules by Photoactivated Localization Microscopy (Palm). *Proc. Natl. Acad. Sci. U. S. A.* **2012**, *109*, 17436.

DOI: 10.1021/acs.chemrev.9b00361
Chem. Rev. 2020, 120, 36−78

(66) Finan, K.; Raulf, A.; Heilemann, M. A Set of Homo-Oligomeric Standards Allows Accurate Protein Counting. *Angew. Chem., Int. Ed.* **2015**, *54*, 12049−12052.
(67) Rollins, G. C.; Shin, J. Y.; Bustamante, C.; Pressé, S. Stochastic Approach to the Molecular Counting Problem in Superresolution Microscopy. *Proc. Natl. Acad. Sci. U. S. A.* **2015**, *112*, E110−E118.
(68) Hummer, G.; Fricke, F.; Heilemann, M. Model-Independent Counting of Molecules in Single-Molecule Localization Microscopy. *Mol. Biol. Cell* **2016**, *27*, 3637−3644.
(69) Jungmann, R.; Avendaño, M. S.; Dai, M.; Woehrstein, J. B.; Agasti, S. S.; Feiger, Z.; Rodal, A.; Yin, P. Quantitative Super-Resolution Imaging with Qpaint. *Nat. Methods* **2016**, *13*, 439.
(70) Manley, S.; Gillette, J. M.; Patterson, G. H.; Shroff, H.; Hess, H. F.; Betzig, E.; Lippincott-Schwartz, J. High-Density Mapping of Single-Molecule Trajectories with Photoactivated Localization Microscopy. *Nat. Methods* **2008**, *5*, 155.
(71) Hansen, A. S.; Woringer, M.; Grimm, J. B.; Lavis, L. D.; Tjian, R.; Darzacq, X. Robust Model-Based Analysis of Single-Particle Tracking Experiments with Spot-On. *eLife* **2018**, *7*, e33125.
(72) Chenouard, N.; Smal, I.; de Chaumont, F.; Maška, M.; Sbalzarini, I. F.; Gong, Y.; Cardinale, J.; Carthel, C.; Coraluppi, S.; Winter, M.; Cohen, A. R.; Godinez, W. J.; Rohr, K.; Kalaidzidis, Y.; Liang, L.; Duncan, J.; Shen, H.; Xu, Y.; Magnusson, K. E. G.; Jaldén, J.; Blau, H. M.; Paul-Gilloteaux, P.; Roudot, P.; Kervrann, C.; Waharte, F.; Tinevez, J.-Y.; Shorte, S. L.; Willemse, J.; Celler, K.; van Wezel, G. P.; Dan, H.-W.; Tsai, Y.-S.; de Solórzano, C. O.; Olivo-Marin, J.-C.; Meijering, E. Objective Comparison of Particle Tracking Methods. *Nat. Methods* **2014**, *11*, 281.
(73) Sahl, S. J.; Hell, S. W.; Jakobs, S. Fluorescence Nanoscopy in Cell Biology. *Nat. Rev. Mol. Cell Biol.* **2017**, *18*, 685.
(74) Wang, H.; Dodd, I. B.; Dunlap, D. D.; Shearwin, K. E.; Finzi, L. Single Molecule Analysis of DNA Wrapping and Looping by a Circular 14mer Wheel of the Bacteriophage 186 Ci Repressor. *Nucleic Acids Res.* **2013**, *41*, 5746−56.
(75) Priest, D. G.; Kumar, S.; Yan, Y.; Dunlap, D. D.; Dodd, I. B.; Shearwin, K. E. Quantitation of Interactions between Two DNA Loops Demonstrates Loop Domain Insulation in E. Coli Cells. *Proc. Natl. Acad. Sci. U. S. A.* **2014**, *111*, E4449−57.
(76) Laurens, N.; Bellamy, S. R.; Harms, A. F.; Kovacheva, Y. S.; Halford, S. E.; Wuite, G. J. Dissecting Protein-Induced DNA Looping Dynamics in Real Time. *Nucleic Acids Res.* **2009**, *37*, 5454−64.
(77) Vanzi, F.; Vladimirov, S.; Knudsen, C. R.; Goldman, Y. E.; Cooperman, B. S. Protein Synthesis by Single Ribosomes. *RNA* **2003**, *9*, 1174−9.
(78) Ucuncuoglu, S.; Schneider, D. A.; Weeks, E. R.; Dunlap, D.; Finzi, L. Multiplexed, Tethered Particle Microscopy for Studies of DNA-Enzyme Dynamics. *Methods Enzymol.* **2017**, *582*, 415−435.
(79) Lovely, G. A.; Brewster, R. C.; Schatz, D. G.; Baltimore, D.; Phillips, R. Single-Molecule Analysis of Rag-Mediated V(D)J DNA Cleavage. *Proc. Natl. Acad. Sci. U. S. A.* **2015**, *112*, E1715−23.
(80) Lu, C. H.; Yeh, H. Y.; Su, G. C.; Ito, K.; Kurokawa, Y.; Iwasaki, H.; Chi, P.; Li, H. W. Swi5-Sfr1 Stimulates Rad51 Recombinase Filament Assembly by Modulating Rad51 Dissociation. *Proc. Natl. Acad. Sci. U. S. A.* **2018**, *115*, E10059−E10068.
(81) Fan, H. F.; Ma, C. H.; Jayaram, M. Single-Molecule Tethered Particle Motion: Stepwise Analyses of Site-Specific DNA Recombination. *Micromachines (Basel)* **2018**, *9*, 216.
(82) Schafer, D. A.; Gelles, J.; Sheetz, M. P.; Landick, R. Transcription by Single Molecules of Rna Polymerase Observed by Light Microscopy. *Nature* **1991**, *352*, 444−8.
(83) Dohoney, K. M.; Gelles, J. Chi-Sequence Recognition and DNA Translocation by Single Recbcd Helicase/Nuclease Molecules. *Nature* **2001**, *409*, 370−4.
(84) Chung, C.; Li, H. W. Direct Observation of Recbcd Helicase as Single-Stranded DNA Translocases. *J. Am. Chem. Soc.* **2013**, *135*, 8920−5.
(85) Plenat, T.; Tardin, C.; Rousseau, P.; Salome, L. High-Throughput Single-Molecule Analysis of DNA-Protein Interactions by Tethered Particle Motion. *Nucleic Acids Res.* **2012**, *40*, e89.
(86) May, P. F. J.; Pinkney, J. N. M.; Zawadzki, P.; Evans, G. W.; Sherratt, D. J.; Kapanidis, A. N. Tethered Fluorophore Motion: Studying Large DNA Conformational Changes by Single-Fluorophore Imaging. *Biophys. J.* **2014**, *107*, 1205−1216.
(87) Blumberg, S.; Gajraj, A.; Pennington, M. W.; Meiners, J. C. Three-Dimensional Characterization of Tethered Microspheres by Total Internal Reflection Fluorescence Microscopy. *Biophys. J.* **2005**, *89*, 1272−81.
(88) Dunlap, D.; Zurla, C.; Manzo, C.; Finzi, L. Probing DNA Topology Using Tethered Particle Motion. *Methods Mol. Biol.* **2011**, *783*, 295−313.
(89) Han, L.; Lui, B. H.; Blumberg, S.; Beausang, J. F.; Nelson, P. C.; Phillips, R. Calibration of Tethered Particle Motion Experiments. *IMA Vol. Math. Its Appl.* **2009**, *150*, 123.
(90) Ashkin, A.; Dziedzic, J. M.; Bjorkholm, J. E.; Chu, S. Observation of a Single-Beam Gradient Force Optical Trap for Dielectric Particles. *Opt. Lett.* **1986**, *11*, 288.
(91) Ngo, T. T.; Zhang, Q.; Zhou, R.; Yodh, J. G.; Ha, T. Asymmetric Unwrapping of Nucleosomes under Tension Directed by DNA Local Flexibility. *Cell* **2015**, *160*, 1135−44.
(92) Bintu, L.; Ishibashi, T.; Dangkulwanich, M.; Wu, Y. Y.; Lubkowska, L.; Kashlev, M.; Bustamante, C. Nucleosomal Elements That Control the Topography of the Barrier to Transcription. *Cell* **2012**, *151*, 738−749.
(93) Morin, J. A.; Cao, F. J.; Lazaro, J. M.; Arias-Gonzalez, J. R.; Valpuesta, J. M.; Carrascosa, J. L.; Salas, M.; Ibarra, B. Active DNA Unwinding Dynamics During Processive DNA Replication. *Proc. Natl. Acad. Sci. U. S. A.* **2012**, *109*, 8115−20.
(94) Dechassa, M. L.; Wyns, K.; Li, M.; Hall, M. A.; Wang, M. D.; Luger, K. Structure and Scm3-Mediated Assembly of Budding Yeast Centromeric Nucleosomes. *Nat. Commun.* **2011**, *2*, 313.
(95) Forget, A. L.; Kowalczykowski, S. C. Single-Molecule Imaging of DNA Pairing by Reca Reveals a Three-Dimensional Homology Search. *Nature* **2012**, *482*, 423−7.
(96) Abbondanzieri, E. A.; Greenleaf, W. J.; Shaevitz, J. W.; Landick, R.; Block, S. M. Direct Observation of Base-Pair Stepping by Rna Polymerase. *Nature* **2005**, *438*, 460−5.
(97) Moffitt, J. R.; Chemla, Y. R.; Izhaky, D.; Bustamante, C. Differential Detection of Dual Traps Improves the Spatial Resolution of Optical Tweezers. *Proc. Natl. Acad. Sci. U. S. A.* **2006**, *103*, 9006−11.
(98) Carter, A. R.; Seol, Y.; Perkins, T. T. Precision Surface-Coupled Optical-Trapping Assay with One-Basepair Resolution. *Biophys. J.* **2009**, *96*, 2926−34.
(99) De Vlaminck, I.; Dekker, C. Recent Advances in Magnetic Tweezers. *Annu. Rev. Biophys.* **2012**, *41*, 453−72.
(100) Koster, D. A.; Croquette, V.; Dekker, C.; Shuman, S.; Dekker, N. H. Friction and Torque Govern the Relaxation of DNA Supercoils by Eukaryotic Topoisomerase Ib. *Nature* **2005**, *434*, 671−4.
(101) Revyakin, A.; Liu, C.; Ebright, R. H.; Strick, T. R. Abortive Initiation and Productive Initiation by Rna Polymerase Involve DNA Scrunching. *Science* **2006**, *314*, 1139−43.
(102) Lipfert, J.; Wiggin, M.; Kerssemakers, J. W.; Pedaci, F.; Dekker, N. H. Freely Orbiting Magnetic Tweezers to Directly Monitor Changes in the Twist of Nucleic Acids. *Nat. Commun.* **2011**, *2*, 439.
(103) Basu, A.; Schoeffler, A. J.; Berger, J. M.; Bryant, Z. Atp Binding Controls Distinct Structural Transitions of Escherichia Coli DNA Gyrase in Complex with DNA. *Nat. Struct. Mol. Biol.* **2012**, *19*, 538−46.
(104) Lebel, P.; Basu, A.; Oberstrass, F. C.; Tretter, E. M.; Bryant, Z. Gold Rotor Bead Tracking for High-Speed Measurements of DNA Twist, Torque and Extension. *Nat. Methods* **2014**, *11*, 456−62.
(105) Basu, A.; Hobson, M.; Lebel, P.; Fernandes, L. E.; Tretter, E. M.; Berger, J. M.; Bryant, Z. Dynamic Coupling between Conformations and Nucleotide States in DNA Gyrase. *Nat. Chem. Biol.* **2018**, *14*, 565−574.

DOI: 10.1021/acs.chemrev.9b00361
Chem. Rev. 2020, 120, 36−78

(106) Lipfert, J.; Kerssemakers, J. W.; Jager, T.; Dekker, N. H. Magnetic Torque Tweezers: Measuring Torsional Stiffness in DNA and Reca-DNA Filaments. *Nat. Methods* **2010**, *7*, 977−80.
(107) Janssen, X. J.; Lipfert, J.; Jager, T.; Daudey, R.; Beekman, J.; Dekker, N. H. Electromagnetic Torque Tweezers: A Versatile Approach for Measurement of Single-Molecule Twist and Torque. *Nano Lett.* **2012**, *12*, 3634−9.
(108) Oberstrass, F. C.; Fernandes, L. E.; Bryant, Z. Torque Measurements Reveal Sequence-Specific Cooperative Transitions in Supercoiled DNA. *Proc. Natl. Acad. Sci. U. S. A.* **2012**, *109*, 6106−11.
(109) Seol, Y.; Neuman, K. C. Combined Magnetic Tweezers and Micro-Mirror Total Internal Reflection Fluorescence Microscope for Single-Molecule Manipulation and Visualization. *Methods Mol. Biol.* **2018**, *1665*, 297−316.
(110) Gunn, K. H.; Marko, J. F.; Mondragon, A. An Orthogonal Single-Molecule Experiment Reveals Multiple-Attempt Dynamics of Type Ia Topoisomerases. *Nat. Struct. Mol. Biol.* **2017**, *24*, 484−490.
(111) Graves, E. T.; Duboc, C.; Fan, J.; Stransky, F.; Leroux-Coyau, M.; Strick, T. R. A Dynamic DNA-Repair Complex Observed by Correlative Single-Molecule Nanomanipulation and Fluorescence. *Nat. Struct. Mol. Biol.* **2015**, *22*, 452−7.
(112) Fan, J.; Leroux-Coyau, M.; Savery, N. J.; Strick, T. R. Reconstruction of Bacterial Transcription-Coupled Repair at Single-Molecule Resolution. *Nature* **2016**, *536*, 234−7.
(113) Kemmerich, F. E.; Swoboda, M.; Kauert, D. J.; Grieb, M. S.; Hahn, S.; Schwarz, F. W.; Seidel, R.; Schlierf, M. Simultaneous Single-Molecule Force and Fluorescence Sampling of DNA Nanostructure Conformations Using Magnetic Tweezers. *Nano Lett.* **2016**, *16*, 381−6.
(114) Ivanov, I. E.; Lebel, P.; Oberstrass, F. C.; Starr, C. H.; Parente, A. C.; Ierokomos, A.; Bryant, Z. Multimodal Measurements of Single-Molecule Dynamics Using Fluorbt. *Biophys. J.* **2018**, *114*, 278−282.
(115) De Vlaminck, I.; Henighan, T.; van Loenhout, M. T.; Pfeiffer, I.; Huijts, J.; Kerssemakers, J. W.; Katan, A. J.; van Langen-Suurling, A.; van der Drift, E.; Wyman, C.; Dekker, C. Highly Parallel Magnetic Tweezers by Targeted DNA Tethering. *Nano Lett.* **2011**, *11*, 5489−93.
(116) Basu, A.; Lagier, S.; Vologodskaia, M.; Fabella, B. A.; Hudspeth, A. J. Direct Mechanical Stimulation of Tip Links in Hair Cells through DNA Tethers. *eLife* **2016**, *5*, No. e16041.
(117) Zhong, Q.; Inniss, D.; Kjoller, K.; Elings, V. B. Fractured Polymer/Silica Fiber Surface Studied by Tapping Mode Atomic Force Microscopy. *Surf. Sci.* **1993**, *290*, L688−L692.
(118) Hansma, H. G.; Sinsheimer, R. L.; Groppe, J.; Bruice, T. C.; Elings, V.; Gurley, G.; Bezanilla, M.; Mastrangelo, I. A.; Hough, P. V. C.; Hansma, P. K. Recent Advances in Atomic Force Microscopy of DNA. *Scanning* **1993**, *15*, 296−299.
(119) Santos, S.; Barcons, V.; Christenson, H. K.; Billingsley, D. J.; Bonass, W. A.; Font, J.; Thomson, N. H. Stability, Resolution, and Ultra-Low Wear Amplitude Modulation Atomic Force Microscopy of DNA: Small Amplitude Small Set-Point Imaging. *Appl. Phys. Lett.* **2013**, *103*, 063702.
(120) Cellai, S.; Mangiarotti, L.; Vannini, N.; Naryshkin, N.; Kortkhonjia, E.; Ebright, R. H.; Rivetti, C. Upstream Promoter Sequences and Alphactd Mediate Stable DNA Wrapping within the Rna Polymerase-Promoter Open Complex. *EMBO Rep.* **2007**, *8*, 271−278.
(121) Maurer, S.; Fritz, J.; Muskhelishvili, G.; Travers, A. Rna Polymerase and an Activator Form Discrete Subcomplexes in a Transcription Initiation Complex. *EMBO J.* **2006**, *25*, 3784.
(122) Tessmer, I.; Moore, T.; Lloyd, R. G.; Wilson, A.; Erie, D. A.; Allen, S.; Tendler, S. J. B. Afm Studies on the Role of the Protein Rdgc in Bacterial DNA Recombination. *J. Mol. Biol.* **2005**, *350*, 254−262.
(123) Verhoeven, E. E. A.; Wyman, C.; Moolenaar, G. F.; Goosen, N. The Presence of Two Uvrb Subunits in the Uvrab Complex Ensures Damage Detection in Both DNA Strands. *EMBO J.* **2002**, *21*, 4196−4205.
(124) Buechner, C. N.; Maiti, A.; Drohat, A. C.; Tessmer, I. Lesion Search and Recognition by Thymine DNA Glycosylase Revealed by Single Molecule Imaging. *Nucleic Acids Res.* **2015**, *43*, 2716−2729.
(125) Chen, L.; Haushalter, K. A.; Lieber, C. M.; Verdine, G. L. Direct Visualization of a DNA Glycosylase Searching for Damage. *Chem. Biol.* **2002**, *9*, 345−350.
(126) Kong, M.; Liu, L.; Chen, X.; Driscoll, K. I.; Mao, P.; Böhm, S.; Kad, N. M.; Watkins, S. C.; Bernstein, Kara A.; Wyrick, John J.; Min, J.-H.; Van Houten, B. Single-Molecule Imaging Reveals That Rad4 Employs a Dynamic DNA Damage Recognition Process. *Mol. Cell* **2016**, *64*, 376−387.
(127) Tessmer, I.; Yang, Y.; Zhai, J.; Du, C.; Hsieh, P.; Hingorani, M. M.; Erie, D. A. Mechanism of Muts Searching for DNA Mismatches and Signaling Repair. *J. Biol. Chem.* **2008**, *283*, 36646−36654.
(128) Wang, H.; Yang, Y.; Schofield, M. J.; Du, C.; Fridman, Y.; Lee, S. D.; Larson, E. D.; Drummond, J. T.; Alani, E.; Hsieh, P.; Erie, D. A. DNA Bending and Unbending by Muts Govern Mismatch Recognition and Specificity. *Proc. Natl. Acad. Sci. U. S. A.* **2003**, *100*, 14822.
(129) Zhang, W.; Dillingham, M. S.; Thomas, C. D.; Allen, S.; Roberts, C. J.; Soultanas, P. Directional Loading and Stimulation of Pcra Helicase by the Replication Initiator Protein Repd. *J. Mol. Biol.* **2007**, *371*, 336−348.
(130) Schneider, S. W.; Lärmer, J.; Henderson, R. M.; Oberleithner, H. Molecular Weights of Individual Proteins Correlate with Molecular Volumes Measured by Atomic Force Microscopy. *Pfluegers Arch.* **1998**, *435*, 362−367.
(131) Ando, T. High-Speed Afm Imaging. *Curr. Opin. Struct. Biol.* **2014**, *28*, 63−68.
(132) Ando, T.; Kodera, N.; Takai, E.; Maruyama, D.; Saito, K.; Toda, A. A High-Speed Atomic Force Microscope for Studying Biological Macromolecules. *Proc. Natl. Acad. Sci. U. S. A.* **2001**, *98*, 12468.
(133) Lee, A. J.; Endo, M.; Hobbs, J. K.; Wälti, C. Direct Single-Molecule Observation of Mode and Geometry of Reca-Mediated Homology Search. *ACS Nano* **2018**, *12*, 272−278.
(134) Sanchez, H.; Suzuki, Y.; Yokokawa, M.; Takeyasu, K.; Wyman, C. Protein−DNA Interactions in High Speed Afm: Single Molecule Diffusion Analysis of Human Rad54. *Integrative Biology* **2011**, *3*, 1127−1134.
(135) Suzuki, Y.; Shin, M.; Yoshida, A.; Yoshimura, S. H.; Takeyasu, K. Fast Microscopical Dissection of Action Scenes Played by Escherichia Coli Rna Polymerase. *FEBS Lett.* **2012**, *586*, 3187−3192.
(136) Buechner, C. N.; Tessmer, I. DNA Substrate Preparation for Atomic Force Microscopy Studies of Protein−DNA Interactions. *J. Mol. Recognit.* **2013**, *26*, 605−617.
(137) Stoddart, D.; Heron, A. J.; Mikhailova, E.; Maglia, G.; Bayley, H. Single-Nucleotide Discrimination in Immobilized DNA Oligonucleotides with a Biological Nanopore. *Proc. Natl. Acad. Sci. U. S. A.* **2009**, *106*, 7702−7.
(138) Purnell, R. F.; Mehta, K. K.; Schmidt, J. J. Nucleotide Identification and Orientation Discrimination of DNA Homopolymers Immobilized in a Protein Nanopore. *Nano Lett.* **2008**, *8*, 3029−34.
(139) Purnell, R. F.; Schmidt, J. J. Discrimination of Single Base Substitutions in a DNA Strand Immobilized in a Biological Nanopore. *ACS Nano* **2009**, *3*, 2533−8.
(140) Butler, T. Z.; Pavlenok, M.; Derrington, I. M.; Niederweis, M.; Gundlach, J. H. Single-Molecule DNA Detection with an Engineered Mspa Protein Nanopore. *Proc. Natl. Acad. Sci. U. S. A.* **2008**, *105*, 20647−52.
(141) Derrington, I. M.; Butler, T. Z.; Collins, M. D.; Manrao, E.; Pavlenok, M.; Niederweis, M.; Gundlach, J. H. Nanopore DNA Sequencing with Mspa. *Proc. Natl. Acad. Sci. U. S. A.* **2010**, *107*, 16060−5.
(142) Manrao, E. A.; Derrington, I. M.; Laszlo, A. H.; Langford, K. W.; Hopper, M. K.; Gillgren, N.; Pavlenok, M.; Niederweis, M.; Gundlach, J. H. Reading DNA at Single-Nucleotide Resolution with a

DOI: 10.1021/acs.chemrev.9b00361
Chem. Rev. 2020, 120, 36−78

Mutant Mspa Nanopore and Phi29 DNA Polymerase. *Nat. Biotechnol.* **2012**, *30*, 349−53.
(143) Cherf, G. M.; Lieberman, K. R.; Rashid, H.; Lam, C. E.; Karplus, K.; Akeson, M. Automated Forward and Reverse Ratcheting of DNA in a Nanopore at 5-a Precision. *Nat. Biotechnol.* **2012**, *30*, 344−8.
(144) Hohng, S.; Joo, C.; Ha, T. Single-Molecule Three-Color Fret. *Biophys. J.* **2004**, *87*, 1328−37.
(145) Lee, J.; Lee, S.; Ragunathan, K.; Joo, C.; Ha, T.; Hohng, S. Single-Molecule Four-Color Fret. *Angew. Chem., Int. Ed.* **2010**, *49*, 9922−5.
(146) Ticau, S.; Friedman, L. J.; Ivica, N. A.; Gelles, J.; Bell, S. P. Single-Molecule Studies of Origin Licensing Reveal Mechanisms Ensuring Bidirectional Helicase Loading. *Cell* **2015**, *161*, 513−525.
(147) Friedman, L. J.; Gelles, J. Mechanism of Transcription Initiation at an Activator-Dependent Promoter Defined by Single-Molecule Observation. *Cell* **2012**, *148*, 679−689.
(148) Hohng, S.; Zhou, R.; Nahas, M. K.; Yu, J.; Schulten, K.; Lilley, D. M.; Ha, T. Fluorescence-Force Spectroscopy Maps Two-Dimensional Reaction Landscape of the Holliday Junction. *Science* **2007**, *318*, 279−83.
(149) Grashoff, C.; Hoffman, B. D.; Brenner, M. D.; Zhou, R.; Parsons, M.; Yang, M. T.; McLean, M. A.; Sligar, S. G.; Chen, C. S.; Ha, T.; Schwartz, M. A. Measuring Mechanical Tension across Vinculin Reveals Regulation of Focal Adhesion Dynamics. *Nature* **2010**, *466*, 263−6.
(150) Zhou, R.; Kozlov, A. G.; Roy, R.; Zhang, J.; Korolev, S.; Lohman, T. M.; Ha, T. Ssb Functions as a Sliding Platform That Migrates on DNA Via Reptation. *Cell* **2011**, *146*, 222−32.
(151) Long, X.; Parks, J. W.; Bagshaw, C. R.; Stone, M. D. Mechanical Unfolding of Human Telomere G-Quadruplex DNA Probed by Integrated Fluorescence and Magnetic Tweezers Spectroscopy. *Nucleic Acids Res.* **2013**, *41*, 2746−55.
(152) Mitra, J.; Makurath, M. A.; Ngo, T. T. M.; Troitskaia, A.; Chemla, Y. R.; Ha, T. Extreme Mechanical Diversity of Human Telomeric DNA Revealed by Fluorescence-Force Spectroscopy. *Proc. Natl. Acad. Sci. U. S. A.* **2019**, *116*, 8350−8359.
(153) Lee, M.; Kim, S. H.; Hong, S. C. Minute Negative Superhelicity Is Sufficient to Induce the B-Z Transition in the Presence of Low Tension. *Proc. Natl. Acad. Sci. U. S. A.* **2010**, *107*, 4985−90.
(154) Comstock, M. J.; Ha, T.; Chemla, Y. R. Ultra-High Resolution Optical Trap with Single Fluorophore Sensitivity. *Nat. Methods* **2011**, *8*, 335−340.
(155) Comstock, M. J.; Whitley, K. D.; Jia, H.; Sokoloski, J.; Lohman, T. M.; Ha, T.; Chemla, Y. R. Direct Observation of Structure-Function Relationship in a Nucleic Acid-Processing Enzyme. *Science* **2015**, *348*, 352−4.
(156) Makurath, M. A.; Whitley, K. D.; Nguyen, B.; Lohman, T. M.; Chemla, Y. R. Regulation of Rep Helicase Unwinding by an Auto-Inhibitory Subdomain. *Nucleic Acids Res.* **2019**, *47*, 2523−2532.
(157) Whitley, K. D.; Comstock, M. J.; Chemla, Y. R. Elasticity of the Transition State for Oligonucleotide Hybridization. *Nucleic Acids Res.* **2017**, *45*, 547−555.
(158) Whitley, K. D.; Comstock, M. J.; Chemla, Y. R. Ultrashort Nucleic Acid Duplexes Exhibit Long Wormlike Chain Behavior with Force-Dependent Edge Effects. *Phys. Rev. Lett.* **2018**, *120*, 068102.
(159) Heller, I.; Sitters, G.; Broekmans, O. D.; Farge, G.; Menges, C.; Wende, W.; Hell, S. W.; Peterman, E. J.; Wuite, G. J. Sted Nanoscopy Combined with Optical Tweezers Reveals Protein Dynamics on Densely Covered DNA. *Nat. Methods* **2013**, *10*, 910−6.
(160) Manosas, M.; Xi, X. G.; Bensimon, D.; Croquette, V. Active and Passive Mechanisms of Helicases. *Nucleic Acids Res.* **2010**, *38*, 5518−26.
(161) Lohman, T. M.; Tomko, E. J.; Wu, C. G. Non-Hexameric DNA Helicases and Translocases: Mechanisms and Regulation. *Nat. Rev. Mol. Cell Biol.* **2008**, *9*, 391.
(162) Lee, J. Y.; Yang, W. Uvrd Helicase Unwinds DNA One Base Pair at a Time by a Two-Part Power Stroke. *Cell* **2006**, *127*, 1349−1360.
(163) Velankar, S. S.; Soultanas, P.; Dillingham, M. S.; Subramanya, H. S.; Wigley, D. B. Crystal Structures of Complexes of Pcra DNA Helicase with a DNA Substrate Indicate an Inchworm Mechanism. *Cell* **1999**, *97*, 75−84.
(164) Arslan, S.; Khafizov, R.; Thomas, C. D.; Chemla, Y. R.; Ha, T. Engineering of a Superhelicase through Conformational Control. *Science* **2015**, *348*, 344−7.
(165) Jia, H.; Korolev, S.; Niedziela-Majka, A.; Maluf, N. K.; Gauss, G. H.; Myong, S.; Ha, T.; Waksman, G.; Lohman, T. M. Rotations of the 2b Sub-Domain of E. Coli Uvrd Helicase/Translocase Coupled to Nucleotide and DNA Binding. *J. Mol. Biol.* **2011**, *411*, 633−48.
(166) Manosas, M.; Perumal, S. K.; Bianco, P. R.; Ritort, F.; Benkovic, S. J.; Croquette, V. Recg and Uvsw Catalyse Robust DNA Rewinding Critical for Stalled DNA Replication Fork Rescue. *Nat. Commun.* **2013**, *4*, 2368.
(167) Zhou, R.; Zhang, J.; Bochman, M. L.; Zakian, V. A.; Ha, T. Periodic DNA Patrolling Underlies Diverse Functions of Pif1 on R-Loops and G-Rich DNA. *eLife* **2014**, *3*, e02190.
(168) Hou, X. M.; Wu, W. Q.; Duan, X. L.; Liu, N. N.; Li, H. H.; Fu, J.; Dou, S. X.; Li, M.; Xi, X. G. Molecular Mechanism of G-Quadruplex Unwinding Helicase: Sequential and Repetitive Unfolding of G-Quadruplex by Pif1 Helicase. *Biochem. J.* **2015**, *466*, 189−99.
(169) Tippana, R.; Hwang, H.; Opresko, P. L.; Bohr, V. A.; Myong, S. Single-Molecule Imaging Reveals a Common Mechanism Shared by G-Quadruplex-Resolving Helicases. *Proc. Natl. Acad. Sci. U. S. A.* **2016**, *113*, 8448−53.
(170) Dawid, A.; Croquette, V.; Grigoriev, M.; Heslot, F. Single-Molecule Study of Ruvab-Mediated Holliday-Junction Migration. *Proc. Natl. Acad. Sci. U. S. A.* **2004**, *101*, 11611−6.
(171) Amit, R.; Gileadi, O.; Stavans, J. Direct Observation of Ruvab-Catalyzed Branch Migration of Single Holliday Junctions. *Proc. Natl. Acad. Sci. U. S. A.* **2004**, *101*, 11605−10.
(172) Shin, S.; Lee, J.; Yoo, S.; Kulikowicz, T.; Bohr, V. A.; Ahn, B.; Hohng, S. Active Control of Repetitive Structural Transitions between Replication Forks and Holliday Junctions by Werner Syndrome Helicase. *Structure* **2016**, *24*, 1292−1300.
(173) Sun, B.; Johnson, D. S.; Patel, G.; Smith, B. Y.; Pandey, M.; Patel, S. S.; Wang, M. D. Atp-Induced Helicase Slippage Reveals Highly Coordinated Subunits. *Nature* **2011**, *478*, 132−5.
(174) Manosas, M.; Spiering, M. M.; Ding, F.; Croquette, V.; Benkovic, S. J. Collaborative Coupling between Polymerase and Helicase for Leading-Strand Synthesis. *Nucleic Acids Res.* **2012**, *40*, 6187−98.
(175) Sun, B.; Singh, A.; Sultana, S.; Inman, J. T.; Patel, S. S.; Wang, M. D. Helicase Promotes Replication Re-Initiation from an Rna Transcript. *Nat. Commun.* **2018**, *9*, 2306.
(176) Hiom, K.; West, S. C. Branch Migration During Homologous Recombination: Assembly of a Ruvab-Holliday Junction Complex in Vitro. *Cell* **1995**, *80*, 787−93.
(177) Whitby, M. C.; Lloyd, R. G. Branch Migration of Three-Strand Recombination Intermediates by Recg, a Possible Pathway for Securing Exchanges Initiated by 3′-Tailed Duplex DNA. *EMBO J.* **1995**, *14*, 3302−10.
(178) Kaplan, D. L.; O'Donnell, M. Dnab Drives DNA Branch Migration and Dislodges Proteins While Encircling Two DNA Strands. *Mol. Cell* **2002**, *10*, 647−57.
(179) McKinney, S. A.; Freeman, A. D.; Lilley, D. M.; Ha, T. Observing Spontaneous Branch Migration of Holliday Junctions One Step at a Time. *Proc. Natl. Acad. Sci. U. S. A.* **2005**, *102*, 5715−20.
(180) Delagoutte, E.; von Hippel, P. H. Molecular Mechanisms of the Functional Coupling of the Helicase (Gp41) and Polymerase (Gp43) of Bacteriophage T4 within the DNA Replication Fork. *Biochemistry* **2001**, *40*, 4459−77.
(181) Dillingham, M. S Superfamily I Helicases as Modular Components of DNA-Processing Machines. *Biochem. Soc. Trans.* **2011**, *39*, 413.

DOI: 10.1021/acs.chemrev.9b00361
Chem. Rev. 2020, 120, 36−78

(182) Korolev, S.; Hsieh, J.; Gauss, G. H.; Lohman, T. M.; Waksman, G. Major Domain Swiveling Revealed by the Crystal Structures of Complexes of E. Coli Rep Helicase Bound to Single-Stranded DNA and Adp. *Cell* **1997**, *90*, 635−647.
(183) Singleton, M. R.; Dillingham, M. S.; Wigley, D. B. Structure and Mechanism of Helicases and Nucleic Acid Translocases. *Annu. Rev. Biochem.* **2007**, *76*, 23−50.
(184) Fiorini, F.; Bagchi, D.; Le Hir, H.; Croquette, V. Human Upf1 Is a Highly Processive Rna Helicase and Translocase with Rnp Remodelling Activities. *Nat. Commun.* **2015**, *6*, 7581.
(185) Kanaan, J.; Raj, S.; Decourty, L.; Saveanu, C.; Croquette, V.; Le Hir, H. Upf1-Like Helicase Grip on Nucleic Acids Dictates Processivity. *Nat. Commun.* **2018**, *9*, 3752.
(186) Brüning, J.-G.; Howard, J. A. L.; Myka, K. K.; Dillingham, M. S.; McGlynn, P. The 2B Subdomain of Rep Helicase Links Translocation Along DNA with Protein Displacement. *Nucleic Acids Res.* **2018**, *46*, 8917−8925.
(187) Guy, C. P.; Atkinson, J.; Gupta, M. K.; Mahdi, A. A.; Gwynn, E. J.; Rudolph, C. J.; Moon, P. B.; van Knippenberg, I. C.; Cadman, C. J.; Dillingham, M. S.; Lloyd, R. G.; McGlynn, P. Rep Provides a Second Motor at the Replisome to Promote Duplication of Protein-Bound DNA. *Mol. Cell* **2009**, *36*, 654−666.
(188) Heller, R. C.; Marians, K. J. Unwinding of the Nascent Lagging Strand by Rep and Pria Enables the Direct Restart of Stalled Replication Forks. *J. Biol. Chem.* **2005**, *280*, 34143−34151.
(189) Syeda, A. H.; Wollman, A. J. M.; Hargreaves, A. L.; Howard, J. A. L.; Brüning, J.-G.; McGlynn, P.; Leake, M. C. Single-Molecule Live Cell Imaging of Rep Reveals the Dynamic Interplay between an Accessory Replicative Helicase and the Replisome. *Nucleic Acids Res.* **2019**, *47*, 6287.
(190) Myong, S.; Rasnik, I.; Joo, C.; Lohman, T. M.; Ha, T. Repetitive Shuttling of a Motor Protein on DNA. *Nature* **2005**, *437*, 1321−1325.
(191) Brendza, K. M.; Cheng, W.; Fischer, C. J.; Chesnik, M. A.; Niedziela-Majka, A.; Lohman, T. M. Autoinhibition of Escherichia Coli Rep Monomer Helicase Activity by Its 2B Subdomain. *Proc. Natl. Acad. Sci. U. S. A.* **2005**, *102*, 10076−10081.
(192) Cheng, W.; Brendza, K. M.; Gauss, G. H.; Korolev, S.; Waksman, G.; Lohman, T. M. The 2B Domain of the *Escherichia Coli* Rep Protein is not Required for DNA Helicase Activity. *Proc. Natl. Acad. Sci. U. S. A.* **2002**, *99*, 16006.
(193) Dillingham, M. S.; Wigley, D. B.; Webb, M. R. Direct Measurement of Single-Stranded DNA Translocation by Pcra Helicase Using the Fluorescent Base Analogue 2-Aminopurine. *Biochemistry* **2002**, *41*, 643−651.
(194) Cheng, W.; Hsieh, J.; Brendza, K. M.; Lohman, T. M. *E. Coli* Rep Oligomers Are Required to Initiate DNA Unwinding in Vitro11edited by D. Draper. *J. Mol. Biol.* **2001**, *310*, 327−350.
(195) Sokoloski, J. E.; Kozlov, A. G.; Galletto, R.; Lohman, T. M. Chemo-Mechanical Pushing of Proteins Along Single-Stranded DNA. *Proc. Natl. Acad. Sci. U. S. A.* **2016**, *113*, 6194−6199.
(196) Dao, V.; Modrich, P. Mismatch-, Muts-, Mutl-, and Helicase Ii-Dependent Unwinding from the Single-Strand Break of an Incised Heteroduplex. *J. Biol. Chem.* **1998**, *273*, 9202−9207.
(197) Husain, I.; Van Houten, B.; Thomas, D. C.; Abdel-Monem, M.; Sancar, A. Effect of DNA Polymerase I and DNA Helicase Ii on the Turnover Rate of Uvrabc Excision Nuclease. *Proc. Natl. Acad. Sci. U. S. A.* **1985**, *82*, 6774−6778.
(198) Maluf, N. K.; Ali, J. A.; Lohman, T. M. Kinetic Mechanism for Formation of the Active, Dimeric Uvrd Helicase-DNA Complex. *J. Biol. Chem.* **2003**, *278*, 31930−31940.
(199) Yokota, H.; Chujo, Y. A.; Harada, Y. Single-Molecule Imaging of the Oligomer Formation of the Nonhexameric Escherichia Coli Uvrd Helicase. *Biophys. J.* **2013**, *104*, 924−933.
(200) Lee, K. S.; Balci, H.; Jia, H.; Lohman, T. M.; Ha, T. Direct Imaging of Single Uvrd Helicase Dynamics on Long Single-Stranded DNA. *Nat. Commun.* **2013**, *4*, 1878.
(201) Matson, S. W. Escherichia Coli Helicase Ii (Urvd Gene Product) Translocates Unidirectionally in a 3′ to 5′ Direction. *J. Biol. Chem.* **1986**, *261*, 10169−10175.
(202) Fischer, C. J.; Maluf, N. K.; Lohman, T. M. Mechanism of ATP-Dependent Translocation of E.Coli Uvrd Monomers Along Single-Stranded DNA. *J. Mol. Biol.* **2004**, *344*, 1287−1309.
(203) Petrova, V.; Chen, S. H.; Molzberger, E. T.; Tomko, E.; Chitteni-Pattu, S.; Jia, H.; Ordabayev, Y.; Lohman, T. M.; Cox, M. M. Active Displacement of Reca Filaments by Uvrd Translocase Activity. *Nucleic Acids Res.* **2015**, *43*, 4133−4149.
(204) Veaute, X.; Delmas, S.; Selva, M.; Jeusset, J.; Le Cam, E.; Matic, I.; Fabre, F.; Petit, M. A. Uvrd Helicase, Unlike Rep Helicase, Dismantles Reca Nucleoprotein Filaments in *Escherichia Coli*. *EMBO J.* **2005**, *24*, 180.
(205) Nguyen, B.; Ordabayev, Y.; Sokoloski, J. E.; Weiland, E.; Lohman, T. M. Large Domain Movements Upon Uvrd Dimerization and Helicase Activation. *Proc. Natl. Acad. Sci. U. S. A.* **2017**, *114*, 12178.
(206) Dessinges, M. N.; Lionnet, T.; Xi, X. G.; Bensimon, D.; Croquette, V. Single-Molecule Assay Reveals Strand Switching and Enhanced Processivity of Uvrd. *Proc. Natl. Acad. Sci. U. S. A.* **2004**, *101*, 6439−44.
(207) Dillingham, M. S.; Wigley, D. B.; Webb, M. R. Demonstration of Unidirectional Single-Stranded DNA Translocation by Pcra Helicase: Measurement of Step Size and Translocation Speed. *Biochemistry* **2000**, *39*, 205−212.
(208) Niedziela-Majka, A.; Chesnik, M. A.; Tomko, E. J.; Lohman, T. M. Bacillus Stearothermophilus Pcra Monomer Is a Single-Stranded DNA Translocase but Not a Processive Helicase in Vitro. *J. Biol. Chem.* **2007**, *282*, 27076−27085.
(209) Park, J.; Myong, S.; Niedziela-Majka, A.; Lee, K. S.; Yu, J.; Lohman, T. M.; Ha, T. Pcra Helicase Dismantles Reca Filaments by Reeling in DNA in Uniform Steps. *Cell* **2010**, *142*, 544−555.
(210) Krejci, L.; Van Komen, S.; Li, Y.; Villemain, J.; Reddy, M. S.; Klein, H.; Ellenberger, T.; Sung, P. DNA Helicase Srs2 Disrupts the Rad51 Presynaptic Filament. *Nature* **2003**, *423*, 305−309.
(211) Veaute, X.; Jeusset, J.; Soustelle, C.; Kowalczykowski, S. C.; Le Cam, E.; Fabre, F. The Srs2 Helicase Prevents Recombination by Disrupting Rad51 Nucleoprotein Filaments. *Nature* **2003**, *423*, 309−312.
(212) Qiu, Y.; Antony, E.; Doganay, S.; Ran Koh, H.; Lohman, T. M.; Myong, S. Srs2 Prevents Rad51 Filament Formation by Repetitive Motion on DNA. *Nat. Commun.* **2013**, *4*, 2281.
(213) Kaniecki, K.; De Tullio, L.; Gibb, B.; Kwon, Y.; Sung, P.; Greene, E. C. Dissociation of Rad51 Presynaptic Complexes and Heteroduplex DNA Joints by Tandem Assemblies of Srs2. *Cell Rep.* **2017**, *21*, 3166−3177.
(214) De Tullio, L.; Kaniecki, K.; Kwon, Y.; Crickard, J. B.; Sung, P.; Greene, E. C. Yeast Srs2 Helicase Promotes Redistribution of Single-Stranded DNA-Bound Rpa and Rad52 in Homologous Recombination Regulation. *Cell Rep.* **2017**, *21*, 570−577.
(215) Bochman, M. L.; Sabouri, N.; Zakian, V. A. Unwinding the Functions of the Pif1 Family Helicases. *DNA Repair* **2010**, *9*, 237−249.
(216) Paeschke, K.; Bochman, M. L.; Garcia, P. D.; Cejka, P.; Friedman, K. L.; Kowalczykowski, S. C.; Zakian, V. A. Pif1 Family Helicases Suppress Genome Instability at G-Quadruplex Motifs. *Nature* **2013**, *497*, 458.
(217) Pyle, A. M. Translocation and Unwinding Mechanisms of Rna and DNA Helicases. *Annu. Rev. Biophys.* **2008**, *37*, 317−336.
(218) Paeschke, K.; Capra, J. A.; Zakian, V. A. DNA Replication through G-Quadruplex Motifs Is Promoted by the Saccharomyces Cerevisiae Pif1 DNA Helicase. *Cell* **2011**, *145*, 678−691.
(219) Boulé, J.-B.; Vega, L. R.; Zakian, V. A. The Yeast Pif1p Helicase Removes Telomerase from Telomeric DNA. *Nature* **2005**, *438*, 57−61.
(220) Wilson, M. A.; Kwon, Y.; Xu, Y.; Chung, W.-H.; Chi, P.; Niu, H.; Mayle, R.; Chen, X.; Malkova, A.; Sung, P.; Ira, G. Pif1 Helicase

DOI: 10.1021/acs.chemrev.9b00361
Chem. Rev. 2020, 120, 36−78

and Polδ Promote Recombination-Coupled DNA Synthesis Via Bubble Migration. *Nature* **2013**, *502*, 393.
(221) Boulé, J.-B.; Zakian, V. A. Roles of Pif1-Like Helicases in the Maintenance of Genomic Stability. *Nucleic Acids Res.* **2006**, *34*, 4147−4153.
(222) Hou, X.-M.; Wu, W.-Q.; Duan, X.-L.; Liu, N.-N.; Li, H.-H.; Fu, J.; Dou, S.-X.; Li, M.; Xi, X.-G. Molecular Mechanism of G-Quadruplex Unwinding Helicase: Sequential and Repetitive Unfolding of G-Quadruplex by Pif1 Helicase. *Biochem. J.* **2015**, *466*, 189.
(223) Handa, N.; Yang, L.; Dillingham, M. S.; Kobayashi, I.; Wigley, D. B.; Kowalczykowski, S. C. Molecular Determinants Responsible for Recognition of the Single-Stranded DNA Regulatory Sequence, X, by Recbcd Enzyme. *Proc. Natl. Acad. Sci. U. S. A.* **2012**, *109*, 8901.
(224) Dillingham, M. S.; Kowalczykowski, S. C. Recbcd Enzyme and the Repair of Double-Stranded DNA Breaks. *Microbiology and Molecular Biology Reviews* **2008**, *72*, 642.
(225) Dillingham, M. S.; Spies, M.; Kowalczykowski, S. C. Recbcd Enzyme Is a Bipolar DNA Helicase. *Nature* **2003**, *423*, 893−897.
(226) Singleton, M. R.; Dillingham, M. S.; Gaudier, M.; Kowalczykowski, S. C.; Wigley, D. B. Crystal Structure of Recbcd Enzyme Reveals a Machine for Processing DNA Breaks. *Nature* **2004**, *432* (7014), 187−193.
(227) Taylor, A. F.; Smith, G. R. Recbcd Enzyme Is a DNA Helicase with Fast and Slow Motors of Opposite Polarity. *Nature* **2003**, *423*, 889−893.
(228) Bianco, P. R.; Brewer, L. R.; Corzett, M.; Balhorn, R.; Yeh, Y.; Kowalczykowski, S. C.; Baskin, R. J. Processive Translocation and DNA Unwinding by Individual Recbcd Enzyme Molecules. *Nature* **2001**, *409*, 374−378.
(229) Liu, B.; Baskin, R. J.; Kowalczykowski, S. C. DNA Unwinding Heterogeneity by Recbcd Results from Static Molecules Able to Equilibrate. *Nature* **2013**, *500*, 482.
(230) Wiktor, J.; van der Does, M.; Büller, L.; Sherratt, D. J.; Dekker, C. Direct Observation of End Resection by Recbcd During Double-Stranded DNA Break Repair in Vivo. *Nucleic Acids Res.* **2018**, *46*, 1821−1833.
(231) Finkelstein, I. J.; Visnapuu, M.-L.; Greene, E. C. Single-Molecule Imaging Reveals Mechanisms of Protein Disruption by a DNA Translocase. *Nature* **2010**, *468*, 983−987.
(232) Terakawa, T.; Redding, S.; Silverstein, T. D.; Greene, E. C. Sequential Eviction of Crowded Nucleoprotein Complexes by the Exonuclease Recbcd Molecular Motor. *Proc. Natl. Acad. Sci. U. S. A.* **2017**, *114*, E6322.
(233) Zananiri, R.; Malik, O.; Rudnizky, S.; Gaydar, V.; Kreiserman, R.; Henn, A.; Kaplan, A. Synergy between Recbcd Subunits Is Essential for Efficient DNA Unwinding. *eLife* **2019**, *8*, e40836.
(234) Beyer, D. C.; Ghoneim, M. K.; Spies, M. Structure and Mechanisms of Sf2 DNA Helicases. *Adv. Exp. Med. Biol.* **2013**, *767*, 47−73.
(235) Jankowsky, E. Rna Helicases at Work: Binding and Rearranging. *Trends Biochem. Sci.* **2011**, *36*, 19−29.
(236) Mills, M.; Harami, G. M.; Seol, Y.; Gyimesi, M.; Martina, M.; Kovacs, Z. J.; Kovacs, M.; Neuman, K. C. Recq Helicase Triggers a Binding Mode Change in the Ssb-DNA Complex to Efficiently Initiate DNA Unwinding. *Nucleic Acids Res.* **2017**, *45*, 11878−11890.
(237) Harami, G. M.; Seol, Y.; In, J.; Ferencziova, V.; Martina, M.; Gyimesi, M.; Sarlos, K.; Kovacs, Z. J.; Nagy, N. T.; Sun, Y.; Vellai, T.; Neuman, K. C.; Kovacs, M. Shuttling Along DNA and Directed Processing of D-Loops by Recq Helicase Support Quality Control of Homologous Recombination. *Proc. Natl. Acad. Sci. U. S. A.* **2017**, *114*, E466−E475.
(238) Klaue, D.; Kobbe, D.; Kemmerich, F.; Kozikowska, A.; Puchta, H.; Seidel, R. Fork Sensing and Strand Switching Control Antagonistic Activities of Recq Helicases. *Nat. Commun.* **2013**, *4*, 2024.
(239) Chatterjee, S.; Zagelbaum, J.; Savitsky, P.; Sturzenegger, A.; Huttner, D.; Janscak, P.; Hickson, I. D.; Gileadi, O.; Rothenberg, E. Mechanistic Insight into the Interaction of Blm Helicase with Intra-Strand G-Quadruplex Structures. *Nat. Commun.* **2014**, *5*, 5556.
(240) Lee, M.; Shin, S.; Uhm, H.; Hong, H.; Kirk, J.; Hyun, K.; Kulikowicz, T.; Kim, J.; Ahn, B.; Bohr, V. A.; Hohng, S. Multiple Rpas Make Wrn Syndrome Protein a Superhelicase. *Nucleic Acids Res.* **2018**, *46* (9), 4689−4698.
(241) Wu, W. Q.; Hou, X. M.; Zhang, B.; Fosse, P.; Rene, B.; Mauffret, O.; Li, M.; Dou, S. X.; Xi, X. G. Single-Molecule Studies Reveal Reciprocating of Wrn Helicase Core Along Ssdna During DNA Unwinding. *Sci. Rep.* **2017**, *7*, 43954.
(242) Bagchi, D.; Manosas, M.; Zhang, W.; Manthei, K. A.; Hodeib, S.; Ducos, B.; Keck, J. L.; Croquette, V. Single Molecule Kinetics Uncover Roles for E. Coli Recq DNA Helicase Domains and Interaction with Ssb. *Nucleic Acids Res.* **2018**, *46*, 8500−8515.
(243) Budhathoki, J. B.; Stafford, E. J.; Yodh, J. G.; Balci, H. Atp-Dependent G-Quadruplex Unfolding by Bloom Helicase Exhibits Low Processivity. *Nucleic Acids Res.* **2015**, *43*, 5961−70.
(244) Wu, W. Q.; Hou, X. M.; Li, M.; Dou, S. X.; Xi, X. G. Blm Unfolds G-Quadruplexes in Different Structural Environments through Different Mechanisms. *Nucleic Acids Res.* **2015**, *43*, 4614−26.
(245) Budhathoki, J. B.; Maleki, P.; Roy, W. A.; Janscak, P.; Yodh, J. G.; Balci, H. A Comparative Study of G-Quadruplex Unfolding and DNA Reeling Activities of Human Recq5 Helicase. *Biophys. J.* **2016**, *110*, 2585−2596.
(246) Croteau, D. L.; Popuri, V.; Opresko, P. L.; Bohr, V. A. Human Recq Helicases in DNA Repair, Recombination, and Replication. *Annu. Rev. Biochem.* **2014**, *83*, 519−52.
(247) Honda, M.; Park, J.; Pugh, R. A.; Ha, T.; Spies, M. Single-Molecule Analysis Reveals Differential Effect of Ssdna-Binding Proteins on DNA Translocation by Xpd Helicase. *Mol. Cell* **2009**, *35*, 694−703.
(248) Qi, Z.; Pugh, R. A.; Spies, M.; Chemla, Y. R. Sequence-Dependent Base Pair Stepping Dynamics in Xpd Helicase Unwinding. *eLife* **2013**, *2*, e00334.
(249) Wu, C. G.; Spies, M. G-Quadruplex Recognition and Remodeling by the Fancj Helicase. *Nucleic Acids Res.* **2016**, *44*, 8742−8753.
(250) Cheng, W.; Arunajadai, S. G.; Moffitt, J. R.; Tinoco, I., Jr.; Bustamante, C. Single-Base Pair Unwinding and Asynchronous Rna Release by the Hepatitis C Virus Ns3 Helicase. *Science* **2011**, *333* (6050), 1746−9.
(251) Craig, J. M.; Laszlo, A. H.; Brinkerhoff, H.; Derrington, I. M.; Noakes, M. T.; Nova, I. C.; Tickman, B. I.; Doering, K.; de Leeuw, N. F.; Gundlach, J. H. Revealing Dynamics of Helicase Translocation on Single-Stranded DNA Using High-Resolution Nanopore Tweezers. *Proc. Natl. Acad. Sci. U. S. A.* **2017**, *114*, 11932−11937.
(252) Craig, J. M.; Laszlo, A. H.; Nova, I. C.; Brinkerhoff, H.; Noakes, M. T.; Baker, K. S.; Bowman, J. L.; Higinbotham, H. R.; Mount, J. W.; Gundlach, J. H. Determining the Effects of DNA Sequence on Hel308 Helicase Translocation Along Single-Stranded DNA Using Nanopore Tweezers. *Nucleic Acids Res.* **2019**, *47*, 2506−2513.
(253) Frick, D. N. The Hepatitis C Virus Ns3 Protein: A Model Rna Helicase and Potential Drug Target. *Curr. Issues Mol. Biol.* **2007**, *9*, 1−20.
(254) Raney, K. D.; Sharma, S. D.; Moustafa, I. M.; Cameron, C. E. Hepatitis C Virus Non-Structural Protein 3 (Hcv Ns3): A Multifunctional Antiviral Target. *J. Biol. Chem.* **2010**, *285*, 22725−31.
(255) Pang, P. S.; Jankowsky, E.; Planet, P. J.; Pyle, A. M. The Hepatitis C Viral Ns3 Protein Is a Processive DNA Helicase with Cofactor Enhanced Rna Unwinding. *EMBO J.* **2002**, *21*, 1168−76.
(256) Beran, R. K.; Serebrov, V.; Pyle, A. M. The Serine Protease Domain of Hepatitis C Viral Ns3 Activates Rna Helicase Activity by Promoting the Binding of Rna Substrate. *J. Biol. Chem.* **2007**, *282*, 34913−20.
(257) Serebrov, V.; Pyle, A. M. Periodic Cycles of Rna Unwinding and Pausing by Hepatitis C Virus Ns3 Helicase. *Nature* **2004**, *430*, 476−80.
(258) Jennings, T. A.; Mackintosh, S. G.; Harrison, M. K.; Sikora, D.; Sikora, B.; Dave, B.; Tackett, A. J.; Cameron, C. E.; Raney, K. D. Ns3 Helicase from the Hepatitis C Virus Can Function as a Monomer

DOI: 10.1021/acs.chemrev.9b00361
Chem. Rev. 2020, 120, 36−78

or Oligomer Depending on Enzyme and Substrate Concentrations. *J. Biol. Chem.* **2009**, *284*, 4806−14.
(259) Ma, Y.; Yates, J.; Liang, Y.; Lemon, S. M.; Yi, M. Ns3 Helicase Domains Involved in Infectious Intracellular Hepatitis C Virus Particle Assembly. *J. Virol.* **2008**, *82*, 7624−39.
(260) Fairman-Williams, M. E.; Guenther, U. P.; Jankowsky, E. Sf1 and Sf2 Helicases: Family Matters. *Curr. Opin. Struct. Biol.* **2010**, *20*, 313−24.
(261) Gu, M.; Rice, C. M. Three Conformational Snapshots of the Hepatitis C Virus Ns3 Helicase Reveal a Ratchet Translocation Mechanism. *Proc. Natl. Acad. Sci. U. S. A.* **2010**, *107*, 521−8.
(262) Kim, J. L.; Morgenstern, K. A.; Griffith, J. P.; Dwyer, M. D.; Thomson, J. A.; Murcko, M. A.; Lin, C.; Caron, P. R. Hepatitis C Virus Ns3 Rna Helicase Domain with a Bound Oligonucleotide: The Crystal Structure Provides Insights into the Mode of Unwinding. *Structure* **1998**, *6*, 89−100.
(263) Appleby, T. C.; Anderson, R.; Fedorova, O.; Pyle, A. M.; Wang, R.; Liu, X.; Brendza, K. M.; Somoza, J. R. Visualizing Atp-Dependent Rna Translocation by the Ns3 Helicase from Hcv. *J. Mol. Biol.* **2011**, *405*, 1139−53.
(264) Lin, C. T.; Tritschler, F.; Lee, K. S.; Gu, M.; Rice, C. M.; Ha, T. Single-Molecule Imaging Reveals the Translocation and DNA Looping Dynamics of Hepatitis C Virus Ns3 Helicase. *Protein Sci.* **2017**, *26*, 1391−1403.
(265) Enemark, E. J.; Joshua-Tor, L. On Helicases and Other Motor Proteins. *Curr. Opin. Struct. Biol.* **2008**, *18*, 243−57.
(266) Lyubimov, A. Y.; Strycharska, M.; Berger, J. M. The Nuts and Bolts of Ring-Translocase Structure and Mechanism. *Curr. Opin. Struct. Biol.* **2011**, *21*, 240−8.
(267) Patel, S. S.; Picha, K. M. Structure and Function of Hexameric Helicases. *Annu. Rev. Biochem.* **2000**, *69*, 651−97.
(268) O'Donnell, M. E.; Li, H. The Ring-Shaped Hexameric Helicases That Function at DNA Replication Forks. *Nat. Struct. Mol. Biol.* **2018**, *25*, 122−130.
(269) Bergvall, M.; Melendy, T.; Archambault, J. The E1 Proteins. *Virology* **2013**, *445*, 35−56.
(270) Auster, A. S.; Joshua-Tor, L. The DNA-Binding Domain of Human Papillomavirus Type 18 E1. Crystal Structure, Dimerization, and DNA Binding. *J. Biol. Chem.* **2004**, *279*, 3733−42.
(271) Enemark, E. J.; Joshua-Tor, L. Mechanism of DNA Translocation in a Replicative Hexameric Helicase. *Nature* **2006**, *442*, 270−5.
(272) Lee, S. J.; Syed, S.; Enemark, E. J.; Schuck, S.; Stenlund, A.; Ha, T.; Joshua-Tor, L. Dynamic Look at DNA Unwinding by a Replicative Helicase. *Proc. Natl. Acad. Sci. U. S. A.* **2014**, *111*, E827−35.
(273) Kulczyk, A. W.; Richardson, C. C. The Replication System of Bacteriophage T7. *Enzymes* **2016**, *39*, 89−136.
(274) Donmez, I.; Patel, S. S. Mechanisms of a Ring Shaped Helicase. *Nucleic Acids Res.* **2006**, *34* (15), 4216−24.
(275) Hacker, K. J.; Johnson, K. A. A Hexameric Helicase Encircles One DNA Strand and Excludes the Other During DNA Unwinding. *Biochemistry* **1997**, *36*, 14080−7.
(276) Johnson, D. S.; Bai, L.; Smith, B. Y.; Patel, S. S.; Wang, M. D. Single-Molecule Studies Reveal Dynamics of DNA Unwinding by the Ring-Shaped T7 Helicase. *Cell* **2007**, *129*, 1299−309.
(277) Itsathitphaisarn, O.; Wing, R. A.; Eliason, W. K.; Wang, J.; Steitz, T. A. The Hexameric Helicase Dnab Adopts a Nonplanar Conformation During Translocation. *Cell* **2012**, *151*, 267−77.
(278) Gao, Y.; Cui, Y.; Fox, T.; Lin, S.; Wang, H.; de Val, N.; Zhou, Z. H.; Yang, W. Structures and Operating Principles of the Replisome. *Science* **2019**, *363*, eaav7003.
(279) Schlierf, M.; Wang, G.; Chen, X. S.; Ha, T. Hexameric Helicase G40p Unwinds DNA in Single Base Pair Steps. *eLife* **2019**, *8*, No. e42001.
(280) Moyer, S. E.; Lewis, P. W.; Botchan, M. R. Isolation of the Cdc45/Mcm2−7/Gins (Cmg) Complex, a Candidate for the Eukaryotic DNA Replication Fork Helicase. *Proc. Natl. Acad. Sci. U. S. A.* **2006**, *103*, 10236−10241.
(281) Bell, S. D.; Botchan, M. R. The Minichromosome Maintenance Replicative Helicase. *Cold Spring Harbor Perspect. Biol.* **2013**, *5*, a012807.
(282) Gambus, A.; Jones, R. C.; Sanchez-Diaz, A.; Kanemaki, M.; van Deursen, F.; Edmondson, R. D.; Labib, K. Gins Maintains Association of Cdc45 with Mcm in Replisome Progression Complexes at Eukaryotic DNA Replication Forks. *Nat. Cell Biol.* **2006**, *8*, 358−66.
(283) Ilves, I.; Petojevic, T.; Pesavento, J. J.; Botchan, M. R. Activation of the Mcm2−7 Helicase by Association with Cdc45 and Gins Proteins. *Mol. Cell* **2010**, *37*, 247−58.
(284) Costa, A.; Ilves, I.; Tamberg, N.; Petojevic, T.; Nogales, E.; Botchan, M. R.; Berger, J. M. The Structural Basis for Mcm2−7 Helicase Activation by Gins and Cdc45. *Nat. Struct. Mol. Biol.* **2011**, *18*, 471−7.
(285) Georgescu, R.; Yuan, Z.; Bai, L.; de Luna Almeida Santos, R.; Sun, J.; Zhang, D.; Yurieva, O.; Li, H.; O'Donnell, M. E. Structure of Eukaryotic Cmg Helicase at a Replication Fork and Implications to Replisome Architecture and Origin Initiation. *Proc. Natl. Acad. Sci. U. S. A.* **2017**, *114*, E697−E706.
(286) Yuan, Z.; Bai, L.; Sun, J.; Georgescu, R.; Liu, J.; O'Donnell, M. E.; Li, H. Structure of the Eukaryotic Replicative Cmg Helicase Suggests a Pumpjack Motion for Translocation. *Nat. Struct. Mol. Biol.* **2016**, *23*, 217−24.
(287) Zhai, Y.; Cheng, E.; Wu, H.; Li, N.; Yung, P. Y.; Gao, N.; Tye, B. K. Open-Ringed Structure of the Cdt1-Mcm2−7 Complex as a Precursor of the Mcm Double Hexamer. *Nat. Struct. Mol. Biol.* **2017**, *24*, 300−308.
(288) Abid Ali, F.; Renault, L.; Gannon, J.; Gahlon, H. L.; Kotecha, A.; Zhou, J. C.; Rueda, D.; Costa, A. Cryo-Em Structures of the Eukaryotic Replicative Helicase Bound to a Translocation Substrate. *Nat. Commun.* **2016**, *7*, 10708.
(289) Burnham, D. R.; Kose, H. B.; Hoyle, R. B.; Yardimci, H. The Mechanism of DNA Unwinding by the Eukaryotic Replicative Helicase. *Nat. Commun.* **2019**, *10*, 2159.
(290) Kose, H. B.; Larsen, N. B.; Duxin, J. P.; Yardimci, H. Dynamics of the Eukaryotic Replicative Helicase at Lagging-Strand Protein Barriers Support the Steric Exclusion Model. *Cell Rep.* **2019**, *26*, 2113−2125.e6.
(291) Wasserman, M. R.; Schauer, G. D.; O'Donnell, M. E.; Liu, S. Replication Fork Activation is Enabled by a Single-Stranded DNA Gate in CMG Helicase. *Cell* **2019**, *178*, 600−611.
(292) Miller, J. M.; Enemark, E. J. Archaeal Mcm Proteins as an Analog for the Eukaryotic Mcm2−7 Helicase to Reveal Essential Features of Structure and Function. *Archaea* **2015**, *2015*, 305497.
(293) Schermerhorn, K. M.; Tanner, N.; Kelman, Z.; Gardner, A. F. High-Temperature Single-Molecule Kinetic Analysis of Thermophilic Archaeal Mcm Helicases. *Nucleic Acids Res.* **2016**, *44*, 8764−8771.
(294) Froelich, C. A.; Kang, S.; Epling, L. B.; Bell, S. P.; Enemark, E. J. A Conserved Mcm Single-Stranded DNA Binding Element Is Essential for Replication Initiation. *eLife* **2014**, *3*, e01993.
(295) Brewster, A. S.; Wang, G.; Yu, X.; Greenleaf, W. B.; Carazo, J. M.; Tjajadi, M.; Klein, M. G.; Chen, X. S. Crystal Structure of a near-Full-Length Archaeal Mcm: Functional Insights for an Aaa+ Hexameric Helicase. *Proc. Natl. Acad. Sci. U. S. A.* **2008**, *105*, 20191−6.
(296) Miller, J. M.; Arachea, B. T.; Epling, L. B.; Enemark, E. J. Analysis of the Crystal Structure of an Active Mcm Hexamer. *eLife* **2014**, *3*, e03433.
(297) Jenkinson, E. R.; Chong, J. P. Minichromosome Maintenance Helicase Activity Is Controlled by N- and C-Terminal Motifs and Requires the Atpase Domain Helix-2 Insert. *Proc. Natl. Acad. Sci. U. S. A.* **2006**, *103*, 7613−8.
(298) Barry, E. R.; McGeoch, A. T.; Kelman, Z.; Bell, S. D. Archaeal Mcm Has Separable Processivity, Substrate Choice and Helicase Domains. *Nucleic Acids Res.* **2007**, *35*, 988−98.
(299) Xu, Y.; Gristwood, T.; Hodgson, B.; Trinidad, J. C.; Albers, S. V.; Bell, S. D. Archaeal Orthologs of Cdc45 and Gins Form a Stable Complex That Stimulates the Helicase Activity of Mcm. *Proc. Natl. Acad. Sci. U. S. A.* **2016**, *113*, 13390−13395.

DOI: 10.1021/acs.chemrev.9b00361
Chem. Rev. 2020, 120, 36−78

(300) Stratmann, S. A.; van Oijen, A. M. DNA Replication at the Single-Molecule Level. *Chem. Soc. Rev.* **2014**, *43*, 1201−1220.
(301) Lee, J. B.; Hite, R. K.; Hamdan, S. M.; Xie, X. S.; Richardson, C. C.; van Oijen, A. M. DNA Primase Acts as a Molecular Brake in DNA Replication. *Nature* **2006**, *439*, 621−4.
(302) Pandey, M.; Syed, S.; Donmez, I.; Patel, G.; Ha, T.; Patel, S. S. Coordinating DNA Replication by Means of Priming Loop and Differential Synthesis Rate. *Nature* **2009**, *462*, 940−3.
(303) Graham, J. E.; Marians, K. J.; Kowalczykowski, S. C. Independent and Stochastic Action of DNA Polymerases in the Replisome. *Cell* **2017**, *169*, 1201−1213.e17.
(304) Tanner, N. A.; Tolun, G.; Loparo, J. J.; Jergic, S.; Griffith, J. D.; Dixon, N. E.; van Oijen, A. M. *E. Coli* DNA Replication in the Absence of Free B Clamps. *EMBO J.* **2011**, *30*, 1830.
(305) Yao, N. Y.; Georgescu, R. E.; Finkelstein, J.; Donnell, M. E. Single-Molecule Analysis Reveals That the Lagging Strand Increases Replisome Processivity but Slows Replication Fork Progression. *Proc. Natl. Acad. Sci. U. S. A.* **2009**, *106*, 13236.
(306) Beattie, T. R.; Kapadia, N.; Nicolas, E.; Uphoff, S.; Wollman, A. J. M.; Leake, M. C.; Reyes-Lamothe, R. Frequent Exchange of the DNA Polymerase During Bacterial Chromosome Replication. *eLife* **2017**, *6*, e21763.
(307) Mueller, S. H.; Spenkelink, L. M.; van Oijen, A. M. When Proteins Play Tag: The Dynamic Nature of the Replisome. *Biophys. Rev.* **2019**, *11*, 641−651.
(308) Gahlon, H. L.; Romano, L. J.; Rueda, D. Influence of DNA Lesions on Polymerase-Mediated DNA Replication at Single-Molecule Resolution. *Chem. Res. Toxicol.* **2017**, *30*, 1972−1983.
(309) Thrall, E. S.; Kath, J. E.; Chang, S.; Loparo, J. J. Single-Molecule Imaging Reveals Multiple Pathways for the Recruitment of Translesion Polymerases after DNA Damage. *Nat. Commun.* **2017**, *8*, 2170.
(310) Friedman, L. J.; Chung, J.; Gelles, J. Viewing Dynamic Assembly of Molecular Complexes by Multi-Wavelength Single-Molecule Fluorescence. *Biophys. J.* **2006**, *91*, 1023−31.
(311) Zhao, G.; Gleave, E. S.; Lamers, M. H. Single-Molecule Studies Contrast Ordered DNA Replication with Stochastic Translesion Synthesis. *eLife* **2017**, *6*, No. e32177.
(312) Larson, M. H.; Landick, R.; Block, S. M. Single-Molecule Studies of Rna Polymerase: One Singular Sensation, Every Little Step It Takes. *Mol. Cell* **2011**, *41*, 249−62.
(313) Michaelis, J.; Treutlein, B. Single-Molecule Studies of RNA Polymerases. *Chem. Rev.* **2013**, *113*, 8377−99.
(314) Dangkulwanich, M.; Ishibashi, T.; Bintu, L.; Bustamante, C. Molecular Mechanisms of Transcription through Single-Molecule Experiments. *Chem. Rev.* **2014**, *114*, 3203−23.
(315) Lisica, A.; Grill, S. W. Optical Tweezers Studies of Transcription by Eukaryotic RNA Polymerases. *Biomol. Concepts* **2017**, *8*, 1−11.
(316) Harada, Y.; Funatsu, T.; Murakami, K.; Nonoyama, Y.; Ishihama, A.; Yanagida, T. Single-Molecule Imaging of RNA Polymerase-DNA Interactions in Real Time. *Biophys. J.* **1999**, *76*, 709−15.
(317) Friedman, L. J.; Mumm, J. P.; Gelles, J. Rna Polymerase Approaches Its Promoter without Long-Range Sliding Along DNA. *Proc. Natl. Acad. Sci. U. S. A.* **2013**, *110*, 9740.
(318) Wang, F.; Redding, S.; Finkelstein, I. J.; Gorman, J.; Reichman, D. R.; Greene, E. C. The Promoter-Search Mechanism of Escherichia Coli RNA Polymerase Is Dominated by Three-Dimensional Diffusion. *Nat. Struct. Mol. Biol.* **2013**, *20*, 174.
(319) Sternberg, S. H.; Redding, S.; Jinek, M.; Greene, E. C.; Doudna, J. A. DNA Interrogation by the Crispr Rna-Guided Endonuclease Cas9. *Nature* **2014**, *507*, 62−7.
(320) Globyte, V.; Lee, S. H.; Bae, T.; Kim, J. S.; Joo, C. Crispr/Cas9 Searches for a Protospacer Adjacent Motif by Lateral Diffusion. *EMBO J.* **2019**, *38*, e99466.
(321) Ragunathan, K.; Liu, C.; Ha, T. Reca Filament Sliding on DNA Facilitates Homology Search. *eLife* **2012**, *1*, e00067.
(322) Chandradoss, S. D.; Schirle, N. T.; Szczepaniak, M.; MacRae, I. J.; Joo, C. A Dynamic Search Process Underlies Microrna Targeting. *Cell* **2015**, *162*, 96−107.
(323) Murakami, K. S.; Masuda, S.; Darst, S. A. Structural Basis of Transcription Initiation: Rna Polymerase Holoenzyme at 4 Å Resolution. *Science* **2002**, *296*, 1280.
(324) Revyakin, A.; Ebright, R. H.; Strick, T. R. Promoter Unwinding and Promoter Clearance by RNA Polymerase: Detection by Single-Molecule DNA Nanomanipulation. *Proc. Natl. Acad. Sci. U. S. A.* **2004**, *101*, 4776.
(325) Tang, G. Q.; Roy, R.; Ha, T.; Patel, S. S. Transcription Initiation in a Single-Subunit RNA Polymerase Proceeds through DNA Scrunching and Rotation of the N-Terminal Subdomains. *Mol. Cell* **2008**, *30*, 567−77.
(326) Kapanidis, A. N.; Margeat, E.; Ho, S. O.; Kortkhonjia, E.; Weiss, S.; Ebright, R. H. Initial Transcription by RNA Polymerase Proceeds through a DNA-Scrunching Mechanism. *Science* **2006**, *314*, 1144−7.
(327) Koh, H. R.; Roy, R.; Sorokina, M.; Tang, G. Q.; Nandakumar, D.; Patel, S. S.; Ha, T. Correlating Transcription Initiation and Conformational Changes by a Single-Subunit RNA Polymerase with near Base-Pair Resolution. *Mol. Cell* **2018**, *70*, 695−706.e5.
(328) Chakraborty, A.; Wang, D.; Ebright, Y. W.; Korlann, Y.; Kortkhonjia, E.; Kim, T.; Chowdhury, S.; Wigneshweraraj, S.; Irschik, H.; Jansen, R.; Nixon, B. T.; Knight, J.; Weiss, S.; Ebright, R. H. Opening and Closing of the Bacterial RNA Polymerase Clamp. *Science* **2012**, *337*, 591.
(329) Koh, H. R.; Roy, R.; Sorokina, M.; Tang, G.-Q.; Nandakumar, D.; Patel, S. S.; Ha, T. Correlating Transcription Initiation and Conformational Changes by a Single-Subunit Rna Polymerase with near Base-Pair Resolution. *Mol. Cell* **2018**, *70*, 695−706.e5.
(330) Zhang, Z.; Revyakin, A.; Grimm, J. B.; Lavis, L. D.; Tjian, R. Single-Molecule Tracking of the Transcription Cycle by Sub-Second Rna Detection. *eLife* **2014**, *3*, e01775.
(331) Gabizon, R.; Lee, A.; Vahedian-Movahed, H.; Ebright, R. H.; Bustamante, C. J. Pause Sequences Facilitate Entry into Long-Lived Paused States by Reducing Rna Polymerase Transcription Rates. *Nat. Commun.* **2018**, *9*, 2930.
(332) Dalal, R. V.; Larson, M. H.; Neuman, K. C.; Gelles, J.; Landick, R.; Block, S. M. Pulling on the Nascent Rna During Transcription Does Not Alter Kinetics of Elongation or Ubiquitous Pausing. *Mol. Cell* **2006**, *23*, 231−9.
(333) Larson, M. H.; Greenleaf, W. J.; Landick, R.; Block, S. M. Applied Force Reveals Mechanistic and Energetic Details of Transcription Termination. *Cell* **2008**, *132*, 971−82.
(334) Deufel, C.; Forth, S.; Simmons, C. R.; Dejgosha, S.; Wang, M. D. Nanofabricated Quartz Cylinders for Angular Trapping: DNA Supercoiling Torque Detection. *Nat. Methods* **2007**, *4*, 223.
(335) Ma, J.; Bai, L.; Wang, M. D. Transcription under Torsion. *Science* **2013**, *340*, 1580.
(336) Ma, J.; Tan, C.; Gao, X.; Fulbright, R. M.; Roberts, J. W.; Wang, M. D. Transcription Factor Regulation of RNA Polymerase's Torque Generation Capacity. *Proc. Natl. Acad. Sci. U. S. A.* **2019**, *116*, 2583.
(337) Bakshi, S.; Dalrymple, R. M.; Li, W.; Choi, H.; Weisshaar, J. C. Partitioning of RNA Polymerase Activity in Live *Escherichia Coli* from Analysis of Single-Molecule Diffusive Trajectories. *Biophys. J.* **2013**, *105*, 2676−2686.
(338) Bakshi, S.; Siryaporn, A.; Goulian, M.; Weisshaar, J. C. Superresolution Imaging of Ribosomes and RNA Polymerase in Live Escherichia Coli Cells. *Mol. Microbiol.* **2012**, *85*, 21−38.
(339) Stracy, M.; Lesterlin, C.; Garza de Leon, F.; Uphoff, S.; Zawadzki, P.; Kapanidis, A. N. Live-Cell Superresolution Microscopy Reveals the Organization of RNA Polymerase in the Bacterial Nucleoid. *Proc. Natl. Acad. Sci. U. S. A.* **2015**, *112*, E4390.
(340) Cisse, I. I.; Izeddin, I.; Causse, S. Z.; Boudarene, L.; Senecal, A.; Muresan, L.; Dugast-Darzacq, C.; Hajj, B.; Dahan, M.; Darzacq, X. Real-Time Dynamics of RNA Polymerase Ii Clustering in Live Human Cells. *Science* **2013**, *341*, 664−7.

DOI: 10.1021/acs.chemrev.9b00361
Chem. Rev. 2020, 120, 36−78

(341) Cho, W. K.; Jayanth, N.; English, B. P.; Inoue, T.; Andrews, J. O.; Conway, W.; Grimm, J. B.; Spille, J. H.; Lavis, L. D.; Lionnet, T.; Cisse, I. I. Rna Polymerase Ii Cluster Dynamics Predict mRNA Output in Living Cells. *eLife* **2016**, *5*, No. e13617.
(342) Tomko, E. J.; Fishburn, J.; Hahn, S.; Galburt, E. A. Tfiih Generates a Six-Base-Pair Open Complex During RNAP II Transcription Initiation and Start-Site Scanning. *Nat. Struct. Mol. Biol.* **2017**, *24*, 1139−1145.
(343) Revyakin, A.; Zhang, Z.; Coleman, R. A.; Li, Y.; Inouye, C.; Lucas, J. K.; Park, S. R.; Chu, S.; Tjian, R. Transcription Initiation by Human RNA Polymerase II Visualized at Single-Molecule Resolution. *Genes Dev.* **2012**, *26*, 1691−702.
(344) Treutlein, B.; Muschielok, A.; Andrecka, J.; Jawhari, A.; Buchen, C.; Kostrewa, D.; Hog, F.; Cramer, P.; Michaelis, J. Dynamic Architecture of a Minimal RNA Polymerase II Open Promoter Complex. *Mol. Cell* **2012**, *46*, 136−46.
(345) Lisica, A.; Engel, C.; Jahnel, M.; Roldan, E.; Galburt, E. A.; Cramer, P.; Grill, S. W. Mechanisms of Backtrack Recovery by RNA Polymerases I and II. *Proc. Natl. Acad. Sci. U. S. A.* **2016**, *113*, 2946−51.
(346) Galburt, E. A.; Grill, S. W.; Wiedmann, A.; Lubkowska, L.; Choy, J.; Nogales, E.; Kashlev, M.; Bustamante, C. Backtracking Determines the Force Sensitivity of RNAP II in a Factor-Dependent Manner. *Nature* **2007**, *446*, 820−3.
(347) Zamft, B.; Bintu, L.; Ishibashi, T.; Bustamante, C. Nascent Rna Structure Modulates the Transcriptional Dynamics of Rna Polymerases. *Proc. Natl. Acad. Sci. U. S. A.* **2012**, *109*, 8948−8953.
(348) Hodges, C.; Bintu, L.; Lubkowska, L.; Kashlev, M.; Bustamante, C. Nucleosomal Fluctuations Govern the Transcription Dynamics of Rna Polymerase Ii. *Science* **2009**, *325*, 626.
(349) Larson, M. H.; Zhou, J.; Kaplan, C. D.; Palangat, M.; Kornberg, R. D.; Landick, R.; Block, S. M. Trigger Loop Dynamics Mediate the Balance between the Transcriptional Fidelity and Speed of RNA Polymerase II. *Proc. Natl. Acad. Sci. U. S. A.* **2012**, *109*, 6555−60.
(350) Schweikhard, V.; Meng, C.; Murakami, K.; Kaplan, C. D.; Kornberg, R. D.; Block, S. M. Transcription Factors Tfiif and Tfiis Promote Transcript Elongation by Rna Polymerase Ii by Synergistic and Independent Mechanisms. *Proc. Natl. Acad. Sci. U. S. A.* **2014**, *111*, 6642−7.
(351) Dangkulwanich, M.; Ishibashi, T.; Liu, S.; Kireeva, M. L.; Lubkowska, L.; Kashlev, M.; Bustamante, C. J. Complete Dissection of Transcription Elongation Reveals Slow Translocation of Rna Polymerase Ii in a Linear Ratchet Mechanism. *eLife* **2013**, *2*, e00971.
(352) Fazal, F. M.; Meng, C. A.; Murakami, K.; Kornberg, R. D.; Block, S. M. Real-Time Observation of the Initiation of Rna Polymerase II Transcription. *Nature* **2015**, *525*, 274−7.
(353) Jin, J.; Bai, L.; Johnson, D. S.; Fulbright, R. M.; Kireeva, M. L.; Kashlev, M.; Wang, M. D. Synergistic Action of Rna Polymerases in Overcoming the Nucleosomal Barrier. *Nat. Struct. Mol. Biol.* **2010**, *17*, 745−52.
(354) Fitz, V.; Shin, J.; Ehrlich, C.; Farnung, L.; Cramer, P.; Zaburdaev, V.; Grill, S. W. Nucleosomal Arrangement Affects Single-Molecule Transcription Dynamics. *Proc. Natl. Acad. Sci. U. S. A.* **2016**, *113*, 12733−12738.
(355) Ucuncuoglu, S.; Engel, K. L.; Purohit, P. K.; Dunlap, D. D.; Schneider, D. A.; Finzi, L. Direct Characterization of Transcription Elongation by RNA Polymerase I. *PLoS One* **2016**, *11*, e0159527.
(356) Vos, S. M.; Tretter, E. M.; Schmidt, B. H.; Berger, J. M. All Tangled Up: How Cells Direct, Manage and Exploit Topoisomerase Function. *Nat. Rev. Mol. Cell Biol.* **2011**, *12*, 827−41.
(357) Le, D. T.; Shannon, K. M. Ras Processing as a Therapeutic Target in Hematologic Malignancies. *Curr. Opin. Hematol.* **2002**, *9*, 308−15.
(358) Schoeffler, A. J.; Berger, J. M. DNA Topoisomerases: Harnessing and Constraining Energy to Govern Chromosome Topology. *Q. Rev. Biophys.* **2008**, *41*, 41−101.
(359) Strick, T. R.; Croquette, V.; Bensimon, D. Single-Molecule Analysis of DNA Uncoiling by a Type Ii Topoisomerase. *Nature* **2000**, *404*, 901−4.
(360) Corbett, K. D.; Shultzaberger, R. K.; Berger, J. M. The C-Terminal Domain of DNA Gyrase a Adopts a DNA-Bending Beta-Pinwheel Fold. *Proc. Natl. Acad. Sci. U. S. A.* **2004**, *101*, 7293−8.
(361) Brown, P. O.; Cozzarelli, N. R. A Sign Inversion Mechanism for Enzymatic Supercoiling of DNA. *Science* **1979**, *206*, 1081−3.
(362) Wang, J. C. Cellular Roles of DNA Topoisomerases: A Molecular Perspective. *Nat. Rev. Mol. Cell Biol.* **2002**, *3*, 430−40.
(363) Peter, B. J.; Arsuaga, J.; Breier, A. M.; Khodursky, A. B.; Brown, P. O.; Cozzarelli, N. R. Genomic Transcriptional Response to Loss of Chromosomal Supercoiling in *Escherichia Coli*. *Genome Biol.* **2004**, *5*, R87.
(364) Chong, S.; Chen, C.; Ge, H.; Xie, X. S. Mechanism of Transcriptional Bursting in Bacteria. *Cell* **2014**, *158*, 314−326.
(365) Gore, J.; Bryant, Z.; Stone, M. D.; Nollmann, M.; Cozzarelli, N. R.; Bustamante, C. Mechanochemical Analysis of DNA Gyrase Using Rotor Bead Tracking. *Nature* **2006**, *439*, 100−104.
(366) Nollmann, M.; Stone, M. D.; Bryant, Z.; Gore, J.; Crisona, N. J.; Hong, S. C.; Mitelheiser, S.; Maxwell, A.; Bustamante, C.; Cozzarelli, N. R. Multiple Modes of Escherichia Coli DNA Gyrase Activity Revealed by Force and Torque. *Nat. Struct. Mol. Biol.* **2007**, *14*, 264−71.
(367) Gubaev, A.; Klostermeier, D. DNA-Induced Narrowing of the Gyrase N-Gate Coordinates T-Segment Capture and Strand Passage. *Proc. Natl. Acad. Sci. U. S. A.* **2011**, *108*, 14085−90.
(368) Lanz, M. A.; Klostermeier, D. Guiding Strand Passage: DNA-Induced Movement of the Gyrase C-Terminal Domains Defines an Early Step in the Supercoiling Cycle. *Nucleic Acids Res.* **2011**, *39*, 9681−94.
(369) Soczek, K. M.; Grant, T.; Rosenthal, P. B.; Mondragon, A. Cryoem Structures of Open Dimers of Gyrase a in Complex with DNA Illuminate Mechanism of Strand Passage. *eLife* **2018**, *7*, No. e41215.
(370) Papillon, J.; Menetret, J. F.; Batisse, C.; Helye, R.; Schultz, P.; Potier, N.; Lamour, V. Structural Insight into Negative DNA Supercoiling by DNA Gyrase, a Bacterial Type 2a DNA Topoisomerase. *Nucleic Acids Res.* **2013**, *41*, 7815−27.
(371) Clapier, C. R.; Cairns, B. R. The Biology of Chromatin Remodeling Complexes. *Annu. Rev. Biochem.* **2009**, *78*, 273−304.
(372) Luger, K.; Mader, A. W.; Richmond, R. K.; Sargent, D. F.; Richmond, T. J. Crystal Structure of the Nucleosome Core Particle at 2.8 a Resolution. *Nature* **1997**, *389*, 251−60.
(373) Luo, Y.; North, J. A.; Rose, S. D.; Poirier, M. G. Nucleosomes Accelerate Transcription Factor Dissociation. *Nucleic Acids Res.* **2014**, *42*, 3017−27.
(374) Liu, X.; Lee, C. K.; Granek, J. A.; Clarke, N. D.; Lieb, J. D. Whole-Genome Comparison of Leu3 Binding in Vitro and in Vivo Reveals the Importance of Nucleosome Occupancy in Target Site Selection. *Genome Res.* **2006**, *16*, 1517−28.
(375) Struhl, K.; Segal, E. Determinants of Nucleosome Positioning. *Nat. Struct. Mol. Biol.* **2013**, *20*, 267−73.
(376) Krietenstein, N.; Wal, M.; Watanabe, S.; Park, B.; Peterson, C. L.; Pugh, B. F.; Korber, P. Genomic Nucleosome Organization Reconstituted with Pure Proteins. *Cell* **2016**, *167*, 709−721.e12.
(377) Hamiche, A.; Sandaltzopoulos, R.; Gdula, D. A.; Wu, C. Atp-Dependent Histone Octamer Sliding Mediated by the Chromatin Remodeling Complex Nurf. *Cell* **1999**, *97*, 833−42.
(378) Langst, G.; Bonte, E. J.; Corona, D. F.; Becker, P. B. Nucleosome Movement by Chrac and Iswi without Disruption or Trans-Displacement of the Histone Octamer. *Cell* **1999**, *97*, 843−52.
(379) Whitehouse, I.; Flaus, A.; Cairns, B. R.; White, M. F.; Workman, J. L.; Owen-Hughes, T. Nucleosome Mobilization Catalysed by the Yeast Swi/Snf Complex. *Nature* **1999**, *400*, 784−7.
(380) Mizuguchi, G.; Shen, X.; Landry, J.; Wu, W. H.; Sen, S.; Wu, C. Atp-Driven Exchange of Histone H2az Variant Catalyzed by Swr1 Chromatin Remodeling Complex. *Science* **2004**, *303*, 343−8.

DOI: 10.1021/acs.chemrev.9b00361
Chem. Rev. 2020, 120, 36−78

(381) Lorch, Y.; Cairns, B. R.; Zhang, M.; Kornberg, R. D. Activated Rsc-Nucleosome Complex and Persistently Altered Form of the Nucleosome. *Cell* **1998**, *94*, 29−34.
(382) Boeger, H.; Griesenbeck, J.; Strattan, J. S.; Kornberg, R. D. Nucleosomes Unfold Completely at a Transcriptionally Active Promoter. *Mol. Cell* **2003**, *11*, 1587−98.
(383) Boeger, H.; Griesenbeck, J.; Strattan, J. S.; Kornberg, R. D. Removal of Promoter Nucleosomes by Disassembly Rather Than Sliding in Vivo. *Mol. Cell* **2004**, *14*, 667−73.
(384) Reinke, H.; Horz, W. Histones Are First Hyperacetylated and Then Lose Contact with the Activated Pho5 Promoter. *Mol. Cell* **2003**, *11*, 1599−607.
(385) Dechassa, M. L.; Sabri, A.; Pondugula, S.; Kassabov, S. R.; Chatterjee, N.; Kladde, M. P.; Bartholomew, B. Swi/Snf Has Intrinsic Nucleosome Disassembly Activity That Is Dependent on Adjacent Nucleosomes. *Mol. Cell* **2010**, *38*, 590−602.
(386) Yang, X.; Zaurin, R.; Beato, M.; Peterson, C. L. Swi3p Controls Swi/Snf Assembly and Atp-Dependent H2a-H2b Displacement. *Nat. Struct. Mol. Biol.* **2007**, *14*, 540−7.
(387) Bruno, M.; Flaus, A.; Stockdale, C.; Rencurel, C.; Ferreira, H.; Owen-Hughes, T. Histone H2a/H2b Dimer Exchange by Atp-Dependent Chromatin Remodeling Activities. *Mol. Cell* **2003**, *12*, 1599−606.
(388) Kagalwala, M. N.; Glaus, B. J.; Dang, W.; Zofall, M.; Bartholomew, B. Topography of the Isw2-Nucleosome Complex: Insights into Nucleosome Spacing and Chromatin Remodeling. *EMBO J.* **2004**, *23*, 2092−104.
(389) Schwanbeck, R.; Xiao, H.; Wu, C. Spatial Contacts and Nucleosome Step Movements Induced by the Nurf Chromatin Remodeling Complex. *J. Biol. Chem.* **2004**, *279*, 39933−41.
(390) Zofall, M.; Persinger, J.; Kassabov, S. R.; Bartholomew, B. Chromatin Remodeling by Isw2 and Swi/Snf Requires DNA Translocation inside the Nucleosome. *Nat. Struct. Mol. Biol.* **2006**, *13*, 339−46.
(391) Saha, A.; Wittmeyer, J.; Cairns, B. R. Chromatin Remodeling by Rsc Involves Atp-Dependent DNA Translocation. *Genes Dev.* **2002**, *16*, 2120−34.
(392) Saha, A.; Wittmeyer, J.; Cairns, B. R. Chromatin Remodeling through Directional DNA Translocation from an Internal Nucleosomal Site. *Nat. Struct. Mol. Biol.* **2005**, *12*, 747−55.
(393) Blosser, T. R.; Yang, J. G.; Stone, M. D.; Narlikar, G. J.; Zhuang, X. Dynamics of Nucleosome Remodelling by Individual Acf Complexes. *Nature* **2009**, *462*, 1022−7.
(394) Hwang, W. L.; Deindl, S.; Harada, B. T.; Zhuang, X. Histone H4 Tail Mediates Allosteric Regulation of Nucleosome Remodelling by Linker DNA. *Nature* **2014**, *512*, 213−7.
(395) Lai, B.; Gao, W.; Cui, K.; Xie, W.; Tang, Q.; Jin, W.; Hu, G.; Ni, B.; Zhao, K. Principles of Nucleosome Organization Revealed by Single-Cell Micrococcal Nuclease Sequencing. *Nature* **2018**, *562*, 281−285.
(396) Racki, L. R.; Yang, J. G.; Naber, N.; Partensky, P. D.; Acevedo, A.; Purcell, T. J.; Cooke, R.; Cheng, Y.; Narlikar, G. J. The Chromatin Remodeller Acf Acts as a Dimeric Motor to Space Nucleosomes. *Nature* **2009**, *462*, 1016−21.
(397) Leonard, J. D.; Narlikar, G. J. A Nucleotide-Driven Switch Regulates Flanking DNA Length Sensing by a Dimeric Chromatin Remodeler. *Mol. Cell* **2015**, *57*, 850−859.
(398) Armache, J.-P.; Gamarra, N.; Johnson, S. L.; Leonard, J. D.; Wu, S.; Narlikar, G. J.; Cheng, Y. Electron Cryo-Microscopy Structures of Remodeler-Nucleosome Intermediates Suggest Allosteric Control through the Nucleosome. 2019, 550970. bioRxiv.org e-Print archive. https://www.biorxiv.org/content/10.1101/550970v1.
(399) Qiu, Y.; Levendosky, R. F.; Chakravarthy, S.; Patel, A.; Bowman, G. D.; Myong, S. The Chd1 Chromatin Remodeler Shifts Nucleosomal DNA Bidirectionally as a Monomer. *Mol. Cell* **2017**, *68*, 76−88.e6.
(400) Ayala, R.; Willhoft, O.; Aramayo, R. J.; Wilkinson, M.; McCormack, E. A.; Ocloo, L.; Wigley, D. B.; Zhang, X. Structure and Regulation of the Human Ino80-Nucleosome Complex. *Nature* **2018**, *556*, 391−395.
(401) Flaus, A.; Owen-Hughes, T. Dynamic Properties of Nucleosomes During Thermal and Atp-Driven Mobilization. *Mol. Cell. Biol.* **2003**, *23*, 7767−79.
(402) Kassabov, S. R.; Zhang, B.; Persinger, J.; Bartholomew, B. Swi/Snf Unwraps, Slides, and Rewraps the Nucleosome. *Mol. Cell* **2003**, *11*, 391−403.
(403) Shundrovsky, A.; Smith, C. L.; Lis, J. T.; Peterson, C. L.; Wang, M. D. Probing Swi/Snf Remodeling of the Nucleosome by Unzipping Single DNA Molecules. *Nat. Struct. Mol. Biol.* **2006**, *13*, 549−54.
(404) Harada, B. T.; Hwang, W. L.; Deindl, S.; Chatterjee, N.; Bartholomew, B.; Zhuang, X. Stepwise Nucleosome Translocation by Rsc Remodeling Complexes. *eLife* **2016**, *5*, No. e10051.
(405) Sabantsev, A.; Levendosky, R. F.; Zhuang, X.; Bowman, G. D.; Deindl, S. Direct Observation of Coordinated DNA Movements on the Nucleosome During Chromatin Remodelling. *Nat. Commun.* **2019**, *10*, 1720.
(406) Deindl, S.; Hwang, W. L.; Hota, S. K.; Blosser, T. R.; Prasad, P.; Bartholomew, B.; Zhuang, X. Iswi Remodelers Slide Nucleosomes with Coordinated Multi-Base-Pair Entry Steps and Single-Base-Pair Exit Steps. *Cell* **2013**, *152*, 442−52.
(407) Li, M.; Xia, X.; Tian, Y.; Jia, Q.; Liu, X.; Lu, Y.; Li, M.; Li, X.; Chen, Z. Mechanism of DNA Translocation Underlying Chromatin Remodelling by Snf2. *Nature* **2019**, *567*, 409−413.
(408) Zhang, Y.; Smith, C. L.; Saha, A.; Grill, S. W.; Mihardja, S.; Smith, S. B.; Cairns, B. R.; Peterson, C. L.; Bustamante, C. DNA Translocation and Loop Formation Mechanism of Chromatin Remodeling by Swi/Snf and. *Mol. Cell* **2006**, *24*, 559−68.
(409) Lia, G.; Praly, E.; Ferreira, H.; Stockdale, C.; Tse-Dinh, Y. C.; Dunlap, D.; Croquette, V.; Bensimon, D.; Owen-Hughes, T. Direct Observation of DNA Distortion by the Rsc Complex. *Mol. Cell* **2006**, *21*, 417−25.
(410) Sirinakis, G.; Clapier, C. R.; Gao, Y.; Viswanathan, R.; Cairns, B. R.; Zhang, Y. The Rsc Chromatin Remodelling Atpase Translocates DNA with High Force and Small Step Size. *EMBO J.* **2011**, *30*, 2364−72.
(411) Conaway, R. C.; Conaway, J. W. The Ino80 Chromatin Remodeling Complex in Transcription, Replication and Repair. *Trends Biochem. Sci.* **2009**, *34*, 71−7.
(412) Bao, Y.; Shen, X. Chromatin Remodeling in DNA Double-Strand Break Repair. *Curr. Opin. Genet. Dev.* **2007**, *17*, 126−31.
(413) van Attikum, H.; Gasser, S. M. Atp-Dependent Chromatin Remodeling and DNA Double-Strand Break Repair. *Cell Cycle* **2005**, *4*, 1011−4.
(414) Zhou, C. Y.; Johnson, S. L.; Lee, L. J.; Longhurst, A. D.; Beckwith, S. L.; Johnson, M. J.; Morrison, A. J.; Narlikar, G. J. The Yeast Ino80 Complex Operates as a Tunable DNA Length-Sensitive Switch to Regulate Nucleosome Sliding. *Mol. Cell* **2018**, *69*, 677−688.e9.
(415) Willhoft, O.; Ghoneim, M.; Lin, C. L.; Chua, E. Y. D.; Wilkinson, M.; Chaban, Y.; Ayala, R.; McCormack, E. A.; Ocloo, L.; Rueda, D. S.; Wigley, D. B. Structure and Dynamics of the Yeast Swr1-Nucleosome Complex. *Science* **2018**, *362*, eaat7716.
(416) Ranjan, A.; Wang, F.; Mizuguchi, G.; Wei, D.; Huang, Y.; Wu, C. H2a Histone-Fold and DNA Elements in Nucleosome Activate Swr1-Mediated H2a.Z Replacement in Budding Yeast. *eLife* **2015**, *4*, e06845.
(417) Farnung, L.; Vos, S. M.; Wigge, C.; Cramer, P. Nucleosome-Chd1 Structure and Implications for Chromatin Remodelling. *Nature* **2017**, *550*, 539−542.
(418) Watanabe, S.; Radman-Livaja, M.; Rando, O. J.; Peterson, C. L. A Histone Acetylation Switch Regulates H2a.Z Deposition by the Swr-C Remodeling Enzyme. *Science* **2013**, *340*, 195−9.
(419) Wang, F.; Ranjan, A.; Wei, D.; Wu, C. Comment on ″A Histone Acetylation Switch Regulates H2a.Z Deposition by the Swr-C Remodeling Enzyme″. *Science* **2016**, *353*, 358.

DOI: 10.1021/acs.chemrev.9b00361
Chem. Rev. 2020, 120, 36−78

(420) Watanabe, S.; Peterson, C. L. Response to Comment on "A Histone Acetylation Switch Regulates H2a.Z Deposition by the Swr-C Remodeling Enzyme". *Science* **2016**, *353*, 358.
(421) Ranjan, A.; Mizuguchi, G.; FitzGerald, P. C.; Wei, D.; Wang, F.; Huang, Y.; Luk, E.; Woodcock, C. L.; Wu, C. Nucleosome-Free Region Dominates Histone Acetylation in Targeting Swr1 to Promoters for H2a.Z Replacement. *Cell* **2013**, *154*, 1232−45.
(422) Brahma, S.; Udugama, M. I.; Kim, J.; Hada, A.; Bhardwaj, S. K.; Hailu, S. G.; Lee, T. H.; Bartholomew, B. Ino80 Exchanges H2a.Z for H2a by Translocating on DNA Proximal to Histone Dimers. *Nat. Commun.* **2017**, *8*, 15616.
(423) Yudkovsky, N.; Logie, C.; Hahn, S.; Peterson, C. L. Recruitment of the Swi/Snf Chromatin Remodeling Complex by Transcriptional Activators. *Genes Dev.* **1999**, *13*, 2369−74.
(424) Tsukiyama, T.; Wu, C. Purification and Properties of an Atp-Dependent Nucleosome Remodeling Factor. *Cell* **1995**, *83*, 1011−20.
(425) Kang, J. G.; Hamiche, A.; Wu, C. Gal4 Directs Nucleosome Sliding Induced by Nurf. *EMBO J.* **2002**, *21*, 1406−13.
(426) McKnight, J. N.; Jenkins, K. R.; Nodelman, I. M.; Escobar, T.; Bowman, G. D. Extranucleosomal DNA Binding Directs Nucleosome Sliding by Chd1. *Mol. Cell. Biol.* **2011**, *31*, 4746−59.
(427) Killian, J. L.; Li, M.; Sheinin, M. Y.; Wang, M. D. Recent Advances in Single Molecule Studies of Nucleosomes. *Curr. Opin. Struct. Biol.* **2012**, *22*, 80−7.
(428) Li, M.; Hada, A.; Sen, P.; Olufemi, L.; Hall, M. A.; Smith, B. Y.; Forth, S.; McKnight, J. N.; Patel, A.; Bowman, G. D.; Bartholomew, B.; Wang, M. D. Dynamic Regulation of Transcription Factors by Nucleosome Remodeling. *eLife* **2015**, *4*, No. e06249.
(429) Rudnizky, S.; Bavly, A.; Malik, O.; Pnueli, L.; Melamed, P.; Kaplan, A. H2a.Z Controls the Stability and Mobility of Nucleosomes to Regulate Expression of the Lh Genes. *Nat. Commun.* **2016**, *7*, 12958.
(430) Rudnizky, S.; Khamis, H.; Malik, O.; Melamed, P.; Kaplan, A. The Base Pair-Scale Diffusion of Nucleosomes Modulates Binding of Transcription Factors. *Proc. Natl. Acad. Sci. U. S. A.* **2019**, *116*, 12161.
(431) Prasad, T. K.; Robertson, R. B.; Visnapuu, M. L.; Chi, P.; Sung, P.; Greene, E. C. A DNA-Translocating Snf2Molecular Motor: Saccharomyces Cerevisiae Rdh54 Displays Processive Translocation and Extrudes DNA Loops. *J. Mol. Biol.* **2007**, *369*, 940−53.
(432) Amitani, I.; Baskin, R. J.; Kowalczykowski, S. C. Visualization of Rad54, a Chromatin Remodeling Protein, Translocating on Single DNA Molecules. *Mol. Cell* **2006**, *23*, 143−8.
(433) Le, T. T.; Yang, Y.; Tan, C.; Suhanovsky, M. M.; Fulbright, R. M., Jr.; Inman, J. T.; Li, M.; Lee, J.; Perelman, S.; Roberts, J. W.; Deaconescu, A. M.; Wang, M. D. Mfd Dynamically Regulates Transcription Via a Release and Catch-up Mechanism. *Cell* **2018**, *172*, 344−357.e15.
(434) Chemla, Y. R.; Aathavan, K.; Michaelis, J.; Grimes, S.; Jardine, P. J.; Anderson, D. L.; Bustamante, C. Mechanism of Force Generation of a Viral DNA Packaging Motor. *Cell* **2005**, *122*, 683−692.
(435) Fuller, D. N.; Raymer, D. M.; Kottadiel, V. I.; Rao, V. B.; Smith, D. E. Single Phage T4 DNA Packaging Motors Exhibit Large Force Generation, High Velocity, and Dynamic Variability. *Proc. Natl. Acad. Sci. U. S. A.* **2007**, *104*, 16868−16873.
(436) Fuller, D. N.; Raymer, D. M.; Rickgauer, J. P.; Robertson, R. M.; Catalano, C. E.; Anderson, D. L.; Grimes, S.; Smith, D. E. Measurements of Single DNA Molecule Packaging Dynamics in Bacteriophage Lambda Reveal High Forces, High Motor Processivity, and Capsid Transformations. *J. Mol. Biol.* **2007**, *373*, 1113−1122.
(437) Smith, D. E.; Tans, S. J.; Smith, S. B.; Grimes, S.; Anderson, D. L.; Bustamante, C. The Bacteriophage Φ29 Portal Motor Can Package DNA against a Large Internal Force. *Nature* **2001**, *413*, 748−752.
(438) Cao, S.; Saha, M.; Zhao, W.; Jardine, P. J.; Zhang, W.; Grimes, S.; Morais, M. C. Insights into the Structure and Assembly of the Bacteriophage ϕ29 Double-Stranded DNA Packaging Motor. *Journal of Virology* **2014**, *88*, 3986.
(439) Morais, M. C.; Koti, J. S.; Bowman, V. D.; Reyes-Aldrete, E.; Anderson, D. L.; Rossmann, M. G. Defining Molecular and Domain Boundaries in the Bacteriophage Phi29 DNA Packaging Motor. *Structure (Oxford, U. K.)* **2008**, *16*, 1267−1274.
(440) Rickgauer, J. P.; Fuller, D. N.; Grimes, S.; Jardine, P. J.; Anderson, D. L.; Smith, D. E. Portal Motor Velocity and Internal Force Resisting Viral DNA Packaging in Bacteriophage Phi29. *Biophys. J.* **2008**, *94*, 159−167.
(441) Chistol, G.; Liu, S.; Hetherington, C. L.; Moffitt, J. R.; Grimes, S.; Jardine, P. J.; Bustamante, C. High Degree of Coordination and Division of Labor among Subunits in a Homomeric Ring Atpase. *Cell* **2012**, *151*, 1017−1028.
(442) Aathavan, K.; Politzer, A. T.; Kaplan, A.; Moffitt, J. R.; Chemla, Y. R.; Grimes, S.; Jardine, P. J.; Anderson, D. L.; Bustamante, C. Substrate Interactions and Promiscuity in a Viral DNA Packaging Motor. *Nature* **2009**, *461*, 669.
(443) Tafoya, S.; Liu, S.; Castillo, J. P.; Atz, R.; Morais, M. C.; Grimes, S.; Jardine, P. J.; Bustamante, C. Molecular Switch-Like Regulation Enables Global Subunit Coordination in a Viral Ring Atpase. *Proc. Natl. Acad. Sci. U. S. A.* **2018**, *115*, 7961.
(444) Keller, N.; Grimes, S.; Jardine, P. J.; Smith, D. E. Single DNA Molecule Jamming and History-Dependent Dynamics During Motor-Driven Viral Packaging. *Nat. Phys.* **2016**, *12*, 757.
(445) Vafabakhsh, R.; Kondabagil, K.; Earnest, T.; Lee, K. S.; Zhang, Z.; Dai, L.; Dahmen, K. A.; Rao, V. B.; Ha, T. Single-Molecule Packaging Initiation in Real Time by a Viral DNA Packaging Machine from Bacteriophage T4. *Proc. Natl. Acad. Sci. U. S. A.* **2014**, *111*, 15096−15101.
(446) Ordyan, M.; Alam, I.; Mahalingam, M.; Rao, V. B.; Smith, D. E. Nucleotide-Dependent DNA Gripping and an End-Clamp Mechanism Regulate the Bacteriophage T4 Viral Packaging Motor. *Nat. Commun.* **2018**, *9*, 5434.
(447) Terakawa, T.; Bisht, S.; Eeftens, J. M.; Dekker, C.; Haering, C. H.; Greene, E. C. The Condensin Complex Is a Mechanochemical Motor That Translocates Along DNA. *Science* **2017**, *358*, 672.
(448) Anderson, D. E.; Losada, A.; Erickson, H. P.; Hirano, T. Condensin and Cohesin Display Different Arm Conformations with Characteristic Hinge Angles. *J. Cell Biol.* **2002**, *156*, 419.
(449) Eeftens, J. M.; Katan, A. J.; Kschonsak, M.; Hassler, M.; de Wilde, L.; Dief, E. M.; Haering, C. H.; Dekker, C. Condensin Smc2-Smc4 Dimers Are Flexible and Dynamic. *Cell Rep.* **2016**, *14*, 1813−1818.
(450) Strick, T. R.; Kawaguchi, T.; Hirano, T. Real-Time Detection of Single-Molecule DNA Compaction by Condensin I. *Curr. Biol.* **2004**, *14*, 874−880.
(451) Eeftens, J. M.; Bisht, S.; Kerssemakers, J.; Kschonsak, M.; Haering, C. H.; Dekker, C. Real-Time Detection of Condensin-Driven DNA Compaction Reveals a Multistep Binding Mechanism. *EMBO J.* **2017**, *36*, 3448.
(452) Ganji, M.; Shaltiel, I. A.; Bisht, S.; Kim, E.; Kalichava, A.; Haering, C. H.; Dekker, C. Real-Time Imaging of DNA Loop Extrusion by Condensin. *Science* **2018**, *360*, 102.
(453) Lee, J. Y.; Finkelstein, I. J.; Crozat, E.; Sherratt, D. J.; Greene, E. C. Single-Molecule Imaging of DNA Curtains Reveals Mechanisms of Kops Sequence Targeting by the DNA Translocase Ftsk. *Proc. Natl. Acad. Sci. U. S. A.* **2012**, *109*, 6531.
(454) Ptacin, J. L.; Nollmann, M.; Becker, E. C.; Cozzarelli, N. R.; Pogliano, K.; Bustamante, C. Sequence-Directed DNA Export Guides Chromosome Translocation During Sporulation in Bacillus Subtilis. *Nat. Struct. Mol. Biol.* **2008**, *15*, 485−493.
(455) Pease, P. J.; Levy, O.; Cost, G. J.; Gore, J.; Ptacin, J. L.; Sherratt, D.; Bustamante, C.; Cozzarelli, N. R. Sequence-Directed DNA Translocation by Purified Ftsk. *Science* **2005**, *307*, 586.
(456) Barre, F.-X. Ftsk and Spoiiie: The Tale of the Conserved Tails. *Mol. Microbiol.* **2007**, *66*, 1051−1055.
(457) Besprozvannaya, M.; Pivorunas, V. L.; Feldman, Z.; Burton, B. M. Spoiiie Protein Achieves Directional DNA Translocation through Allosteric Regulation of Atpase Activity by an Accessory Domain. *J. Biol. Chem.* **2013**, *288*, 28962−28974.

DOI: 10.1021/acs.chemrev.9b00361
Chem. Rev. 2020, 120, 36−78

(458) Massey, T. H.; Mercogliano, C. P.; Yates, J.; Sherratt, D. J.; Löwe, J. Double-Stranded DNA Translocation: Structure and Mechanism of Hexameric Ftsk. *Mol. Cell* **2006**, *23*, 457−469.
(459) Löwe, J.; Ellonen, A.; Allen, M. D.; Atkinson, C.; Sherratt, D. J.; Grainge, I. Molecular Mechanism of Sequence-Directed DNA Loading and Translocation by Ftsk. *Mol. Cell* **2008**, *31*, 498−509.
(460) Ptacin, J. L.; Nöllmann, M.; Bustamante, C.; Cozzarelli, N. R. Identification of the Ftsk Sequence-Recognition Domain. *Nat. Struct. Mol. Biol.* **2006**, *13*, 1023−1025.
(461) Levy, O.; Ptacin, J. L.; Pease, P. J.; Gore, J.; Eisen, M. B.; Bustamante, C.; Cozzarelli, N. R. Identification of Oligonucleotide Sequences That Direct the Movement of the ≪Em≫Escherichia Coli≪/Em≫ Ftsk Translocase. *Proc. Natl. Acad. Sci. U. S. A.* **2005**, *102*, 17618.
(462) Bigot, S.; Saleh, O. A.; Lesterlin, C.; Pages, C.; El Karoui, M.; Dennis, C.; Grigoriev, M.; Allemand, J. F.; Barre, F. X.; Cornet, F. Kops: DNA Motifs That Control *E. Coli* Chromosome Segregation by Orienting the Ftsk Translocase. *EMBO J.* **2005**, *24*, 3770.
(463) Bigot, S.; Saleh, O. A.; Cornet, F.; Allemand, J.-F.; Barre, F. X. Oriented Loading of Ftsk on Kops. *Nat. Struct. Mol. Biol.* **2006**, *13*, 1026−1028.
(464) Sivanathan, V.; Allen, M. D.; de Bekker, C.; Baker, R.; Arciszewska, L. K.; Freund, S. M.; Bycroft, M.; Löwe, J.; Sherratt, D. J. The Ftsk Γ Domain Directs Oriented DNA Translocation by Interacting with Kops. *Nat. Struct. Mol. Biol.* **2006**, *13*, 965−972.
(465) Graham, J. E.; Sherratt, D. J.; Szczelkun, M. D. Sequence-Specific Assembly of Ftsk Hexamers Establishes Directional Translocation on DNA. *Proc. Natl. Acad. Sci. U. S. A.* **2010**, *107*, 20263.
(466) Lee, J. Y.; Finkelstein, I. J.; Arciszewska, L. K.; Sherratt, D. J.; Greene, E. C. Single-Molecule Imaging of Ftsk Translocation Reveals Mechanistic Features of Protein-Protein Collisions on DNA. *Mol. Cell* **2014**, *54*, 832−843.
(467) Liu, N.; Chistol, G.; Bustamante, C. Two-Subunit DNA Escort Mechanism and Inactive Subunit Bypass in an Ultra-Fast Ring Atpase. *eLife* **2015**, *4*, e09224.
(468) Liu, N.; Chistol, G.; Cui, Y.; Bustamante, C. Mechanochemical Coupling and Bi-Phasic Force-Velocity Dependence in the Ultra-Fast Ring Atpase Spoiiie. *eLife* **2018**, *7*, e32354.
(469) Burton, B. M.; Marquis, K. A.; Sullivan, N. L.; Rapoport, T. A.; Rudner, D. Z. The Atpase Spoiiie Transports DNA across Fused Septal Membranes During Sporulation in Bacillus Subtilis. *Cell* **2007**, *131*, 1301−1312.
(470) Haber, J. E. Vivo Biochemistry: Physical Monitoring of Recombination Induced by Site-Specific Endonucleases. *BioEssays* **1995**, *17*, 609−620.
(471) Lee, G.; Yoo, J.; Leslie, B. J.; Ha, T. Single-Molecule Analysis Reveals Three Phases of DNA Degradation by an Exonuclease. *Nat. Chem. Biol.* **2011**, *7*, 367−374.
(472) Yoo, J.; Lee, G. Allosteric Ring Assembly and Chemo-Mechanical Melting by the Interaction between 5′-Phosphate and Λ Exonuclease. *Nucleic Acids Res.* **2015**, *43*, 10861−10869.
(473) Perkins, T. T.; Dalal, R. V.; Mitsis, P. G.; Block, S. M. Sequence-Dependent Pausing of Single Lambda Exonuclease Molecules. *Science* **2003**, *301*, 1914.
(474) Hwang, W.; Yoo, J.; Lee, Y.; Park, S.; Hoang, P. L.; Cho, H.; Yu, J.; Hoa Vo, T. M.; Shin, M.; Jin, M. S.; Park, D.; Hyeon, C.; Lee, G. Dynamic Coordination of Two-Metal-Ions Orchestrates Λ-Exonuclease Catalysis. *Nat. Commun.* **2018**, *9*, 4404.
(475) Zhang, G.; Deng, E.; Baugh, L.; Kushner, S. R. Identification and Characterization of Escherichia Coli DNA Helicase Ii Mutants That Exhibit Increased Unwinding Efficiency. *J. Bacteriol.* **1998**, *180*, 377−387.
(476) Meiners, M. J.; Tahmaseb, K.; Matson, S. W. The Uvrd303 Hyper-Helicase Exhibits Increased Processivity. *J. Biol. Chem.* **2014**, *289*, 17100−17110.
(477) Ma, W.; Whitley, K. D.; Chemla, Y. R.; Luthey-Schulten, Z.; Schulten, K. Free-Energy Simulations Reveal Molecular Mechanism for Functional Switch of a DNA Helicase. *eLife* **2018**, *7*, e34186.
(478) Lin, S.; Alam, T. I.; Kottadiel, V. I.; VanGessel, C. J.; Tang, W.-C.; Chemla, Y. R.; Rao, V. B. Altering the Speed of a DNA Packaging Motor from Bacteriophage T4. *Nucleic Acids Res.* **2017**, *45*, 11437−11448.
(479) Motré, A.; Li, Y.; Kong, H. Enhancing Helicase-Dependent Amplification by Fusing the Helicase with the DNA Polymerase. *Gene* **2008**, *420*, 17−22.
(480) Vincent, M.; Xu, Y.; Kong, H. Helicase-Dependent Isothermal DNA Amplification. *EMBO Rep.* **2004**, *5*, 795.
(481) McKnight, J. N.; Tsukiyama, T.; Bowman, G. D. Sequence-Targeted Nucleosome Sliding in Vivo by a Hybrid Chd1 Chromatin Remodeler. *Genome Res.* **2016**, *26*, 693−704.
(482) Donovan, D. A.; Crandall, J. G.; Banks, O. G. B.; Jensvold, Z. D.; McKnight, L. E.; McKnight, J. N. E-ChRPs: Engineered Chromatin Remodeling Proteins for Precise Nucleosome Positioning. **2019**, 480913.
(483) Hua, B.; Panja, S.; Wang, Y.; Woodson, S. A.; Ha, T. Mimicking Co-Transcriptional Rna Folding Using a Superhelicase. *J. Am. Chem. Soc.* **2018**, *140*, 10067−10070.
(484) Mitra, J.; Ha, T. Nanomechanics and Co-Transcriptional Folding of Spinach and Mango. *Nat. Commun.* **2019**, *10*, 650119.
(485) Fegan, A.; White, B.; Carlson, J. C. T.; Wagner, C. R. Chemically Controlled Protein Assembly: Techniques and Applications. *Chem. Rev.* **2010**, *110*, 3315−3336.
(486) Putyrski, M.; Schultz, C. Protein Translocation as a Tool: The Current Rapamycin Story. *FEBS Lett.* **2012**, *586*, 2097−2105.
(487) Chen, J.; Zheng, X. F.; Brown, E. J.; Schreiber, S. L. Identification of an 11-Kda Fkbp12-Rapamycin-Binding Domain within the 289-Kda Fkbp12-Rapamycin-Associated Protein and Characterization of a Critical Serine Residue. *Proc. Natl. Acad. Sci. U. S. A.* **1995**, *92*, 4947.
(488) Banaszynski, L. A.; Liu, C. W.; Wandless, T. J. Characterization of the Fkbp·Rapamycin·Frb Ternary Complex. *J. Am. Chem. Soc.* **2005**, *127*, 4715−4721.
(489) Karginov, A. V.; Zou, Y.; Shirvanyants, D.; Kota, P.; Dokholyan, N. V.; Young, D. D.; Hahn, K. M.; Deiters, A. Light Regulation of Protein Dimerization and Kinase Activity in Living Cells Using Photocaged Rapamycin and Engineered Fkbp. *J. Am. Chem. Soc.* **2011**, *133*, 420−423.
(490) Dagliyan, O.; Shirvanyants, D.; Karginov, A. V.; Ding, F.; Fee, L.; Chandrasekaran, S. N.; Freisinger, C. M.; Smolen, G. A.; Huttenlocher, A.; Hahn, K. M.; Dokholyan, N. V. Rational Design of a Ligand-Controlled Protein Conformational Switch. *Proc. Natl. Acad. Sci. U. S. A.* **2013**, *110*, 6800.
(491) Dagliyan, O.; Krokhotin, A.; Ozkan-Dagliyan, I.; Deiters, A.; Der, C. J.; Hahn, K. M.; Dokholyan, N. V. Computational Design of Chemogenetic and Optogenetic Split Proteins. *Nat. Commun.* **2018**, *9*, 4042.
(492) Kaplan, J. H.; Forbush, B.; Hoffman, J. F. Rapid Photolytic Release of Adenosine 5′-Triphosphate from a Protected Analog: Utilization by the Sodium:Potassium Pump of Human Red Blood Cell Ghosts. *Biochemistry* **1978**, *17*, 1929−1935.
(493) Kamei, T.; Fukaminato, T.; Tamaoki, N. A Photochromic Atp Analogue Driving a Motor Protein with Reversible Light-Controlled Motility: Controlling Velocity and Binding Manner of a Kinesin−Microtubule System in an in Vitro Motility Assay. *Chem. Commun.* **2012**, *48*, 7625−7627.
(494) Boyden, E. S.; Zhang, F.; Bamberg, E.; Nagel, G.; Deisseroth, K. Millisecond-Timescale, Genetically Targeted Optical Control of Neural Activity. *Nat. Neurosci.* **2005**, *8*, 1263−8.
(495) Tye, K. M.; Deisseroth, K. Optogenetic Investigation of Neural Circuits Underlying Brain Disease in Animal Models. *Nat. Rev. Neurosci.* **2012**, *13*, 251−66.
(496) Selimbeyoglu, A.; Kim, C. K.; Inoue, M.; Lee, S. Y.; Hong, A. S. O.; Kauvar, I.; Ramakrishnan, C.; Fenno, L. E.; Davidson, T. J.; Wright, M.; Deisseroth, K. Modulation of Prefrontal Cortex Excitation/Inhibition Balance Rescues Social Behavior in Cntnap2-Deficient Mice. *Sci. Transl. Med.* **2017**, *9*, eaah6733.

DOI: 10.1021/acs.chemrev.9b00361
Chem. Rev. 2020, 120, 36−78

(497) Repina, N. A.; Rosenbloom, A.; Mukherjee, A.; Schaffer, D. V.; Kane, R. S. At Light Speed: Advances in Optogenetic Systems for Regulating Cell Signaling and Behavior. *Annu. Rev. Chem. Biomol. Eng.* **2017**, *8*, 13−39.
(498) Astori, S.; Wimmer, R. D.; Luthi, A. Manipulating Sleep Spindles–Expanding Views on Sleep, Memory, and Disease. *Trends Neurosci.* **2013**, *36*, 738−48.
(499) Govorunova, E. G.; Cunha, S. R.; Sineshchekov, O. A.; Spudich, J. L. Anion Channelrhodopsins for Inhibitory Cardiac Optogenetics. *Sci. Rep.* **2016**, *6*, 33530.
(500) Zhang, K.; Cui, B. Optogenetic Control of Intracellular Signaling Pathways. *Trends Biotechnol.* **2015**, *33*, 92−100.
(501) Toettcher, J. E.; Voigt, C. A.; Weiner, O. D.; Lim, W. A. The Promise of Optogenetics in Cell Biology: Interrogating Molecular Circuits in Space and Time. *Nat. Methods* **2011**, *8*, 35−8.
(502) Konermann, S.; Brigham, M. D.; Trevino, A.; Hsu, P. D.; Heidenreich, M.; Cong, L.; Platt, R. J.; Scott, D. A.; Church, G. M.; Zhang, F. Optical Control of Mammalian Endogenous Transcription and Epigenetic States. *Nature* **2013**, *500*, 472−476.
(503) Lungu, O. I.; Hallett, R. A.; Choi, E. J.; Aiken, M. J.; Hahn, K. M.; Kuhlman, B. Designing Photoswitchable Peptides Using the Aslov2 Domain. *Chem. Biol.* **2012**, *19*, 507−17.
(504) Motta-Mena, L. B.; Reade, A.; Mallory, M. J.; Glantz, S.; Weiner, O. D.; Lynch, K. W.; Gardner, K. H. An Optogenetic Gene Expression System with Rapid Activation and Deactivation Kinetics. *Nat. Chem. Biol.* **2014**, *10*, 196−202.
(505) Idevall-Hagren, O.; Dickson, E. J.; Hille, B.; Toomre, D. K.; De Camilli, P. Optogenetic Control of Phosphoinositide Metabolism. *Proc. Natl. Acad. Sci. U. S. A.* **2012**, *109*, E2316−23.
(506) Strickland, D.; Lin, Y.; Wagner, E.; Hope, C. M.; Zayner, J.; Antoniou, C.; Sosnick, T. R.; Weiss, E. L.; Glotzer, M. Tulips: Tunable, Light-Controlled Interacting Protein Tags for Cell Biology. *Nat. Methods* **2012**, *9*, 379−84.
(507) Toettcher, J. E.; Weiner, O. D.; Lim, W. A. Using Optogenetics to Interrogate the Dynamic Control of Signal Transmission by the Ras/Erk Module. *Cell* **2013**, *155*, 1422−34.
(508) Toettcher, J. E.; Gong, D.; Lim, W. A.; Weiner, O. D. Light-Based Feedback for Controlling Intracellular Signaling Dynamics. *Nat. Methods* **2011**, *8*, 837−9.
(509) Vazquez, A. L.; Fukuda, M.; Kim, S. G. Inhibitory Neuron Activity Contributions to Hemodynamic Responses and Metabolic Load Examined Using an Inhibitory Optogenetic Mouse Model. *Cereb. Cortex* **2018**, *28*, 4105−4119.
(510) Yang, X.; Jost, A. P.; Weiner, O. D.; Tang, C. A Light-Inducible Organelle-Targeting System for Dynamically Activating and Inactivating Signaling in Budding Yeast. *Mol. Biol. Cell* **2013**, *24*, 2419−30.
(511) Zhang, K.; Duan, L.; Ong, Q.; Lin, Z.; Varman, P. M.; Sung, K.; Cui, B. Light-Mediated Kinetic Control Reveals the Temporal Effect of the Raf/Mek/Erk Pathway in Pc12 Cell Neurite Outgrowth. *PLoS One* **2014**, *9*, e92917.
(512) Bugaj, L. J.; Spelke, D. P.; Mesuda, C. K.; Varedi, M.; Kane, R. S.; Schaffer, D. V. Regulation of Endogenous Transmembrane Receptors through Optogenetic Cry2 Clustering. *Nat. Commun.* **2015**, *6*, 6898.
(513) Adhikari, A.; Lerner, T. N.; Finkelstein, J.; Pak, S.; Jennings, J. H.; Davidson, T. J.; Ferenczi, E.; Gunaydin, L. A.; Mirzabekov, J. J.; Ye, L.; Kim, S. Y.; Lei, A.; Deisseroth, K. Basomedial Amygdala Mediates Top-Down Control of Anxiety and Fear. *Nature* **2015**, *527*, 179−85.
(514) Ferenczi, E. A.; Zalocusky, K. A.; Liston, C.; Grosenick, L.; Warden, M. R.; Amatya, D.; Katovich, K.; Mehta, H.; Patenaude, B.; Ramakrishnan, C.; Kalanithi, P.; Etkin, A.; Knutson, B.; Glover, G. H.; Deisseroth, K. Prefrontal Cortical Regulation of Brainwide Circuit Dynamics and Reward-Related Behavior. *Science* **2016**, *351*, aac9698.
(515) Eleftheriou, C.; Cesca, F.; Maragliano, L.; Benfenati, F.; Maya-Vetencourt, J. F. Optogenetic Modulation of Intracellular Signalling and Transcription: Focus on Neuronal Plasticity. *J. Exp. Neurosci.* **2017**, DOI: 10.1177/1179069517703354.
(516) Schmidt, D.; Cho, Y. K. Natural Photoreceptors and Their Application to Synthetic Biology. *Trends Biotechnol.* **2015**, *33*, 80−91.
(517) Zhou, X. X.; Pan, M.; Lin, M. Z. Investigating Neuronal Function with Optically Controllable Proteins. *Front. Mol. Neurosci.* **2015**, *8*, 37.
(518) Baumschlager, A.; Aoki, S. K.; Khammash, M. Dynamic Blue Light-Inducible T7 Rna Polymerases (Opto-T7rnaps) for Precise Spatiotemporal Gene Expression Control. *ACS Synth. Biol.* **2017**, *6*, 2157−2167.
(519) Renicke, C.; Schuster, D.; Usherenko, S.; Essen, L. O.; Taxis, C. A Lov2 Domain-Based Optogenetic Tool to Control Protein Degradation and Cellular Function. *Chem. Biol.* **2013**, *20*, 619−26.
(520) Halavaty, A. S.; Moffat, K. N- and C-Terminal Flanking Regions Modulate Light-Induced Signal Transduction in the Lov2 Domain of the Blue Light Sensor Phototropin 1 from Avena Sativa. *Biochemistry* **2007**, *46*, 14001−9.
(521) Niopek, D.; Wehler, P.; Roensch, J.; Eils, R.; Di Ventura, B. Optogenetic Control of Nuclear Protein Export. *Nat. Commun.* **2016**, *7*, 10624.
(522) Yumerefendi, H.; Lerner, A. M.; Zimmerman, S. P.; Hahn, K.; Bear, J. E.; Strahl, B. D.; Kuhlman, B. Light-Induced Nuclear Export Reveals Rapid Dynamics of Epigenetic Modifications. *Nat. Chem. Biol.* **2016**, *12*, 399−401.
(523) Christie, J. M.; Swartz, T. E.; Bogomolni, R. A.; Briggs, W. R. Phototropin Lov Domains Exhibit Distinct Roles in Regulating Photoreceptor Function. *Plant J.* **2002**, *32*, 205−19.
(524) Harper, S. M.; Neil, L. C.; Gardner, K. H. Structural Basis of a Phototropin Light Switch. *Science* **2003**, *301*, 1541−4.
(525) Harper, S. M.; Christie, J. M.; Gardner, K. H. Disruption of the Lov-Jalpha Helix Interaction Activates Phototropin Kinase Activity. *Biochemistry* **2004**, *43*, 16184−92.
(526) Taslimi, A.; Vrana, J. D.; Chen, D.; Borinskaya, S.; Mayer, B. J.; Kennedy, M. J.; Tucker, C. L. An Optimized Optogenetic Clustering Tool for Probing Protein Interaction and Function. *Nat. Commun.* **2014**, *5*, 4925.
(527) Bugaj, L. J.; Choksi, A. T.; Mesuda, C. K.; Kane, R. S.; Schaffer, D. V. Optogenetic Protein Clustering and Signaling Activation in Mammalian Cells. *Nat. Methods* **2013**, *10*, 249−52.
(528) Zhang, P.; Fan, B.; Yang, P.; Temirov, J.; Messing, J.; Kim, H. J.; Taylor, J. P. Chronic Optogenetic Induction of Stress Granules Is Cytotoxic and Reveals the Evolution of Als-Ftd Pathology. *eLife* **2019**, *8*, No. 39578.
(529) Shin, Y.; Berry, J.; Pannucci, N.; Haataja, M. P.; Toettcher, J. E.; Brangwynne, C. P. Spatiotemporal Control of Intracellular Phase Transitions Using Light-Activated Optodroplets. *Cell* **2017**, *168*, 159−171.e14.
(530) Lee, S.; Park, H.; Kyung, T.; Kim, N. Y.; Kim, S.; Kim, J.; Heo, W. D. Reversible Protein Inactivation by Optogenetic Trapping in Cells. *Nat. Methods* **2014**, *11*, 633−6.
(531) Dagliyan, O.; Dokholyan, N. V.; Hahn, K. M. Engineering Proteins for Allosteric Control by Light or Ligands. *Nat. Protoc.* **2019**, *14*, 1863−1883.
(532) Dagliyan, O.; Tarnawski, M.; Chu, P. H.; Shirvanyants, D.; Schlichting, I.; Dokholyan, N. V.; Hahn, K. M. Engineering Extrinsic Disorder to Control Protein Activity in Living Cells. *Science* **2016**, *354*, 1441−1444.
(533) Wang, X.; He, L.; Wu, Y. I.; Hahn, K. M.; Montell, D. J. Light-Mediated Activation Reveals a Key Role for Rac in Collective Guidance of Cell Movement in Vivo. *Nat. Cell Biol.* **2010**, *12*, 591−7.
(534) Yoo, S. K.; Deng, Q.; Cavnar, P. J.; Wu, Y. I.; Hahn, K. M.; Huttenlocher, A. Differential Regulation of Protrusion and Polarity by Pi3k During Neutrophil Motility in Live Zebrafish. *Dev. Cell* **2010**, *18*, 226−36.
(535) Zhou, X. X.; Fan, L. Z.; Li, P.; Shen, K.; Lin, M. Z. Optical Control of Cell Signaling by Single-Chain Photoswitchable Kinases. *Science* **2017**, *355*, 836−842.
(536) Luo, J.; Kong, M.; Liu, L.; Samanta, S.; Van Houten, B.; Deiters, A. Optical Control of DNA Helicase Function through Genetic Code Expansion. *ChemBioChem* **2017**, *18*, 466−469.

DOI: 10.1021/acs.chemrev.9b00361
Chem. Rev. 2020, 120, 36−78

(537) Strickland, D.; Yao, X.; Gawlak, G.; Rosen, M. K.; Gardner, K. H.; Sosnick, T. R. Rationally Improving Lov Domain-Based Photoswitches. *Nat. Methods* **2010**, *7*, 623−6.

DOI: 10.1021/acs.chemrev.9b00361
Chem. Rev. 2020, 120, 36−78